UNIVERSITÀ DEGLI STUDI DI MILANO

Scuola di Dottorato in
Biotecnologie applicate alle Scienze Biomediche
XXVI ciclo

Dipartimento di Biotecnologie Mediche
e Medicina Traslazionale

THE NOVEL DESMOSOMAL PROTEIN POF1B IS ESSENTIAL FOR CELL-CELL ADHESION STRENGTH

COORDINATORE: Prof. Enrico Ginelli
TUTOR: Dott.ssa Grazia Pietrini

Tesi di Dottorato di:
ARIANNA CRESPI
Matricola: R09284

Anno Accademico 2012-2013

The novel desmosomal protein POF1B is essential for cell-cell adhesion strength

Contents

1
chapter

Abstract

POF1B is a candidate gene for premature ovarian failure (POF); it is mainly expressed in polarized epithelial tissues, but its function in these tissues and the relationship with the disorder are unknown. In polarized epithelial MDCK cells the human stably expressed POF1B showed a tight junction localization that was lost by the POF1B R329Q variant associated with POF. Although the apico-basal polarity markers and ultrastructure of the tight junctions were maintained in cells expressing the mutant, tight junction assembly, as well as the organization of the monolayer appeared altered. Moreover, cells expressing the POF1B R329Q variant showed defects in ciliogenesis and cystogenesis as a result of misorientation of primary cilia and mitotic division. All of these defects were explained by interference of the mutant with the content and organization of F-actin at the junctions. Subsequently, by means of morphological and biochemical criteria we documented that POF1B is actually a desmosome-associated protein. Both in Caco-2 human intestinal cells and in stratified HaCaT keratinocyte cell lines, indeed, endogenous POF1B colocalized with desmoplakin and plakophilin 2 at the desmosomal plaque and in cytoplasmic particles aligned along intermediate filaments. POF1B co-fractionated with desmosomes and intermediate filament components and showed properties characteristic of desmosomes (i.e. detergent insolubility and calcium independence). Furthermore, POF1B was required for desmosome assembly and function, as the stable downregulation of the protein in HaCaT cells caused a decrease in desmosome number and size, and these desmosomes had very weak electron dense plaques. Among the cell-cell adhesion structures, desmosomes are the most essential for mechanical coupling. The

reduced capability of POF1B-silenced keratinocytes to respond to mechanical stress revealed the protein's crucial role in these junctions. Moreover, altered desmosomes in POF1B-downregulated keratinocytes were associated with altered cell proliferation and differentiation. The localization of POF1B in simple and stratified epithelia, as well as its relocation to desmosomes in human skin tumors, further indicated the protein's role in desmosome function, and suggested its involvement in human diseases associated with impairment of these junctions.

2
chapter

General introduction

2.1 Cell polarity

Cell polarity is a fundamental feature of almost all cells. It allows cell orientation in a variety of different ways. For example, cells of an epithelial sheet display both apico-basal and planar polarity, while migrating mesenchymal cells have a clear front-to-back organization. This property is essential in many aspects of cell developmental biology and involves different processes, such as cell migration, directional cell growth, asymmetric cell division, activation of immune response and vectorial transport of molecules in both unicellular and multicellular organisms (Drubin and Nelson, 1996; Nelson, 2003). Cell polarity relies on molecular polarity determinants that, localizing in specific domains of the plasma membrane, act to polarize and asymmetrically organize other cellular systems, such as plasma membrane proteins, organelles, and cytoskeletal components (Thompson, 2013).

One clear example of polarization is represented by epithelial cells, in which it is possible to observe an apico-basal polarity axis, characterized by asymmetric distribution of proteins between the junctional domain (cell-cell and cell-matrix) and the extra-junctional domain (the apical domain). Moreover, epithelial cells exhibit planar cell polarity: a secondary axis of polarity that is perpendicular to the apico-basal direction (Simons and Mlodzik, 2008; Song *et al*., 2010), and that is crucial for the appearance of highly organized cellular structures, such as primary cilia, as well as for the orientation of cell divisions.

2.2 Epithelial polarity

Development and maintenance of polarized epithelia are crucial for all multicellular organisms. Evolutionarily, epithelia are the most archetypal polarized tissues in metazoa, with ~60% of mammalian cell types being of epithelial or epithelial-derived origin (Bryant and Mostov, 2008). Epithelia are coherent sheets of cells that form a barrier against the outside world and the establishment and maintenance of their polarity are necessary steps for the normal physiological function of the organism. Epithelial sheets can be “one-cell thick” in the case of simple epithelia, such as part of the respiratory, urinary and digestive systems, or “many cells thick” for stratified epithelia, such as skin, tongue and esophagus. Polarized epithelial cells are present in all body cavities and occur in tissues that carry out specialized vectorial transport functions of absorption and secretion.

2.2.1 Planar cell polarity (PCP)

The presence of an axis of polarity within the plane of the epithelium appears clear observing an epithelial sheet inside its organ (see *Cartoon 1*). This axis gives rise to the planar cell polarity (PCP), also named "tissue polarity". Not just epithelia possess PCP, but also mesenchymal cells take advantage of PCP during migration and cell intercalation.

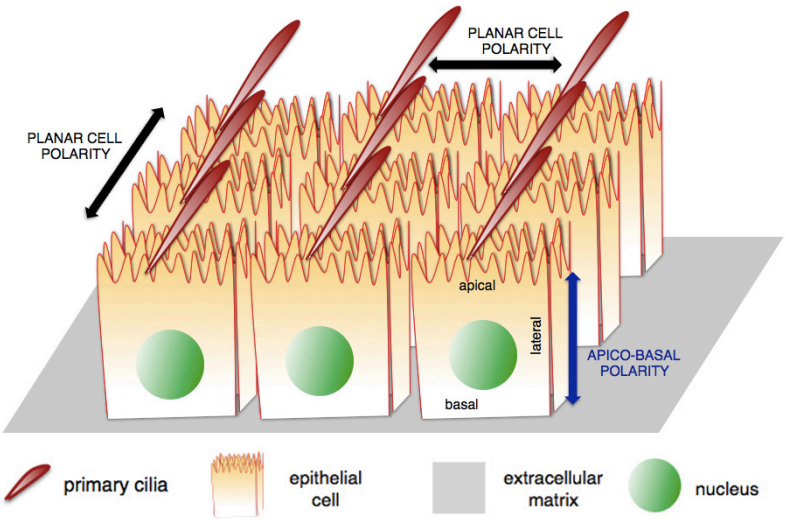

Cartoon 1. *Apico-basal polarity and planar cell polarity in epithelial sheet.*

The establishment of PCP is due to the coordination of two evolutionary conserved classes of factors: the Frizzled (Fz)/ Flamingo (Fmi) core genes and the Fat/Dachsous PCP system (Simons and Mlodzik, 2008). The signaling deriving from the interactions between these factors leads to PCP and allows the organization of a tissue in which hundreds of cells acquire the same orientation within the organ. PCP is a geometric property of cells that ensures oriented cellular behaviors along the plane of the cell sheet. Most tissues, indeed, require a three-dimensional organization both during the development and the adulthood to maintain proper functions. Clear examples of tissues that exhibit PCP are those performing a vectorial function in the plane of the

epithelium, such as the respiratory epithelium that transports mucus aborally thanks to coordinated ciliary beating, or the oviduct epithelium that transports the fertilized ovum to the uterus (Simons and Mlodzik, 2008). Deficiencies in PCP factors are linked to different damages such as defects of axis elongation, inner ear patterning, neural tube closure, directed ciliary beating, and left/right patterning (Wallingford, 2012).

PCP is tightly associated with cilia in vertebrates. These organelles possess a microtubules-based structure and are present on most eukaryotic cells. They can be classified in two subtypes: the motile and the immotile cilia, the latter are also named "primary cilia". Their microtubules core is the axoneme, that is formed by nine peripheral microtubule doublets. The motile cilia have also a central couple of microtubules and thus this configuration is referred to as "9+2" arrangement. The axoneme of primary cilia lacking this central pair is known as "9+0" arrangement (see *Cartoon 2*).

Cilia emerge from the basal body that is the microtubules-organizing center (MTOC), deriving from the mother centriole. This organelle is associated with transition fibers that regulate the traffic of proteins into the cilia compartment (Berbari *et al.*, 2010).

The importance of cilia in the organism is highlighted by the presence of numerous human syndromes, named "ciliophaties", in which cilia functions are disrupted. These disorders are associated with different clinical features including defects of the left-right body axis, abnormalities in neural tube closure, polydactyly, cystic kidney, liver and pancreatic diseases, anosmia, retinal degeneration, cognitive defects and obesity (Sharma *et al.*, 2008).

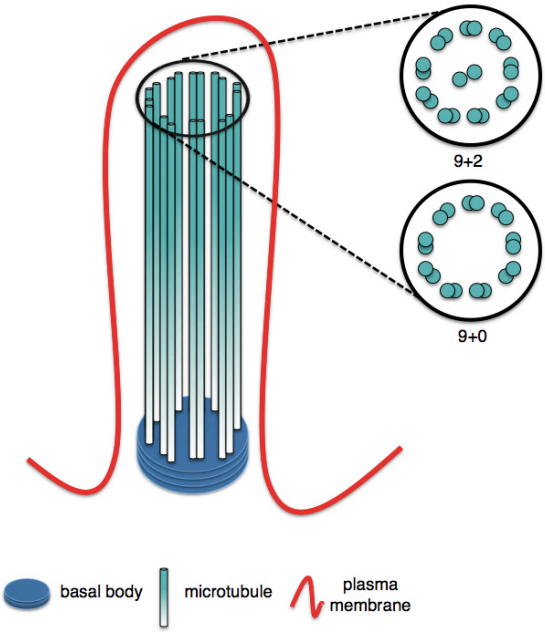

Cartoon 2. *Motile and immotile cilia structure.*

Motile cilia are found in large number at the apical surface of epithelial cells; for example, they are present in the epithelia of trachea and in the ependymal cells lining the brain ventricles. PCP effectors are involved in the control of ciliogenesis by coordinating apical actin assembly in cells with motile cilia (Oishi *et al.*, 2006), and, furthermore, PCP factors are the responsible for the directional motile cilia beating. Motile cilia, in fact, have to beat in a rhythmic manner to propel fluids in specific compartments, and the normal functions of many organs rely upon oriented fluid flow across epithelial surfaces (Wallingford, 2012).

The primary cilium is also an essential organelle because it is a sensory input involved in olfaction and photo-reception. Moreover, primary cilia are fundamental during development, since they act as mechanosensory in the establishment of left-right asymmetry and play critical roles in cell-cell communication by sensing extracellular signals (Berbari *et al*., 2010).

Another clear manifestation of PCP is the regular orientation of cell divisions, a phenotype that is observed in many tissues. The correct orientation of mitotic division has a crucial role in early embryo body plan specification, axis determination and cell fate diversity generation, as well as in the morphogenesis of tissues and organs (Segalen and Bellaïche, 2009). In response to cell-cell contacts and other cues, the Wnt/Frizzled (Wnt/Fz) and the Fat/Dachsous/Four-jointed (Fat/Ds/Fj) PCP pathways drive tissue morphogenesis by regulating the orientation of mitotic spindle and symmetric cell division within a field of cells.

2.2.2 Apico-basal polarity

The polarized organization of epithelia is the basis for the function of these cells, especially in vectorial transport of ions and solutes. The generation of polarized phenotype is a multistage process requiring extracellular cues and the reorganization of proteins in the cytoplasm and on the plasma membrane; once established, this phenotype is maintained by the segregation and retention of specific proteins and lipids in distinct apical and baso-lateral plasma membrane domains.

The apical surfaces of epithelial cells provide the luminal interface and are specialized in regulating the exchange of

materials with the external medium. The lateral surfaces, through specific cell-cell junctions, allow the connection with adjacent cells while the basal surfaces contact the underlying connective tissue (Nelson, 2003). The basal and lateral surfaces are fairly similar in composition and organization and are often referred together as the baso-lateral surface. The apical and baso-lateral surfaces, on the contrary, show very different compositions (Bryant and Mostov, 2008). The physical border between apical and lateral domains is provided by the tight junctions (TJs).

The polarization of cells into tissues requires the integration of different polarizing cues deriving from inter-dependent biological processes. First of all, cells must sense their environment and, in particular, their spatial relationship with neighboring cells. Cells can interact with the extracellular matrix (ECM) through various receptors, such as integrin, dystroglycan and proteoglycan molecules (Hynes, 1992; Clark and Brugge, 1995) and can communicate with other cells through adhesion molecules. The contacts with ECM are sufficient to initiate the segregation of membrane and cytoskeleton elements between contacting and non-contacting surfaces of cells (Vega Salas *et al.*, 1987). Moreover, when cells interact with neighboring cells, the site of the interaction is marked by adhesion receptors; here specialized cytoskeletal and signaling networks assemble and position other cytoskeletal complexes and protein-sorting compartments. Subsequently, protein sorting from these compartments to the cell surface and the retention at plasma membrane reinforce and maintain the structural and functional specializations of these membrane domains.

Three polarity complexes guide the polarization process: Crumbs, Par and Scribble (*Cartoon 3*). Interactions of these

complexes with each other modulate the formation of junctions and epithelial polarity. The Crumbs and Scribble complexes regulate the formation of the apical and lateral surfaces, respectively, whereas the Par complex modulates the balance between the two surfaces by multiple interactions (Pieczynski and Margolis, 2011).

The Par complex consists of Par3 (partitioning defective-3), Par6 (partitioning defective-6) and aPKC (atypical PKC); these genes were originally identified in searching for genes required for the establishment of anterior/posterior polarity in *C. elegans* zygotes. Subsequent studies showed that Par complex is also required for the initial stages of polarization in *Drosophila* embryos, in the *Drosophila* neuroblast asymmetric cell division, for the establishment of mammalian epithelial apico-basal polarity and in the axon-dendrite polarization of neurons (Chen and Zhang, 2013). Crumbs complex is restricted to the apical plasma membrane domain. The most relevant component, Crumbs (Crb), was first identified in *Drosophila* as an essential protein in the maintaining of apico-basal polarity and for the integrity of embryonic epithelia. The composition, localization and function of this complex is conserved from flies to humans. It is composed by: Crb, PALS1 (protein associated with LIN7 1) and PATJ (PALS1-associated tight junction protein). Crb is a transmembrane protein, whereas the other two components are cytoplasmatic scaffolding proteins (Bulgakova and Knust, 2009). The baso-lateral polarity complex is formed by SCRIB (scribble), Lgl (lethal giant larvae) and Dlg (discs large). The exact dynamic of the physical interactions between these proteins has not yet been clearly defined.

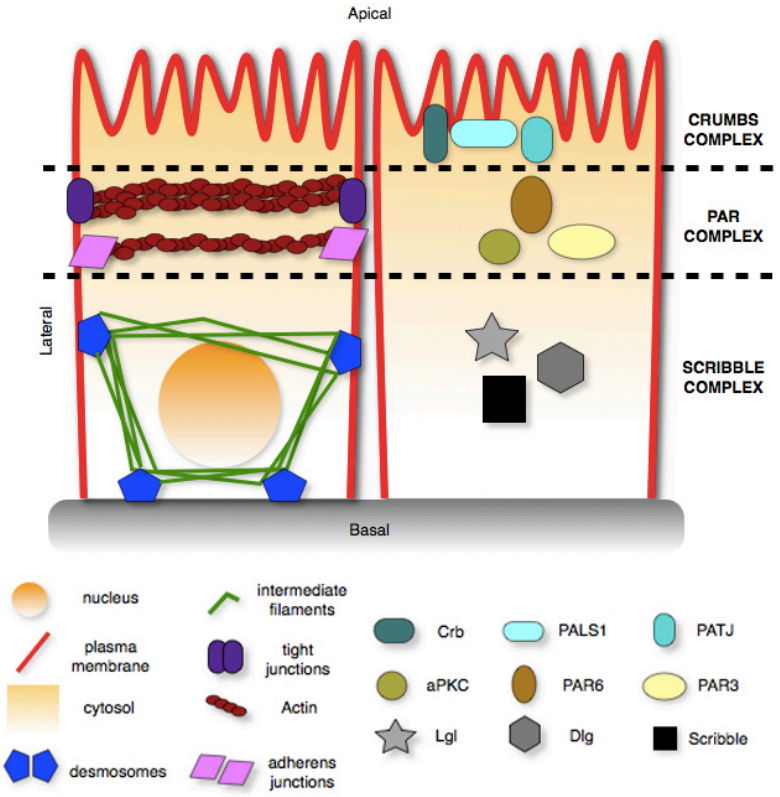

Cartoon 3. *Distribution of polarity complexes in epithelial cells.*

These polarity complexes, besides interacting with each others, have been found to interact with cytoskeleton-related proteins, such as 14.3.3 protein for Par complex, YMO1 (yurt/ mosaic eyes like 1) protein for Crumbs complex and myosin II for Scribble complex. These interactions modulate the dynamic of actin cytoskeleton, one of the fundamental events in controlling cell shape and polarity (Assémat *et al.*, 2008).

2.3 Cell junctions

Polarity complexes are intimately linked to cell junctions and regulate their localization and assembly within cells, contributing to tissue organization.

The formation of cell-cell junctions is the prerequisite for the establishment of adequate architecture within the epithelium and it is considered the primary epithelial polarity landmark: it depends on the formation of adhesions between neighboring cells and, in particular, on the distribution of TJs at the apex of cells (the opposite cellular pole compared to the cellular pole in contact with the ECM), in order to physically segregate the apical from the baso-lateral plasma membrane.

Cell junctions are classified into tight junctions (TJs), adherens junctions (AJs), and desmosomes. (see *Cartoon 4*); besides them a fourth type of cell-cell adhesion exists: the gap junctions, that are not mentioned in this thesis.

Polarity proteins regulate the proper establishment of cell junction complexes; for example, Par complex ensures the proper localization and maintenance of TJs at the apical side of the cells. Crumbs proteins regulate TJ formation through their reciprocal interaction with Par proteins. Scribble proteins interact with AJs to allow their proper segregation away from TJs (Bazzoun *et al.*, 2013).

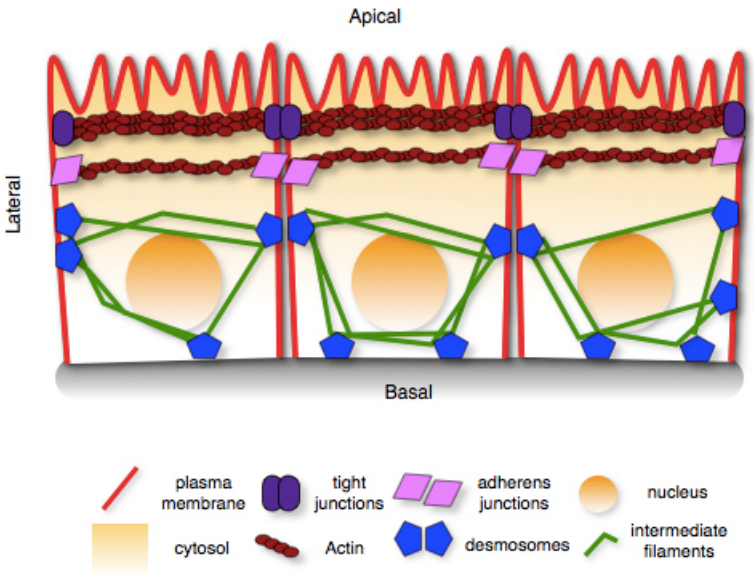

Cartoon 4. *Cell-cell junctions in epithelial cells.*

Cell-cell junctions consist of transmembrane proteins that, through their intracellular domains, interact with cytoplasmatic partners and cytoskeleton, and, through their extracellular domains, mediate the communication between neighboring cells in a homo- or heterotypic manner.

2.3.1 Tight junctions (TJs)

TJs are the most important contributors to epithelial polarity since, as mentioned before, they provide a physical border between apical and lateral domains, preventing the movement of

macromolecules from one plasma membrane domain to another. TJs are belt-like structures that restrict paracellular transport by forming selectively permeable barriers in the apical region of the cells (Bazzoun *et al.*, 2013).

As depicted in *Cartoon 5*, TJs consist of transmembrane components that bind directly to protein partners on adjacent cells and a large number of cytoplasmatic associated proteins (Shin *et al.*, 2006). Three main families of membrane spanning proteins are found in TJs: occludins, claudins and junctional adhesion molecules (JAMs).

Occludins contain four transmembrane domains, two extracellular loops and two intracellular domains (Feldman *et al.*, 2005). They directly interact with the proteins of the zonula

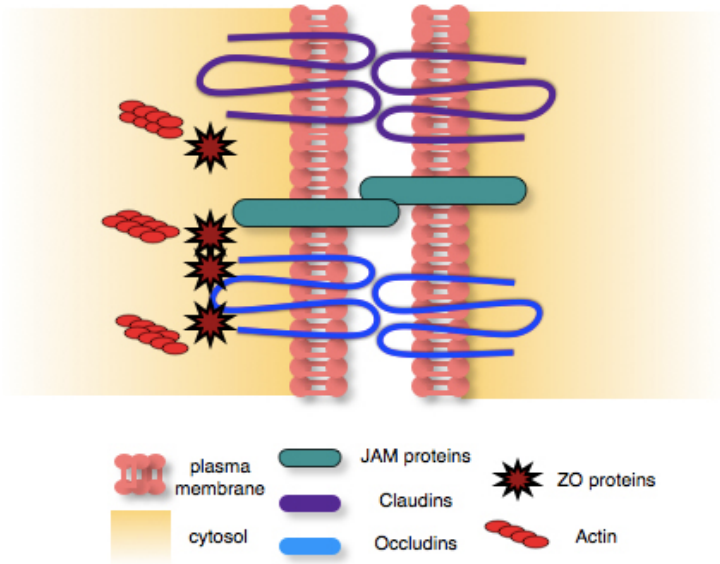

Cartoon 5. *Schematic representation of TJ proteins in epithelial cells.*

occludens family: ZO-1, ZO-2 and ZO-3 (Chiba *et al.*, 2008) and indirectly also with the actin cytoskeleton and JAMs, via ZO proteins.

Claudins (at least 23 family members are present in humans) contain four transmembrane domains, two extracellular loops and two intracellular domains. They interact with ZO family proteins, PALS1 and PATJ. Claudins are fundamental for the barrier function of TJs since, directly, regulate ion charge selectivity, permeability dependence on ion concentration and competition for movement of molecules; moreover they are also known to recruit occludins to tight junctions (Tsukita and Furuse, 2002; Bazzoun *et al.*, 2013).

JAMs are members of the immunoglobulin superfamily of proteins. There are four members: JAM-A, JAM-B, JAM-C and JAM4/JAML (Mandell and Parkos, 2005). JAM-A and JAM-C localize to TJs, whereas JAM-B is distributed along the entire lateral membrane (Aurrand-Lions *et al.*, 2001). These TJ components are characterized by the presence of one single transmembrane domain, en extracellular sequence containing two Ig-like motifs and a cytoplasmatic tail. Except for JAML, all JAM proteins have a PDZ (postsynaptic density 95/disc-large/zona occludens)-binding motif at their C-termini that appears to be involved in the interaction with TJ scaffolding proteins, including ZO-1, calcium/calmodulin-dependent serine protein kinase (CASK/LIN2), membrane-associated guanylate kinase with inverted domain structure 1 (MAGI-1), multi-PDZ domain protein 1 (MUPP1), and partitioning defective 3 (Par3) (Ebnet *et al.*, 2001, Itoh *et al.*, 2001).

Zonula occludens (ZO) proteins belong to the membrane-associated guanylate kinase (MAGUK) family; this group of proteins comprises ZO-1, ZO-2 and ZO-3. ZO-1 was the first TJ protein described and ZO-2 and -3 were subsequently identified by co-immunoprecipitation studies as binding partners of ZO-1 (reviewed in Gonzalez-Mariscal *et al*., 2000; Runkle and Mu, 2013). The principal role of ZO proteins is to link the membrane TJ proteins to the actin cytoskeleton. Collectively, MAGUKs contain a core structure consisting of one or more PDZ domains, a Src homology 3 (SH3) domain, and a guanylate kinase (GUK) domain (reviewed in Gonzalez-Mariscal *et al*., 2000). ZO-1 localizes to the TJs of epithelial and endothelial cells. Besides the MAGUK core structure of PDZ, SH3, and GUK domains, ZO-1 also contains two nuclear localization signals that allow its localization to the nucleus during the maturation of the epithelial monolayer. In the nucleus ZO-1 acts as key regulator of proliferation by interacting with the Y-box transcription factor ZONAB (ZO-1-associated nucleic acid-binding protein) (Balda and Matter, 2000; Balda *et al*., 2003). All ZO proteins interact directly with the C-terminal domain of occludins through their first PDZ domain (reviewed in Gonzalez-Mariscal *et al*., 2000; Feldman *et al*., 2005).

Besides these principal components of TJ complexes, other macromolecules allow the formation of TJs and, thus, the maintenance of epithelial cell polarity. Indeed, since the discovery of ZO-1, as the first protein at TJs and its molecular cloning (Stevenson *et al*., 1986; Itoh *et al*., 1993), the number of proteins that are localized at TJs has steadily increased. These proteins comprise scaffolding and adaptor proteins, regulatory proteins like small GTPases, G-proteins, kinases and phosphatases, as well

as transcription factors or factors regulating RNA processing (reviewed in Shin *et al*., 2006).

2.3.2 Adherens junctions (AJs)

AJs are multiprotein complexes that play essential roles in epithelial cell differentiation and apico-basal polarity. They also contribute to the control of cell polarity in other cell types and, in fact, they promote neuronal morphogenesis, growth cone guidance and directed migration during embryonic development (reviewed in Etienne-Manneville, 2011). Besides polarity, AJs also promote cell-cell communication and transfer signals that mediate contact inhibition of cell growth, increase resistance to apoptosis, and regulate cell shape. In epithelial cells AJs can be detected at the apical region of the intercellular cleft and appear as a zipper-like seal between adjacent cells (Rudini and Dejana, 2008).

The core of the AJs includes interactions among transmembrane glycoproteins of the classical cadherin superfamily and the catenin family members (reviewed in Hartsock and Nelson, 2007). Together, these proteins control the formation, maintenance and function of adherens junctions (see *Cartoon 6*).

Classical cadherins are calcium-dependent adhesion receptors belonging to a superfamily of approximately 80 members. Since these cadherins show distinct tissue distribution patterns, they were originally named from the tissue in which they were predominantly expressed: E-cadherin in epithelia, N-cadherin in the nervous system and VE-cadherin in the vascular

endothelium (Etienne-Manneville, 2011). Classical cadherins are composed of an extracellular domain formed of five cadherin repeats (EC), a single transmembrane domain and a highly conserved cytoplasmic tail. Through the EC domains neighboring cadherins form homophilic cis- and trans- interactions (Halbleib and Nelson, 2006). With their cytoplasmic tail, cadherins form a multiprotein complex with β-catenin, α-catenin, γ-catenin (plakoglobin) and p120-catenin (p120ctn), members of the armadillo repeat domain containing family of proteins. β-catenin and p120ctn, when released from junctions and free in the cytosol, may translocate to the nucleus where they regulate cell transcription.

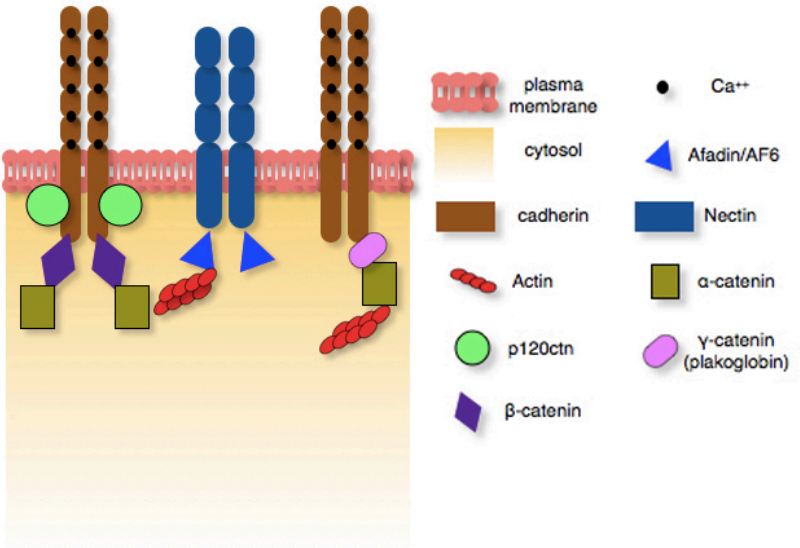

Cartoon 6. *Schematic representation of adherens junction components.*

Nectins are another integral molecules of AJs. The four members of the nectin family are calcium-independent immunoglobulin-like proteins. Their cytoplasmic domain associates with the actin-binding protein AF6/afadin that, interacting with α-catenin, provide a physical connection between the cadherin and the nectin complexes (reviewed in Etienne-Manneville, 2011).

The catenin family consists of p120-catenin, β-catenin, γ-catenin and α-catenin. These catenins interact with a number of cytoplasmic proteins that can affect the dynamics and strength of cadherin-mediated adhesion and mediate a wide variety of intracellular signaling pathways. For example, association of p120-catenin with E-cadherin has been proposed to stabilize E-cadherin at the plasma membrane during the formation of cell-cell contact; moreover, p120ctn also functions as a regulator of cell motility through the actin cytoskeleton by interacting with Rho family GTPases (Noren *et al*., 2000). β-catenin, which was originally identified in *Drosophila*, as the segment polarity protein armadillo (McCrea *et al*., 1991), contains 13 repeats of the characteristic armadillo domain of ~42 amino acids that form triple α-helix (Huber *et al*., 1997) and binds the C-terminal cytoplasmic domain of E-cadherin in a phospho-regulated manner. α-catenin is the link between the cadherin/β-catenin complex and the actin cytoskeleton.

2.3.3 Desmosomes

Desmosomes are cell-cell junctions widely distributed along the lateral membranes of epithelial cells. They mechanically integrate

adjacent cells by coupling adhesive interactions mediated by desmosomal cadherins to intermediate filament cytoskeleton. The desmosome was first observed by Giulio Bizzozero (1846-1901) in the spinous layer of epidermis. Bizzozero's observations of these small dense nodules, subsequently named "nodes of Bizzozero," led him to the hypothesis that these structures were adhesive cell-cell contact points. The term desmosome was later coined by Josef Schaffer in 1920 and is derived from the Greek words "desmo", meaning bond, and "soma", meaning body (Wells, 2005; Calkins and Setzer, 2007).

Among the intercellular junctions, desmosomes are those more specialized in providing strong adhesion that is prominent in tissues routinely subjected to considerable physical stress, such as heart, skin, bladder and gastro-intestinal tract. When assembled, these junctions play essential roles in tissue morphogenesis and maintenance: their disruption is a hallmark of many blistering and cancer diseases (McGrath *et al*., 1997; McKoy *et al*., 2000).

Desmosomes occur predominantly in epithelial tissues providing dynamic barriers between body compartments. An epithelial sheet has to be confluent to ensure barrier function of the epithelium. If confluence is damaged in healthy individual, the epithelium repairs itself to restore the barrier as rapidly as possible. Desmosomes are the mayor contributors to this process (Garrod, 2010)

At the ultrastructural level, the desmosome appears as a dense cytoplasmatic plaque, approximately 0,2-0,5 μm in diameter that assembles into a mirror image arrangement at cell-cell interface (Kowalczyk and Green, 2013). As shown in *Cartoon 7*, this plaque consists of two electron-dense regions: the outer

dense plaque (ODP) that is located closer to the plasma membrane, and the inner dense plaque (IDP), localized further away from the membrane. The ODP is composed of two major armadillo family members, plakoglobin (PG) and plakophilin (PKP), which mediate the binding of cadherin cytoplasmic tails to the N-terminus of desmoplakin (DSP), which itself constitutes most of the IDP and interacts with the intermediate filaments (IFs) (Al-Amoudi *et al*., 2011).

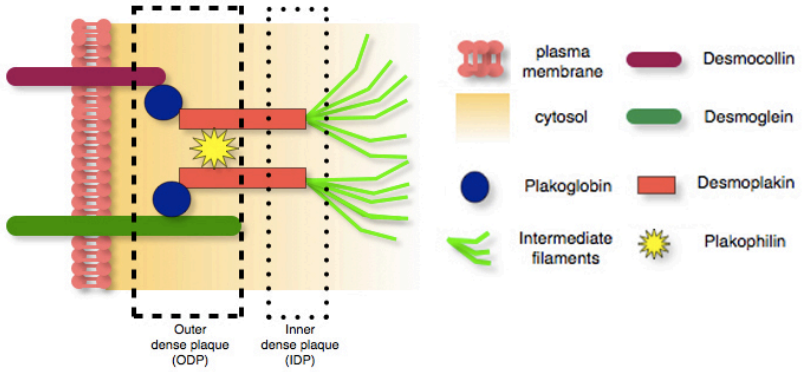

Cartoon 7. *Schematic representation of desmosome components.*

Desmosomal cadherins are the desmosome counterparts of the classic cadherins present in AJs. They comprise two subtypes of proteins: desmogleins (DSGs) and desmocollins (DSCs), both of which are single-pass transmembrane glycoproteins that mediate adhesion in a calcium-dependent manner through their extracellular domains and interact with desmosomal plaque proteins with their cytoplasmatic tails (Saito *et al*., 2012). Cadherin-based adhesive intercellular junctions drive tissue morphogenesis during development and are essential

for the maintenance of adult tissue architecture in virtually all complex tissues (Gumbiner, 2005; Stepniak *et al*., 2009).

In humans, there are four genes encoding DSG (DSG1-4) and three genes encoding DSC (DSC1-3). DSG2 and DSC2 are predominantly expressed in heart and simple epithelia, whereas the other isoforms are expressed in complex tissues, such as the epidermis and the oral cavity (Delva *et al*., 2009). Both cadherins are composed of five extracellular cadherin repeats, each of which form Ig-like globular domains (of approximately 110 amino acids), separated by calcium binding sites (see *Cartoon 8*). The cytoplasmic domains of DSG and DSC consist of an intracellular anchor (IA) and a cadherin-like sequence (ICS). DSGs have additional sequences with unknown functions, including a prolin-rich linker (IPL), a repeat unit domain (RUD) and a desmoglein terminal domain (DTD). Each DSC RNA can be spliced to yield an "a" and a "b" isoform; in the "b" splice variant the ICS domain is truncated and terminates with an additional 11 residues in DSC1 and 2, and eight amino acids in DSC3, not found in the "a" isoform (Getsios *et al*., 2004a; Getsios *et al*., 2004b; Kowalczyk and Green, 2013).

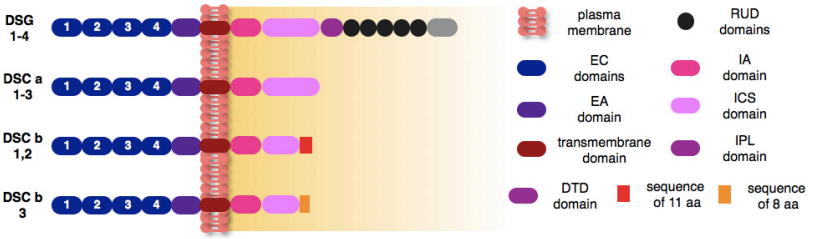

Cartoon 8. *Structure of desmosomal cadherins.*

The desmosomal cadherins show complex developmental and differentiation pattern of expression, and their regulation is important during epithelial differentiation and homeostasis (Holthofer *et al*., 2007).

Armadillo (Arm) family of proteins are cadherin binding partners that play important roles in cell signaling and tissue integrity (*Cartoon 9*). Desmosomes contain two components of this family of proteins: plakophilins (PKP) and plakoglobin (PG). Similarly to their AJ counterparts (β-catenin and p120 catenin), PG and PKPs are also present in the nucleus, where they indirectly regulate cell growth, survival and differentiation through their influence on β-catenin signaling, and directly through the activation of transcriptional pathways (Yin and Green, 2004; Hatzfeld, 2007; Holthofer *et al*., 2007; Keil *et al*., 2007).

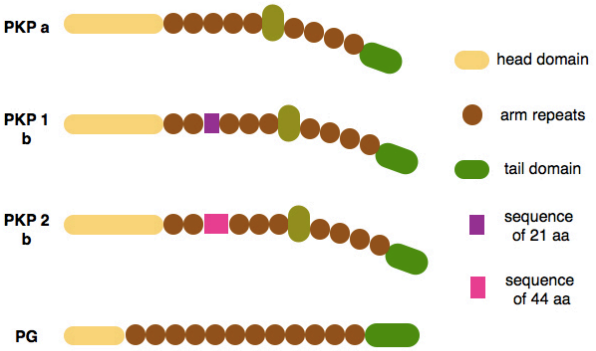

Cartoon 9. *Structure of Armadillo desmosomal proteins.*

Armadillo was originally discovered in *Drosophila*, where acts as a regulator of segment polarity; later it has been found

that Arm was the homolog of the vertebrate junctional and signaling proteins β-catenin and plakoglobin (Peifer *et al*., 1992). The armadillo proteins are characterized by the presence of a central domain, containing repeating units of a 42 amino acid sequence homology domain (arm repeats) (Peifer *et al*., 1992). In the desmosome PG and PKP are fundamental in tethering the plaque to IFs and, moreover, they play critical roles in signal transduction pathways: they are indeed found in both soluble and membrane-associated compartments with a regulated equilibrium between these two forms. (Bass-Zubek *et al*., 2009; Pieperhoff *et al*., 2010; Clevers and Nusse, 2012).

Plakoglobin is the founding member of the armadillo family and it is also known as junction plakoglobin (JUP) and γ-catenin. It binds to the ICS domain of desmogleins and desmocollins and forms a bridge between these cadherins and the intermediate filaments binding protein desmoplakin. Structurally, the protein contains 12-arm repeats flanked by distinct amino- and carboxy-terminal domains (Peifer *et al*., 1992; Huber *et al*., 1997; Garrod and Chidgey, 2008).

Plakophilins are members of the p120-catenin subfamily and are characterized by the presence of nine arm-repeats with an insert between repeats 5 and 6 that introduces a bend into the overall structure; in humans there are three plakophilins (PKP1-3), which exhibit different patterns of expression in the organism. Both PKP1 and 2 exist as two isoforms: the shorter “a” and the longer “b” forms, differing in the addition of 21 amino acids in arm-repeat three (PKP1) and the addition of 44 amino acids in arm-repeat four (PKP2) (Mertens *et al*., 1996; Schmidt *et al*., 1997).

Desmoplakin (DSP) is the most important member of the plakin family: a group of proteins that regulate the interaction between the intermediate filament cytoskeleton and the desmosomal plaque (see *Cartoon 10*). Besides DSP this family of proteins includes plectin, envoplakin and periplakin, all characterized by the presence of plakin-repat domains, responsible for the interaction with cytoskeleton elements (Sonnenberg and Liem, 2007).

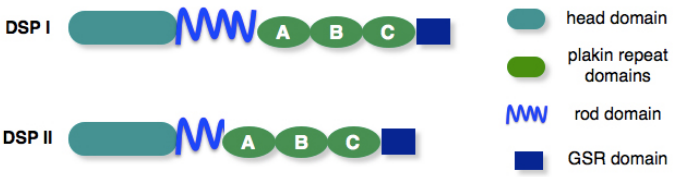

Cartoon 10. *Desmoplakins structure.*

DSP contains globular amino- and carboxy-termini, connected by a central, α-helical coiled-coil rod domain. The amino-terminal head domain provides binding sites for PG and PKP, and thereby targets the protein to the armadillo complex at the desmosome (Delva *et al.*, 2009). The carboxy-terminal domain contains three plakin-repeat domains, called A, B and C subdomains; between the B and C subdomains there is a specialized linker sequence that is conserved in many plakin-family members (Leung *et al.*, 2002). These plakin repeats show a globular structure that accommodates a groove lined with basic residues, and which has been proposed to contribute to intermediate filament binding (Nikolic *et al.*, 1996; Fontao *et al.*, 2003). Moreover, the C-terminal tail of desmoplakin corresponds

to a glycine-serine-arginine rich domain (GSR), fundamental in regulating interaction of DSP with IFs (Choi *et al*., 2002; Yin and Green, 2004). DSP can exist as two isoforms (I and II), with DSPII missing approximately two-thirds of the central rod domain; both the DSPs are broadly expressed in epithelia, but DSPII is not present in the heart and its expression is lower in simple epithelia.

Desmosome regulation

Although desmosomes are very strong and resistant spot-welds between adjacent cells, they posses a dynamic nature consisting of a constant remodeling of the plaque. This is a post-translational regulation that takes into account the calcium concentration, the kinase/phosphatase activity, the proteolytic processing and a strict cross-talk with AJs. *De novo* assembly of cell-cell junctions depends on calcium concentration and occurs from distinct cytoplasmic pools of cadherins and plaque components.

Desmosomal cadherins and PG co-fractionate and are recruited to cell surface thanks to the participation of microtubule cytoskeleton and kinesin motor proteins (Green *et al.,* 2010; Nekrasova *et al*., 2011). Several lines of evidence suggest that DSCs may initiate desmosome assembly while DSGs are transported to nucleation sites in a secondary stage (Burdett and Sullivan, 2002). It has been reported that DSC and DSG localize in cholesterol-rich raft domains and assembly and compartmentalize into functional junctions in association with lipids (reviewed in Nekrasova and Green, 2013).

In response to cell-cell contacts DSP forms non-membrane bound particles in the cytoplasm in strict association

with IFs; these desmosomal precursors then translocate to nascent desmosomes to reinforce the plaque (Godsel, *et al.*, 2005). A portion of the cellular pool of PKP2 is associated with these DSP precursors and plays an essential role in regulating both the association of DSP with IFs and its dynamic behavior recruiting protein kinase C α (PKCα) in proximity to DSP; this action results in DSP phosphorylation and conversion to an assembly-competent state (Bass-Zubek *et al.*, 2008). PKP2 recruits itself to cell-cell interfaces through its C-terminal domain, and DSP through its N-terminal domain (Holthofer *et al.*, 2007).

As mentioned before, the calcium-dependance of desmosomal adhesions has been largely used to manipulate desmosome formation: when cells are grown in low calcium medium (~ 0,05 mM Ca^{++}) desmosomal components are recruited to cell adhesions, but are rapidly degraded due to the inability of desmosomal cadherins to interact with each others without calcium. When calcium is added at the adequate concentration (~ 1,2 mM Ca^{++}), junction assembly is triggered and desmosomal proteins are then stabilized (Kowalczyk and Green, 2013).

Desmosomal hyper-adhesion

The prominent feature of desmosomes is to permit the cells to resist to mechanical stresses, thanks to their ability to connect adjacent cells providing very strong adhesion. This characteristic is underlined by the capability of desmosomes to acquire a calcium-independent behavior in epithelial sheets that have matured for several days. This condition, typical and exclusive of desmosomes, among the cell junctions, is called hyper-adhesion

(Garrod and Kimura, 2008). In this situation, desmosome components assume stable adhesive properties and represent the only spot-welds persisting between adjacent cells even with calcium deprivation: this hyper-adhesive and calcium-independent behavior, indeed, has been never observed for the other adhesions such as TJs and AJs. In hyper-adhesive state cells adopt a stellate conformation, since they remain merely attached at points where desmosomes accumulate during the retraction process (Wallis *et al*., 2000). The confluence is a prerequisite to develop hyper-adhesion: it has been observed that if a confluent sheet is scratch wounded, the cells reacquire calcium dependence in proximity to the wound edge (Wallis *et al*., 2000). This calcium-independent property of desmosomes is a constant feature *in vivo*: desmosomes become hyper-adhesive by E14 and maintain this state in adult tissues (reviewed in Nekrasova and Green, 2013); in several papers it has been observed that desmosomes in tissues such as epidermis, trachea, esophagus, tongue, liver and cardiac muscle are hyper-adhesive and, unlike AJs, they remain stable even after 6 hours-treatment with the calcium-chelanting agent ethylene glycol tetra acetic acid [EGTA] (Garrod *et al*., 2005; Wallis *et al*., 2000). The mechanism underlying the acquisition of hyper-adhesion by desmosomes is still unclear, but it has been hypothesized that this state may depend on conformational changes in cadherin ectodomains (Garrod and Kimura, 2008).

Desmosomes and diseases

Cell-cell connectivity is an absolute requirement for the correct functioning of cells; the importance of cell junctions is demonstrated by their involvement in a wide-ranging variety of diseases, of genetic, auto-immune, cancerous and infectious etiology. Among all the adhesions, the precise role of desmosomes in maintaining adhesive strength between neighboring cells is supported by human diseases and mouse models in which desmosomal constituents are affected by mutations, bacterial toxins and auto-antibodies. All these mutations lead to diseases characterized by epithelial blistering and fragility, in particular, in the presence of mechanical stress. (Yin and Green, 2004). Patients carrying mutations in desmosomal proteins often exhibit defects in hair development (patients with mutations in DSP, PG or DSG4) and, more important, mutations in almost all the desmosomal proteins can cause cardiomyopathies.

Below are listed some examples of pathologies in which desmosomal proteins play a pivotal role.

Pemphigus

Pemphigus vulgaris (PV) is characterized by loss of keratinocyte cell-cell adhesions (acantholysis) and blister formation, in the mucosal membranes caused by auto-antibodies directed against DSG3, and this phenotype is evident also in DSG3 knock out mice (Koch *et al.*, 1997). The superficial layer of the epidermis is affected in a similar way in pemphigus foliaceus

(PF), which is determined by antibodies anti-DSG1 that inactivate the protein (Amagai, 1999). The different patterns of disease in PV and PF reflect the distribution and expression levels of DSG1 and DSG3, which differ significantly between the epidermis and the mucosa (Shirakata *et al*., 1998).

Paraneoplastic pemphigus (PNP) is a muco-cutaneous blistering disease associated with malignant neoplasia. The pathology is characterized by the presence of serum antibodies which recognize desmosomal proteins including DSPI, DSPII, DSG3, the desmosome-associate proteins envoplakin and periplakin, and the hemidesmosomal component BPAG1 (reviewed in Chidgey, 2002).

Bullous impetigo

The infectious pathology bullous impetigo, and its generalized form staphylococcal scalded skin syndrome (SSSS), are both characterized by epidermal blister formation that share analogies with PF; this is a result of the fact that the DSG1 is affected in both cases. In bullous impetigo DSG1 is the target of exfoliative toxins (ETs) and toxins produced by some strains of pathogenic Staphylococcus aureus bacteria (reviewed in Brooke *et al*., 2012).

Palmoplantar keratoderma

Palmoplantar keratodermas (PPKs) are a heterogeneous group of genetic skin diseases primarily affecting the palm and

sole. The striated form is characterized by longitudinal hyperkeratotic lesions on the palms and localized keratin masses on the soles. Affected skin loses cell-cell contacts and shows disruption of normal desmosome-IF interactions; moreover, desmosomes are small and of abnormal appearance. The genetic causes of the disease are autosomal dominant mutations in the gene encoding DSG1, in particular occurring in the extracellular domain of the protein or in DSP gene, resulting in null allele and haploinsufficiency (reviewed in Chidgey, 2002).

Hailey-Hailey and Darier's diseases

Darier's disease (also known as dyskeratosis follicularis) is an autosomal dominant skin condition characterized by keratotic papules, which form into larger skin lesions. The molecular cause of the pathology is the loss-of-function mutation in ATP2A2, the gene encoding for SERCA2, the calcium pump that allows the translocation of calcium from the cytosol to the endoplasmic reticulum (ER) lumen. The most important feature of this disease is the acantholysis of keratinocytes, a phenomenon due to abnormalities in desmosome formation. The impairment of the pump causes apoptosis of keratinocytes for ER-stress response on one hand, and reduces trafficking of DSP to desmosomes resulting in skin fragility, on the other hand (reviewed in Brooke *et al.*, 2012).

A similar clinical condition is found in Hailey-Hailey-affected patients, in which the typical phenotype is characterized by persistent blistering and erosion of the skin. This disorder is inherited in an autosomal dominant fashion, and it is caused by

mutations in ATP2C1, another gene encoding for an ER calcium pump. Also in this case the desmosome ultrastructure is disrupted in lesional skin, demonstrating, in this way, the importance of intracellular calcium homeostasis for normal epidermal function (reviewed in Chidgey, 2002).

Lethal acantholytic epidermolysis bullosa (LAEB)

LAEB is a skin disorder characterized by extensive epidermal dislodgment with structurally normal desmosomes that, however, lack intermediate filament insertion; the symptoms comprise epidermal erosion and massive fluid loss.

In these patients heterozygous nonsense mutations in DSP leading to truncation of almost the complete DSP C-terminus have been identified. Recently, also an out-of-frame DSP mutation has been found in the DSP rod domain (Bolling *et al.*, 2010).

Arrhythmogenic right ventricular cardiomiopathy (ARVC)

One important clinical condition arising from mutations in desmosomal proteins is the arrhythmogenic right ventricular cardiomyopathy (ARVC), an inherited disorder that leads to progressive heart muscle failure. It is characterized by arrhythmias, sudden cardiac death, and the typical phenotype is the replacement of the right ventricular free wall of myocardium with fibro-fatty tissue. The degenerative process may be diffuse o

segmental and in the 50% of the cases there is also an involvement of the left ventricle (Bauce *et al.*, 2011).

Clinical manifestations of the disease occur between the second and the fourth decade of life and include functional abnormalities and arrhythmias of the right ventricle, electrocardiographic depolarization/repolarization changes and sudden cardiac death. The histological hallmarks of the disease are myocytes loss, myocardium inflammation, fibrosis and adiposis (Peters *et al.*, 2012). ARVC is characterized by different pathological patterns: there is a "silent" phenotype in which asymptomatic victims of sudden death show cardiomyopathic abnormalities in the right ventricle; in the "overt" disease there are segmental or global right ventricular structural changes, histological evidence of left ventricular involvement and symptomatic ventricular arrhythmias; in the "end-stage" pattern a bi-ventricular cardiomyopathy, mimicking dilated cardiomyopathy, leads to a progressive heart failure and may require orthotopic cardiac transplantation (Rampazzo, 2006; Bauce *et al.*, 2011; Peters *et al.*, 2012; Campuzano *et al.*, 2012).

The prevalence of ARVC is estimated to be between 1: 2000 and 1: 5000 and it is three times more common in women (Peters *et al.*, 2012); in Italy it was reported that between 12,5 and 25% of sudden cardiac deaths in young under the age of 35 years were caused by ARVC (Rampazzo, 2006). The disease is heterogeneous with intra-interfamilial variability and both benign and malignant forms exist.

In the heart, proper mechanical and electrical coupling of cardiomyocytes is crucial for the normal propagation of the electric impulse throughout the myocardium. Junctional complexes localized at the termini of cardiomyocytes are

responsible for the integration of structural informations and for cell-cell communications. These connections between cardiomyocytes are called intercalated discs (ICDs) and consist of three main junctional complexes: the AJs, the gap junctions and the desmosomes. ARVC is considered a disease of the desmosome, as defects in cardiac desmosomes might impair cell-cell contacts and thus diminish the response of myocardium to mechanical stresses. Since desmosomal proteins are particularly expressed in both myocardium and skin, ARVC is occasionally associated with cutaneous manifestations like palmoplantar keratoderma and woolly hair (Rasmussen *et al.*, 2013).

ARVC can be both an autosomal dominant and recessive hereditable condition, characterized by incomplete penetrance and variable expressivity of the phenotype. Fifty percent of ARVC patients have a mutations in one of the genes encoding desmosome proteins expressed in the heart (12 chromosome loci discovered so far); besides these proteins, an increasing number of non-desmosomal proteins seem to be involved in the development of the disease (lamin A/C, desmin, titin and striatin) (Pilichou *et al.*, 2011; Rickelt and Pieperhoff, 2012). Co-inheritance of multiple desmosomal genes sequence variations has been reported to be associated with a more severe cardiac phenotype.

Non-syndromic ARVC (without cutaneous abnormalities) has been associated with mutations in DSP and PG, which appear to be inherited in a dominant manner (Bolling and Jonkman, 2009; Asimaki *et al.*, 2007), and in DSG2 and DSC2, both inherited in autosomal or recessive manner (Simpson *et al.*, 2009; reviewed in Brooke *et al.*, 2012). The majority of ARVC patients, however, carry dominant or recessive mutations for

PKP2, mostly found in its carboxy-terminal domain. Mutations in PKP1 result in skin fragility and severe ectodermal dysplasia, whereas no disease-causing mutations have been reported PKP3 (reviewed in Brooke *et al.*, 2012).

Heart and skin abnormalities are also present in the Naxos disease, a human autosomal recessive pathology, characterized by ARVC, palmoplantar keratoderma and woolly hair. The genetic cause is a homozygous deletion in the PG gene that results in a truncation in the C-terminal end of the protein (reviewed in Chidgey, 2002). Carvajal syndrome is an autosomal recessive disease caused by mutation in DSP gene. It has been described as cardio-cutaneous abnormalities and predominantly left-sided cardiomyopathy (Pilichou *et al.*, 2011).

Desmosomes and cancer

The role of desmosomal proteins in human cancer development and progression is not yet clear, since contradictory results have been produced in this field. According to the tumor type, desmosome components have been found either up-regulated or down-regulated, increasing the confusion about it.

For example, several studies have revealed an increased expression of DSG2, DSG3 and PKP3, compared to normal tissue, in some cancers of the skin, head and neck, prostate and lung, with a correlation between their expression and tumor progression. On the contrary, a loss or a reduction of different desmosomal markers (DSP, PG, DSG1-3, DSC2,3, and PKP1-3) has been observed in various human epithelial tumors, such as skin, head and neck, gastric, colorectal, bladder, breast, prostate,

cervical and endometrial cancers. Moreover, in some studies no obvious changes in the level of desmosomal proteins have been observed during cancer progression (reviewed in Brooke *et al.*, 2012).

Also in *in vitro* models conflicting results have been obtained: in some cases, the overexpression of desmosomal proteins seems to advantage tumor progression through the promotion of proliferation and invasiveness, and the inhibition of apoptosis; conversely, other papers indicate that overexpressed desmosomal components suppress tumor behavior (Dusek and Attardi, 2011).

It is clear, however, that loss of desmosomal adhesion is a prerequisite for epithelial-mesenchymal transition, and so they are implicated in the conversion from early stage tumor to invasive cancer. Desmosomal components can contribute to tumor progression altering signaling transduction pathways, such as the Wnt/β-catenin pathway. This intervention has been hypothesized for the desmosomal armadillo protein PG (reviewed in Chidgey and Dawson, 2007).

PG, as mentioned before, is a desmosomal marker that can localize also at the AJs where it is closely associated with β-catenin and so can interact with many components of the Wnt/β-catenin pathway; this cascade of signals can develop in a canonical or a non-canonical pathway. In the first case, in the absence of the Wnt signal, β-catenin is phosphorylated by glycogen synthase kinase 3b (GSK3b) and then is targeted for proteosomal degradation. When, on the contrary, Wnt interacts with its receptors, the phosphorylation is blocked and β-catenin accumulates in the cytoplasm and enters in the nucleus, where it converts DNA binding proteins of the T-cell factor (Tcf)/ lymphoid

enhancer factor (Lef) family into transcriptional activators. In some instances, seems that the activation of this signaling is associated with cancer progression. It is controversial if PG has a positive or negative role in the Wnt/β-catenin signaling. It can block β-catenin phosphorylation permitting its accumulation in the cytoplasm and thus its translocation in the nucleus, but it has been observed that it can be a negative regulator of this cascade. PG, in fact, may interfere with gene expression by competing with β-catenin for binding to Tcf/Lef thus suppressing β-catenin/Tcf/Lef target gene transcription (reviewed in Chidgey and Dawson, 2007; Swope *et al*., 2013). In support of this idea, Garcia-Gras and colleagues have demonstrated that the translocation of PG in the nucleus of human cardiomyocytes (due to siRNA downregulation of DSP), leads to the suppression of Wnt/β-catenin signaling; this, in turn, causes a transcriptional switch from myogenesis to adipogenesis and accumulation of fat droplets in the cells (Garcia-Gras *et al*., 2006).

2.4 Polarity and cytoskeleton

Epithelial cell junctions contribute to cell integrity and provide platforms to orchestrate cell shape changes. To perform these functions, cell-cell adhesions have to intimately collaborate with the cytoskeleton. It consists of three major groups of filamentous structures: microtubules, actin filaments, and intermediate filaments (IFs). An asymmetric distribution of cytoskeletal elements is necessary in order to organize cells into structures such as tissues and organs.

Actin dynamics are fundamental in promoting cell migration, structural maintenance, cell division, endocytosis, vesicle trafficking and for the establishment of intercellular apical adhesions. Microtubules act mainly during cell division accurately positioning the spindles; this phenomenon results essential for asymmetric mitotic and meiotic cell divisions that are crucial for animal development and oocyte maturation, respectively (McNally, 2013). Microtubules also sustain vectorial movements through molecular motors and thus carry vesicles, cytosolic components, or other cytoskeletal structures to either the apical or baso-lateral domains of the plasma membrane. IFs, although often considered barely mechanical components of the cell, fundamental in providing strong resistance to deformation stress, are also dynamic, mobile, and, in the case of simple epithelia, also polarized components of the cytoskeleton acting as potent scaffolds, capable of compartmentalize proteins within the cytoplasm (Oriolo *et al.*, 2007).

2.4.1 Actin cytoskeleton

In polarized epithelial cells, cell-cell contacts mature to form apical junctions (TJs and AJs). They are physically supported by actin cytoskeleton that forms a cortical belt in the most apical end of the lateral membrane domain (*Cartoon 11*). Here, cortical sub-membrane actin makes up also the core of the apical microvilli, but a uniform thin layer of F-actin also decorates the inner surface of the baso-lateral membrane (Hofer *et al.*, 1998); moreover, at the basal domain of the cell, actin filaments form stress fibers and support focal adhesions. While actin monomers are not polarized,

the organization of actin microfilaments, on the other hand, shows an evident polarization.

Actin exists as either monomeric globular G-actin or polymeric filamentous F-actin. Actin filaments are double helical polymers of globular subunits. The filament grows at the barbed-end while is less active at the pointed-ends. Profilin, an actin-associated protein, catalyzes the exchange of ADP (adenosine diphosphate) for ATP (adenosine triphosphate) in the actin monomers and maintains a pool of monomers ready to elongate

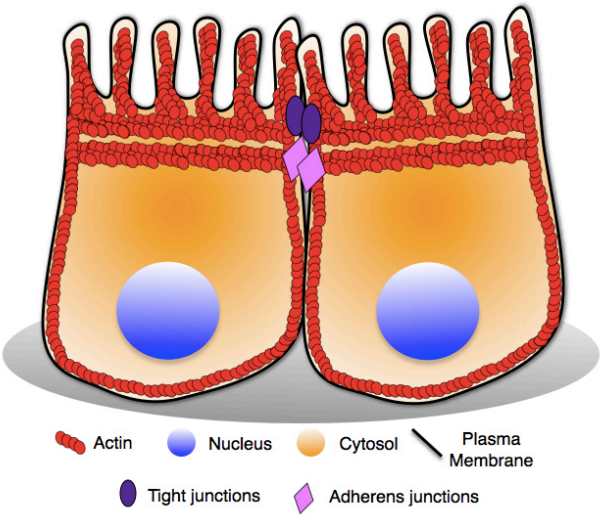

Cartoon 11. *Distribution of actin cytoskeleton in epithelial cells.*

the barbed ends. During the nucleation phase, several actin regulators initiate the formation of new actin filaments: first of all, actin monomers form trimers that act as a nucleus for the subsequent elongation of the filament; then, nucleation-promoting

proteins such as Arp2/3 complex and formins act in efficiently promoting *de novo* actin polymerization, since dimers and trimers of actin are very unstable. Once elongation is started, the filament grows rapidly until capping proteins block the barbed ends (reviewed in Miyoshi and Takai, 2008).

Tight and adherens junctions are strictly associated with actin filaments, as the alteration of actin cytoskeleton destabilizes the junctional complex and vice versa. For this reason, actin cytoskeleton is considered a prerequisite for the maintenance of epithelial cell polarity.

The capability of cells to modify their shape or to start migration depends on the actin cytoskeleton; in particular, the GTPases of the Rho family (Rho, Rac, and Cdc42) participate in regulating the actin cytoskeleton, in order to allow cellular movements. This family of Rho GTPases regulate independent pathways to assemble distinct filamentous actin structures. Rho regulates the assembly of stress fibers that provide the driving force for movement; Rac mediates the formation of lamellipodia and membrane ruffles; lastly Cdc42 promotes the formation of filopodia (reviewed in Delorme-Axford and Coyne, 2011).

2.4.2 Microtubule cytoskeleton

Microtubules are asymmetric structures with a fast-growing plus-end and a slow-growing minus end. This type of cytoskeleton in simple epithelia is distributed throughout the cytoplasm in a parallel array (*Cartoon 12*).

Thanks to their association with molecular motors, microtubules represent the tracks for polarized traffic in the cell. In

this contest, the polarized positioning of plus- and minus-ends of microtubules is a fundamental parameter in polarized membrane trafficking. Furthermore, microtubule dynamics play a central role also in the positioning of the organelles involved in intracellular trafficking such as endoplasmic reticulum (ER), Golgi apparatus and endosomes/lysosomes.

Microtubule filaments consist of 13 protofilaments, each consisting of a linear array of α/β-tubulin dimers. In most

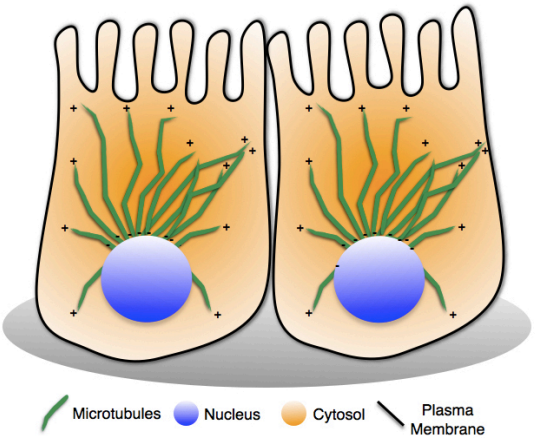

Cartoon 12. *Localization of microtubules in epithelial cells.*

vertebrate cells, interphase microtubules are organized radially with their slow-growing minus ends that nucleate from the centrosome that acts as microtubule organizing center (MTOC); this organelle typically is localized in proximity to the nucleus and is composed of two centrioles, each formed by nine triplets of microtubules, surrounded by pericentriolar material, where proteins implicated in microtubule nucleation are accumulated

(reviewed in Siegrist and Doe, 2007; Sugioka and Sawa, 2012; De Forges *et al*., 2012).

During the microtubule filaments elongation, heterodimers of guanoside triphosphate (GTP)-bound tubulin are added to the plus-ends. After this incorporation, the GTP is kept unhydrolyzed for a short time and in this case the microtubule has a GTP-cap which enables efficient polymerization. Once the GTP is hydrolyzed to GDP (guanoside diphosphate), the cap is lost and microtubules undergo rapid disassembly. The regulation of the dynamic of this process in also under the control of several microtubule-associated proteins (MAPs).

During cell mitosis microtubule cytoskeleton is essential to ensure proper segregation of chromosomes and is also directly implicated in nuclear envelope breakdown.

2.4.3 Intermediate filaments (IFs)

IFs are a family of cytoskeletal proteins consisting of more than 70 members. They are involved in several cellular processes: besides their participation in the response to mechanical stress, IFs are also key regulators of cell growth, proliferation, organelle transport and malignant transformation. The importance of intermediate filaments in such different processes is highlighted by the broad range of diseases targeting IFs. Among them, there are many epithelial blistering disorders, neurophaties, cardiomyopathies and metabolic syndromes (Arin, 2009; Otten *et al*., 2010; Haines and Lane, 2012).

Five types of intermediate filaments exist: the type I comprises acid cytokeratins K9-K28; type II IFs includes the basic

keratins K1-K8 and K71-K80; the cardiac muscular desmin, as well as vimentin and GFAP (glial fibrillary acidic protein) are type III IFs; the fourth class mainly comprehends neurofilaments (NFs) and the type V includes the ubiquitous nuclear lamins (reviewed in Bragulla and Homberger, 2009; Toivola *et al.*, 2011).

The primary structure of IFs is maintained throughout all the members of the family: they possess a central α-helical rod domain of conserved length comprising four heptad repeat-containing segments (1A, 1B, 2A and 2B), interrupted by three short linker sequences (L1, L12 and L2). Besides the rod domain, IFs show variable head and tail domains, localized at the N- and C-termini, respectively; this globular portions of the proteins play important functions in their assembly, regulation and organization (Lee *et al.*, 2012).

A distinguishing feature of intermediate filaments, in comparison to the other cytoskeletal components, is their lack of polarity because of the full symmetry of their units The nucleation of a new filament starts with the parallel association of monomers through their coiled-coil domains, in order to form a dimer that, interacting anti-parallel with another dimer, leads to the formation of a tetramer. The terminal structure of an intermediate filament is a polymer of eight tetramers resulting in a diameter of 10 nm (Lee *et al.*, 2012). Epithelial tissues are characterized by the presence of type I and II IFs. These cytokeratins are obligate heterodymers of one type I and one type II keratin. Conversely, other types of IFs, such as desmin, lamins and vimentin can individually sustain their assembly yielding homopolymeric filaments.

In simple epithelia IFs show an apical distribution, immediately below microvilli. Moreover, numerous bundles of IFs extend from the lateral domain of plasma membrane where they

are connected with desmosomes (see *Cartoon 13*), and a distinct basal network of filaments in observed in association with the presence of hemidesmosomes (reviewed in Oriolo *et al*., 2007).

The establishment of new IF network initiates with filament nucleation in proximity to focal adhesions in the cell periphery. Within the growing network, particles of filaments contribute to filament elongation and filaments continue to move toward the nucleus. Part of the filaments disassemble into soluble oligomers that rapidly diffuse throughout the cytoplasm and are

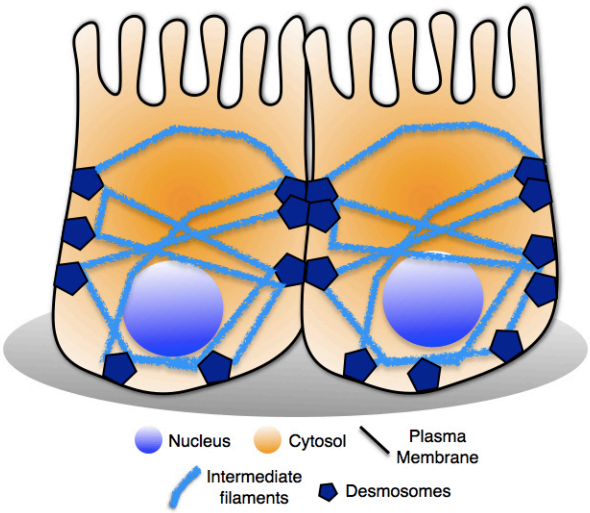

Cartoon 13. *Localization of IFs in polarized epithelial cells.*

then available for another round of nucleation (Kölsch *et al*., 2010; Windoffer *et al*., 2011). The inward-transport of IF particles relies on actin and microtubule cytoskeletons. When filaments mature, they are anchored to desmosomes and hemidesmosomes, and in

addition form a shell for the nucleus (Leube *et al*., 2011; Windoffer *et al*., 2011).

The remodeling of the cytoskeleton is crucial for different basic cell functions; also IFs can respond to various extracellular and intracellular stimuli, and their regulation mainly depends on phosphorylation events.

2.5 Polarity of stratified epithelia

Epithelial tissues are characterized by cells exhibiting different shapes: squamous, cuboidal, columnar or polyhedral. Moreover, epithelia are distinguished in simple, transitional or stratified, according to the number of layers (reviewed in Bragulla and Homberger, 2009).

Two types of simple epithelia are distinguished: single-layered and multi-layered epithelia. In the first case all the cells are connected to the basal membrane and extend to the surface of the epithelium (e.g. duodenum, jejunum, renal tubules and alveoli). Conversely, in the multi-layered epithelium, called also pseudostratified, although all cells are attached with the basement membrane, not all of them necessarily extend to the surface (e.g. respiratory epithelium).

In transitional epithelia, cells can modify their appearance during stretching, since in the relaxed state they appear small and polyhedral, whereas with the stretching cells become flatten. In this epithelium at least some cells attach to the basement membrane and extend to the surface of the epithelium (e.g. epithelium of the renal pelvis, ureter and urinary bladder).

The peculiar feature of stratified epithelia is that only the basal cells are attached to the basal membrane and only the most superficial layer forms the epithelial surface. The basal cells are the only ones that are mitotically active, whereas cells of the intermediate stratum undergo various processes of differentiation, such as keratinization. Generally, stratified epithelia can be keratinized, "wet", but non-cornified (e.g. epithelium of the oral cavity, esophagus, vagina and urethra), or "dry", keratinized and cornified epithelia, such as epidermis.

The skin covers the whole body and acts as a barrier against the outside world. The cells of the external layers (stratum corneum) are cornified and dead, as they do not have organelles and nucleus. Cornification process requires the previous keratinization of cells and the addition of a proteinaceous layer, called cornified envelope (CE), composed of insoluble complexes of proteins. Beneath the cornified layers, epidermis presents the stratum granulosum under which there are several cell layers of stratum spinosum. Finally, the basal stratum is attached to the basal membrane, an extracellular matrix that is secreted by both the basal keratinocytes and underlying fibroblasts (Morita *et al.*, 2001; Simpson *et al.*, 2011, see *Cartoon 14*).

The typical polarized phenotype of simple epithelia is quite maintained in the basal keratinocytes of the epidermis, that possess many of the same polarity constituents; however, there are some differences in the establishment and in the role of polarized proteins in this tissues (Muroyama and Lachler, 2013). For example basal keratinocytes lack TJs which are only expressed only in the differentiated granular layer. For this reason, TJs are considered polarized when looking polarity across the whole epidermis and not at single cell level. The apical

surface is thus referred as the side opposite to the basement membrane (Tsukita and Furuse, 2002). Also cytoplasmatic organelles display polarization both in simple and in basal keratinocytes, but the most important function of polarity in the skin is the orientation of mitotic spindles and asymmetric division, which ensure the stratification of the epidermis (Muroyama and Lachler, 2013).

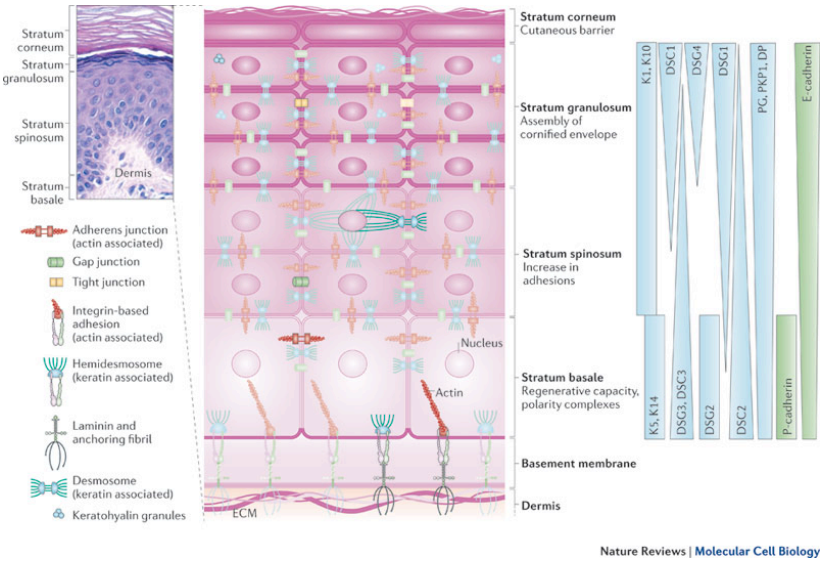

Cartoon 14. *Stratification of the skin and marker distribution (from Simpson et al., 2011).*

The differentiation process of keratinocytes depends in large part on changes in the composition and organization of epidermal cytoarchitecture. These phenomena drive a correct tissue morphogenesis and ensure that each layer can accomplish specific functions, from the regenerative capacity of the basal

stratum to the assembly of CE in the more apical layers. In this contest, it is possible to observe a graded distribution of specific cytoskeletal and cell-cell adhesion markers, such as desmosomes (Simpson *et al.*, 2011, see *Cartoon 14*, right).

2.6 POF1B (Premature Ovarian Failure 1B)

POF1B is a novel gene in evolution, found only in vertebrates, characterized by the presence of a large coiled coil region in the C-terminal half of the protein, corresponding to aa 334-443 (see *Cartoon 15*). The human protein exhibits a molecular weight of 68 kDa and consists of 589 amino acids. In the present study it has been used a GFP-tagged human POF1B.

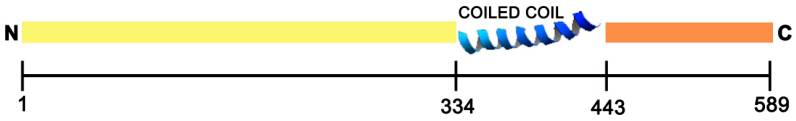

Cartoon 15. *Structure of POF1B.*

The coiled coil domain of POF1B shows significant homology to the myosin heavy chain rod domain (from residue 629 to 870 of the consensus sequence of the myosin rod domain), as well as to the C-terminal coiled coil region of barmotin/7H6, a tight junction associated protein (Lacombe *et al.*, 2006; Rizzolio *et al.*, 2007).

POF1B, both in human and in mouse, is specifically and highly expressed almost exclusively in polarized epithelial tissues such as the epidermis, where it is enriched in the granular layer, and in oro-pharyngeal and gastro-intestinal tracts. Moreover, it is worth of interest that the expression of the protein during mouse development starts in the external layers of the epidermis just before the formation of the epidermal permeability barrier. It has been also observed that POF1B shows a complex pattern of expression according to the tissue: in skin it colocalized with marker of the granular layer, such as involucrin and filaggrin and did not show any co-distribution with desmosomal markers; on the contrary, in human duodenum, it clearly colocalized with desmosomal desmoglein (Rizzolio *et al.*, 2007).

POF1B has been proposed as a candidate gene for premature ovarian failure (POF; OMIM 311360), a disorder characterized by primary or secondary amenorrhea, hypoestrogenism and elevated serum gonadotropin level before 40 years of age. This disease has a frequency of 2-3% among females. Different factors have been proposed as cause of POF, such as the presence of autoantibodies, environmental factors, infections, stress and anti-tumoral therapies (Coulam *et al.*, 1986), but the frequent finding of POF familial cases suggests a major genetic component (de Moraes-Ruehsen and Jones, 1967). On the basis of five kindreds, it has been proposed that POF may be a mendelian disorder, paternally or maternally inherited as an autosomal or X-linked dominant trait (Mattison *et al.*, 1984).

A “critical region” for normal ovarian functions has been reported on the long arm of the X chromosome (Xq13.3-q26/27) (Krauss *et al.*, 1987; Bione *et al.*, 1998; Davis *et al.*, 2000). Within this region, two regions called “POF1” and “POF2” have been

identified; the number of genes involved in POF is small and localized to either POF1 or POF2. POF1 extends from Xq21-qter, while POF2 extends from Xq13.3 to Xq21.1 and harbors POF1B among other genes implicated in POF (see *Cartoon 16*) (Therman *et al.*, 1990).

Regarding a possible role of POF1B in the etiology of POF there aren't strong evidence yet but, in support of this hypothesis, it was first identified in a patient presenting secondary amenorrhea at the age of 17 years (Riva *et al.*, 1996) and furthermore it was found interrupted by a balanced translocation in an isolated case of POF (Bione *et al.*, 2004). Moreover, a

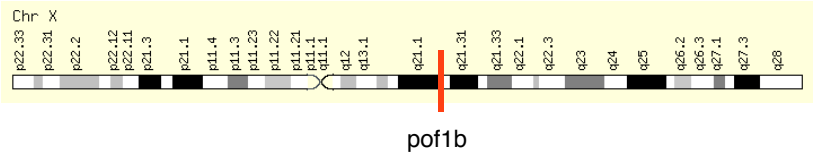

Cartoon 16. *Localization of pof1b gene in X chromosome.*

recent study of a Lebanese family with POF, showing linkage to Xq21, identified a G-to-A transition at nucleotide 1132 in exon 10 of the *pof1b* gene that resulted in an Arg-to-Gln (R329Q) mutation (see *Cartoon 17*). Through *in vitro* assays the authors demonstrated that this mutant variant of POF1B exhibited greatly diminished binding affinity with non-muscle actin filaments, compared to the wild type protein (Lacombe *et al.*, 2006).

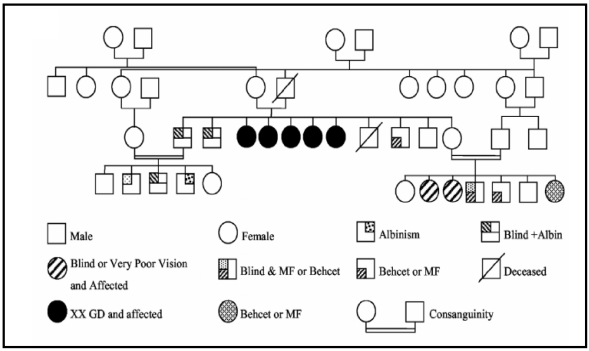

Cartoon 17. *Pedigree of the POF1B R329Q-affected family (Lacombe et al., 2006).*

3
chapter

Aims of the thesis

The aim of this study was to analyze the precise localization and function of POF1B, a cytosolic protein with unknown function that is mainly expressed in epithelial tissues. Moreover, another aim of the thesis was to clarify the impact on POF1B role of a point mutation (R329Q) recently found in a Lebanese family affected by premature ovarian failure.

To these purposes we first generated stable clones expressing the human GFP-tagged POF1B and the variant carrying the R329Q mutation in canine polarized epithelial MDCK cells. These clones were investigated by means of morphological and functional assays in comparison with untransfected MDCK cells (Chapter 4).

Subsequently, the analysis moved to an epithelial cell line of intestinal origin (human Caco-2 cells) where POF1B is highly expressed. We here focused on the traffic and the localization of the endogenous protein (Chapter 5).

The physiological role of POF1B in epithelial cells was evaluated taking advantage of the small hairpin RNA technique (shRNA). We were never able to obtain POF1B shRNA-expressing clones in Caco-2 cells, while stable clones down-regulated for endogenous POF1B were obtained in human HaCaT keratinocytes (Chapter 6). Both ultrastructural and functional analyses were performed on POF1B-silenced HaCaT cells, in comparison with non trasfected (nt) and pSuper-expressing cells.

Lastly, we investigated the localization of POF1B in several tissues, with the purpose to understand its differential distribution in simple and stratified epithelia (Chapter 7).

4

chapter

POF1B regulates epithelial polarity in MDCK cells

POF1B is a candidate gene for premature ovarian failure (Lacombe *et al.*, 2006) mainly expressed in epithelial tissues where it localizes at cell-cell adhesions (Rizzolio *et al.*, 2007), but its role in ovarian and epithelial tissues are unknown.

We start to investigate POF1B role in the most used polarized epithelial cell line: the MDCK (Madin-Darby canine kidney) cells. We here established clones expressing the GFP-tagged wild type protein (WT) and the POF-associated variant, (R329Q mutation) found in a POF-affected family by Lacombe and colleagues in 2006 (Mut). These cell lines were analyzed by means of morphological and biochemical assays in comparison with non trasfected MDCK cells (M). All the data obtained in MDCK cells have been published in 2011 by our lab (Padovano *et al.*, 2011).

4.1 The R329Q substitution prevents the localization of POF1B to tight junctions

The specific spatial and temporal expression in gastrointestinal tracts and granular layer of the epidermis has led to the suggestion that POF1B has a role in the acquisition and/or maintenance of epithelial polarity (Rizzolio *et al.*, 2007). Because TJs are the most relevant junctions for acquisition and maintenance of the polarized phenotype, we first investigated the TJ localization of endogenous POF1B in human jejunum (Fig. 1A), using specific antibodies against POF1B (red) and Na^+/K^+-ATPase, which is a marker of the lateral surface, or JAM1, a TJ marker (green). POF1B localizes along the entire lateral

junctional domain. Staining was punctuated along the surface homogeneously labelled by the Na^+/K^+-ATPase antibody. A yellow color indicating the colocalization was not seen in the merged image because the green staining of the pump was predominant; however, the red staining of POF1B was clearly enriched in a more apical region of the lateral surface that is devoid of Na^+ pumps (Fig. 1A, see the lack of overlap between the green and red peak of fluorescence in the apical position). The green JAM1 staining was enriched in an apical portion of the lateral junctional domain and the colocalization with POF1B was revealed by the yellow staining and by the overlap of the fluorescence peaks. These data indicate a localization of POF1B along the entire lateral junctional surface, and its enrichment at the level of the tight junctions in human jejunum.

We then investigated the effects of the over-expression of full-length POF1B (WT) and its R329Q variant (Mut) on the surface polarization of epithelial cells. To this end, we stably expressed the cDNAs fused to the green fluorescent protein (GFP) in the MDCK polarized epithelial cell line, a cell model that is widely used to study the role of polarity proteins. At least three independent WT and Mut clones were selected and the localization of the transfectants was characterized by confocal and Western blot analysis (Figs 1, 2). Vertical confocal sections (x-z) showed a similar distribution of POF1B to that observed in human jejunum, and the localization of the WT (green staining) construct extended beyond the staining of the β-catenin (red staining) marker of adherens junctions (AJs). The localization of POF1B at the cytoplasmic face of TJs was further confirmed by its colocalization with the PAR3 marker of this domain (Fig. 1B,

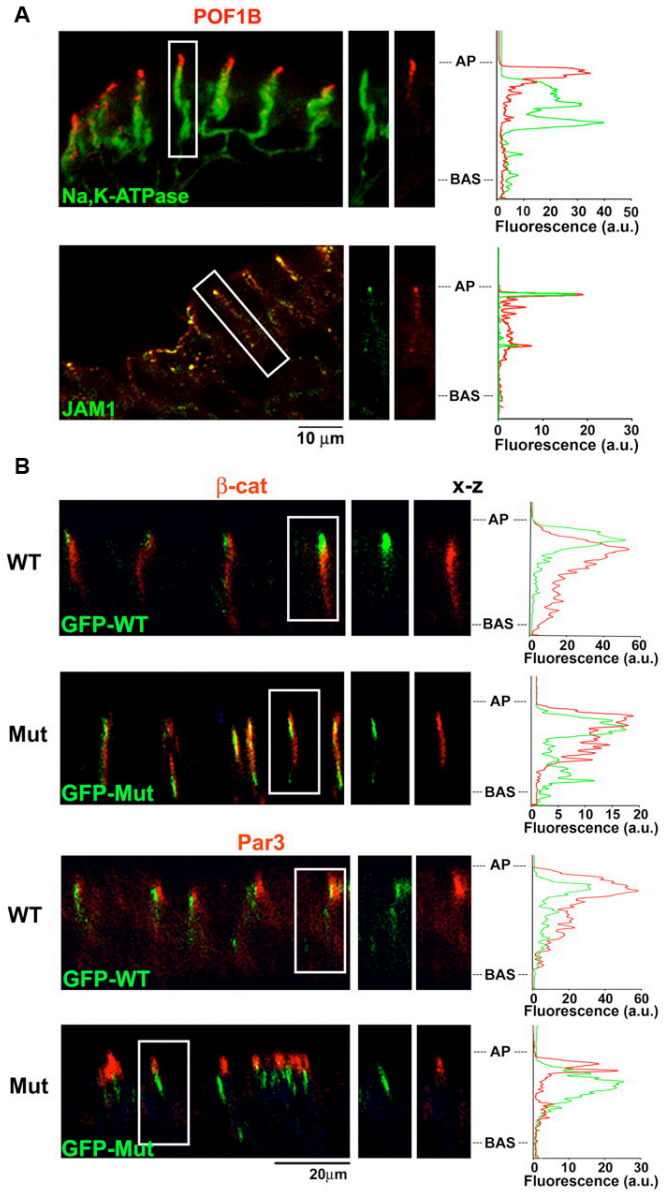

Figure 1

see next page for legend

Figure 1. POF1B R329Q fails to localize to TJs in fully polarized MDCK cells. (A) *Confocal analysis of immunofluorescence double staining for POF1B (red) and the Na^+/K^+-ATPase marker of AJs or the JAM1 marker of TJs in human jejunum (green).* ***(B)*** *Immunofluorescence analyses of MDCK cells stably expressing wild-type GFP-POF1B (WT) or GFP-POF1B R329Q (Mut). Cells grown at confluency for > 3 days in Transwell filters were double stained for the indicated markers and analyzed by confocal microscopy. Vertical (x-z) confocal sections are stained for the β-catenin marker of AJs (β-cat) and the PAR3 marker of TJs (red). POF1B localization is revealed by GFP fluorescence (green). (A, B) Red and green pixel intensity along the lateral surface of the corresponding images is expressed in fluorescence arbitrary units (a.u.). AP, apical region; BAS, basal region (Padovano et al., 2011).*

compare the green peak with the red of β-catenin or with that of PAR3). By contrast, the localization of Mut did not extend in the apical direction beyond that of β-catenin, and the mutant did not colocalize with PAR3 at the TJ level (Fig. 1B, see the almost complete overlap between the Mut peak with that of β-catenin but not with PAR3).

4.2 Apico-basal polarity is maintained in MDCK cells expressing POF1B R329Q

The effects of POF1B overexpression on polarity markers was investigated by Western blot analysis in MDCK cell lysates. Approximately a threefold reduced expression of the apical marker gp135 and the tight junctional marker Claudin2 (Cla2) was revealed in Mut cells (Fig. 2A, B). However, Claudin2 and gp135, as well as all the junctional polarity markers tested, maintained

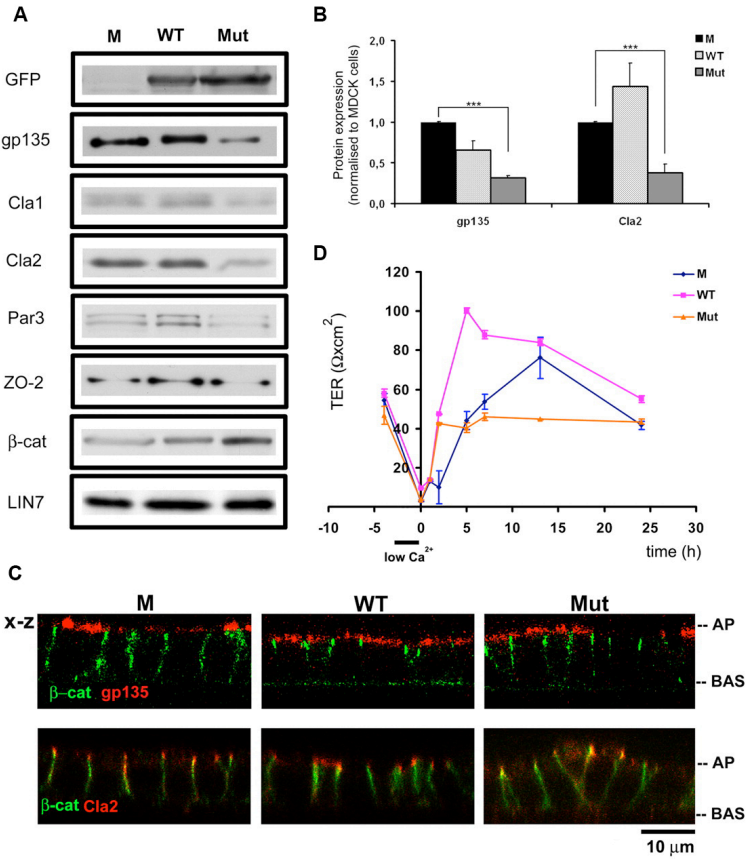

Figure 2

Figure 2. Altered mechanism of TER acquisition in POF1B R329Q cells. (A) *Representative Western blot analysis of the total expression of junctional markers in control MDCK cells (M), MDCK cell lines overexpressing GFP-POF1B or GFP-POF1B R329Q. Equal amounts of cell extracts were loaded onto 10% SDS-PAGE and the transferred proteins were immunoprobed for GFP (to quantify the expression of the WT and Mut constructs in the cell lines) and markers of the apical surface (gp135), tight junctions (Cla1, Cla2, Par3, ZO-2 and LIN7) and adherens junctions (β-cat and LIN7).*

see next page for legend

*(**B**) Quantification of the expression of gp135 and Cla2 in transfected and untransfected cells. The results are the means +/- S.E.M. of three independent experiments performed in control, and two stable clones for WT and Mut; one of these experiments, normalized to control MDCK cells, is shown in A (*** p < 0,001). **(C)** Vertical confocal sections (x-z) of double immunofluorescence staining for β-catenin (green) and the apical marker gp135 or the tight junctional marker Cla2 (red) in control (M) and transfected (WT or Mut) MDCK cells. AP: apical surface; BAS: basal surface. **(D)** TER assay in control (M), WT and Mut cell lines. Cell monolayers grown at confluence for more than five days on Transwell filters were incubated with low calcium medium (low Ca^{++}) to disassemble the junctions. Junction reassembly induced by calcium replacement was followed by measuring TER at the indicated times. Each value +/- S.E.M. represents the average of three experiments performed in two stable clones. (Padovano et al., 2011).*

their specific surface localization (Fig. 2C), thus suggesting that apico-basal polarity is maintained in Mut cells.

The reduced expression of these markers was not due to variability among the cell lines, because it was observed in three independent clones, and it was associated with the level of expression of the transfectants, whereas significant changes in the expression of other markers were not confirmed (data not shown).

Because claudins influence the charge selectivity and electrical resistance of junctions, we measured transepithelial electrical resistance (TER) (Fig. 2D) and paracellular permeability to FITC-Dextran (not shown). WT cell monolayers grown at confluency for more than 5 days showed significantly higher TER values than control MDCK cells or MDCK cells transfected with the variant. Incubation with a low-calcium medium to disassemble the junctions abolished TER in all of the cells, whereas the replacement with regular medium induced junction reassembly.

The WT-expressing cells peaked earlier than untransfected MDCK cells, whereas the TER peak was virtually absent in cell lines expressing the mutant. However, apico-basal polarity and steady-state TER in Mut cells were not affected, and the altered TER acquisition profile did not correlate with an increased permeability of FITC-Dextran (data not shown), suggesting that POF1B R329Q does not interfere with TJ barrier properties for large solutes.

4.3 Altered organization of the monolayer in MDCK cells expressing POF1B R329Q

No remarkable differences in TJ ultrastructure in cells expressing the different constructs were observed by means of conventional electron microscopy (data not shown). The ultrastructural analysis, however, revealed that the MDCK monolayer expressing the mutant contained cells of various shapes and sizes that sometimes appeared as a pseudo-stratified monolayer (Fig. 3A), although these cells were still capable of forming morphologically normal junctions, as shown by the presence of TJs in highly dysmorphic cells (Fig. 3B).

Defects in cell size and monolayer organization were also observed by confocal analysis of Mut distribution. POF1B and POF1B R329Q were particularly enriched at sub-apical and basal levels (Fig. 3C,D), although the latter staining was more discontinuous (compare sub-apical and basal staining in 3D image reconstructions and horizontal sections), and thus rarely seen in vertical sections (Fig. 1B). The enrichments were resolved as two rings, one at the sub-apical and the other at the

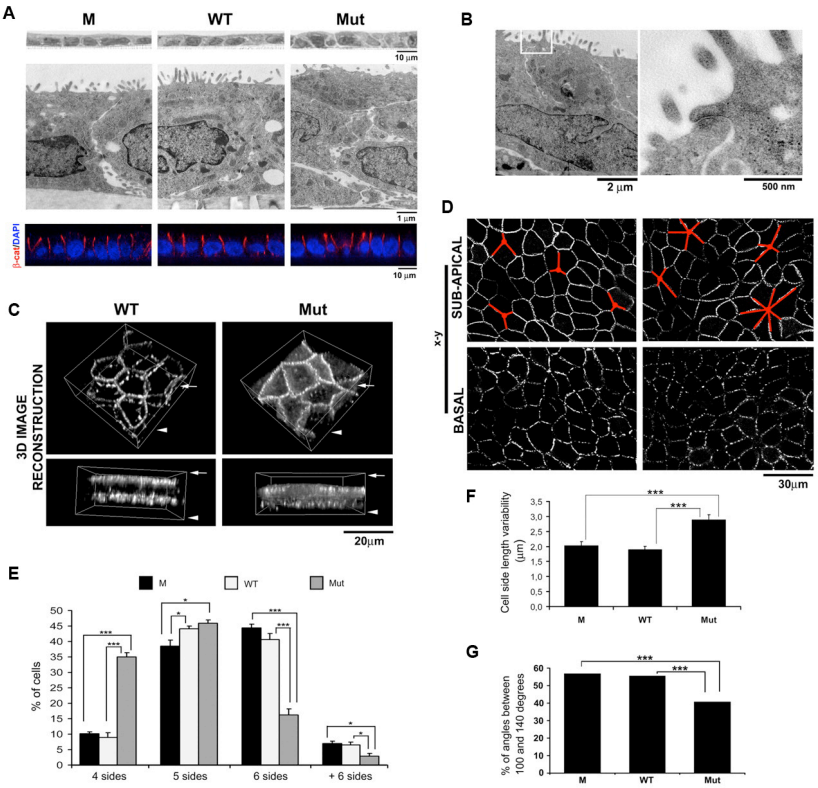

Figure 3

Figure 3. Altered cell morphology and monolayer organization in cells expressing POF1B R329Q. *Control MDCK cells (M), MDCK cell lines transfected with POF1B (WT) or POF1B R329Q (Mut) were grown confluent on Transwell filters for > 3 days and processed for EM or immunofluorescence. (**A**) Semithin sections (top), TEM images (middle) and immunofluorescence staining (bottom) using the β-catenin antibody (red) and DAPI (blue). (**B**) Ultrastructural analysis in highly dysmorphic Mut cells; a 4X magnification is shown on the right.*

see next page for legend

(C) *Immunofluorescence analysis of POF1B localization. Tilted volume rendering of entire volume of cells (3D-image reconstructions) showing 3D apical (upper) and side (lower) views of a group of cells. Arrows and arrowheads indicate the apical and basal region of the cell monolayer, respectively.* ***(D)*** *Horizontal (x-y) confocal sections of POF1B localization in WT and Mut cell lines taken at the sub-apical and basal region of the cell monolayers. A red mask is drawn on sub-apical sections to highlight cell arrangement in the monolayer.* ***(E)*** *Quantification of cells with four (quadrilateral), five (pentagonal), six (hexagonal) or more than six sides (n=350 for each cell line).* ***(F)*** *Cell side length variability was measured within each cell on an average of 50 cells in at least three different experiments.* ***(G)*** *Angles measured in 100 cells per each cell line using a macro developed in ImageJ (see the Materials and Methods). Data in E-G are the means +/- S.E.M. of three independent experiments performed with two stable clones for each transfectant. * p < 0,05; ** p < 0,01; *** p < 0,001 (Padovano et al., 2011).*

basal level in both horizontal sections (x-y) and 3D reconstructions (Fig. 3C,D). Low levels of POF1B were found between the apical and basal enrichments, whereas the mutant protein showed a more diffuse localization between the two rings, which in 3D-images, partially masked the lower ring.

In horizontal sections of Mut monolayers, we noticed that more than three cells often contacted each other at a single point (Fig. 3D, vertices, compare the red masks drawn on WT and Mut sub-apical sections) and the number of hexagonal cells was considerably reduced, whereas the number of cells with four sides increased threefold (Fig. 3E). Moreover, Mut cells showed a greater variability in the length of their sides (mean value, 7,8 +/- 0,15 µm) and the percentage of angles between 100 and 140 degrees was significantly reduced (the ideal measure of each angle if three cells contact each other at a single point is 120 degrees) (Fig. 3F,G). It is known that epithelial cells tend to pack

into regular hexagons to reach a thermodynamically favorable state and so, an increased divergence from the shape of regular polygons in which all angles are equal in size and all sides have the same length (equiangular and equilateral polygon), is a clear sign of a perturbed organization of the monolayer (Carthew, 2005).

4.4 Decreased levels and altered organization of F-actin in MDCK cells expressing POF1B R329Q

Irregularity of cell shape, which disturbs the monolayer polarity, might be a consequence of dysfunctional POF1B. Because cell shape and specialized cellular functions depend on an underlying network of dynamic actin polymers (F-actin) that ensure mechanical stability and flexibility of the cortex (Van Itallie *et al.*, 2009), we analyzed the effects of POF1B expression on the actin cytoskeleton.

We first verified that both POF1B apical and basal rings contained F-actin in 3D reconstructions of cells stained with phalloidin to detect F-actin (Fig. 4A, yellow, only colocalization signals were represented). Note that the distribution of POF1B (WT and Mut) is maintained, but the Mut distribution appeared more diffuse along the entire lateral surface and less enriched at the apical ring (compare with the 3D images in Fig. 3B), suggesting a major overlap between F-actin and WT, as compared with Mut. Because confluent MDCK cells had an apical actin cytoskeleton ring that included and circumscribed the microvilli, which was located at the same level of the apical junctions (TJs and AJs), we analyzed whether WT and Mut

codistributed with the apical actin in 3D side reconstructions of the indicated regions (Fig. 4B). The apical ring of WT POF1B was completely embedded into the F-actin apical enrichment, whereas the Mut staining was partially underneath the phalloidin staining of F-actin, further suggesting the exclusion of Mut from apical junctional domains. A twofold increase in colocalization of WT and phalloidin (99%) compared with that of Mut (63%) was measured using Manders' colocalization coefficients (Fig. 4B, histogram).

A different distribution and content of F-actin was also observed at cell-cell contacts in Mut cells; F-actin showed a spot-like distribution along the adhesion surface and the staining was particularly marked in three-cell vertices (vertices at which three cells and three sides meet) in control cells and cells expressing WT POF1B, but not in Mut cells, (Fig. 4C, see arrowheads). Peaks of fluorescence in Mut cells, obtained using ImageJ surface plot analysis, were also lower in intensity (mainly in the blue range of the scale, whereas peaks of fluorescence in WT reach the red range of intensity) in the vertices. No significant difference was observed in apical and basal actin in Mut cells.

The effect of WT or Mut expression on F-actin was then qualitatively analyzed by measuring the F-actin to G-actin ratio (Fig. 4D), and the F-actin content was quantified by FACS analysis (Fig. 4E). The ratio assay is based on the differential extractability of F-actin and G-actin from cells by detergent (Blikstad and Carlsson, 1982). In these experiments, actin was mainly found in the detergent-insoluble F-actin fraction (70%) in control and WT MDCK cells, whereas only 50% of the cellular actin was found in the F-actin fraction in Mut cells. Moreover, FACS analysis revealed a 40% increase and a 20% decrease in F-actin content, respectively in WT and Mut cells, when compared

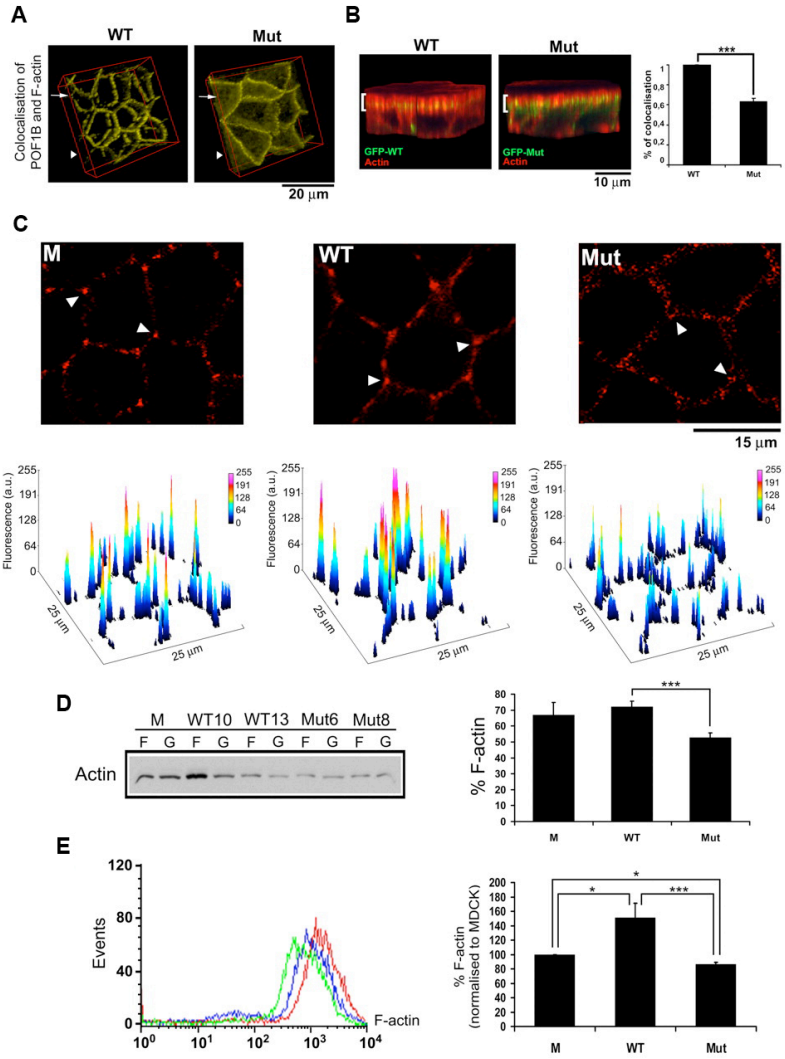

Figure 4

Figure 4. F-actin defects in cells expressing POF1B R329Q*. Cells grown confluent on Transwell filters (A-C), or Petri dishes (D,E) for > 4 days were stained for labelled phalloidin (A-C,E) and analyzed as indicated.*

see next page for legend

*(**A**) 3D image reconstruction representing colocalization of POF1B and labelled phalloidin (yellow). POF1B and F-actin not colocalizing are not considered. (**B**) 3D side view (left) and quantification of the percentage of POF1B and phalloidin colocalization (right) evaluated by Manders' colocalization coefficients in the apical region of the cells (brackets) (n=10 cells analyzed for each stable cell line; *** p < 0,001). (**C**) Horizontal confocal sections (upper) and their corresponding surface plot analysis (lower); the fluorescence intensity is expressed in arbitrary unit (a.u.). (**D**) A representative detergent extraction experiment. Equal volumes of insoluble F- and soluble G-fractions were loaded onto 10% SDS-PAGE and blotted into nitrocellulose; the amount of actin in each fraction was evaluated using specific antibodies (left). Quantification showing mean +/- S.E.M. of three independent experiments is presented in the right panel. *** p < 0,001. (**E**) A representative graph of F-actin signals in WT (red), Mut (green) and control MDCK cells (blue), and F-actin content comparison in transfected (WT and Mut) and untransfected (M) (set to 100%) cell lines, as determined by FACS analysis. Data represent mean +/- S.E.M. of three independent experiments performed with at least two stable clones for each transfectant. * p < 0,05; *** p < 0,001 (Padovano et al., 2011).*

with control MDCK cells. This result supports a role for POF1B in the stabilization of F-actin at cell-cell contacts and suggests that the mutant interferes with this process.

4.5 Altered ciliogenesis and cystogenesis in MDCK cells expressing POF1B R329Q

In a variety of cell systems, cytoskeleton arrangements are regulated by the tissue polarity or planar cell polarity (PCP) pathway. PCP corresponds to a secondary axis of polarity that is perpendicular to the apico-basal direction (Simons and Mlodzik,

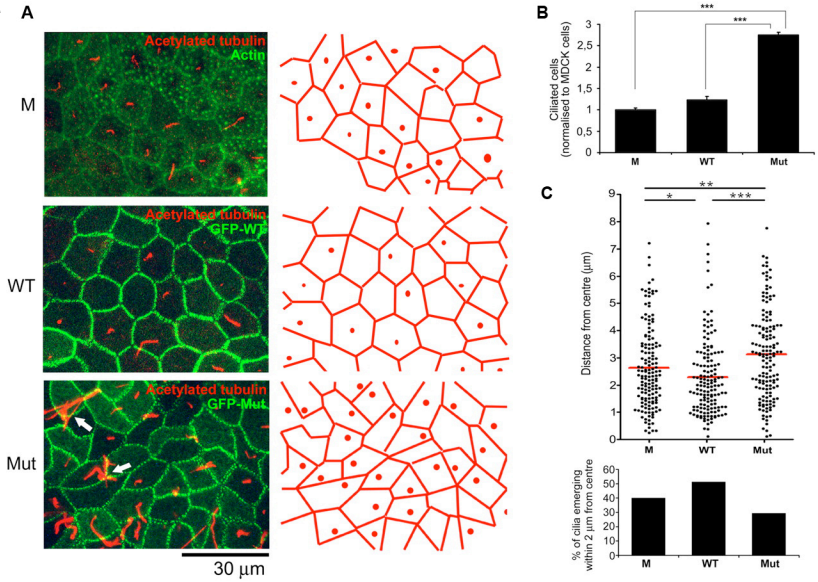

Figure 5

Figure 5. Defects in ciliogenesis in cell lines expressing POF1B R329Q*. Cells grown confluent for > 4 days in Transwell filters were stained for the indicated markers.* ***(A)*** *Confocal z-stack projections of horizontal sections of cell monolayers in control MDCK cells (M) and MDCK cells expressing GFP-POF1B (WT) or GFP-POF1B R329Q (Mut) stained with acetylated tubulin to visualize primary cilia (red), phalloidin in M or GFP in WT and Mut (green). The red masks representing the cell boundary and the base of primary cilia were obtained from confocal sections taken from the sub-apical region through the emergence of primary cilia. Arrows indicates interlaced cilia tips.* ***(B)*** *The number of ciliated cells in monolayers expressing WT or Mut was normalized to MDCK cells (n=350 for each cell line).* ***(C)*** *Scatter plot of the distance from cilia emergence and cell centre (n=150 for each cell line) measured using a macro developed in ImageJ. Red lines indicate mean values and dots indicate individual data points of the ciliated cells analyzed. The lower histogram represents the percentage of the primary cilia emerging within 2 µm from the centre. The values are means +/- S.E.M. from three independent experiments performed with two stable clones for each transfectant. * p < 0,05; ** p < 0,01; *** p < 0,001 (Padovano et al., 2011).*

as for the orientation of cell division. Primary cilia are sensory microtubule-based structures emanating from the apical surface of many cells, including MDCK cells (Singla and Reiter, 2006), stained by antibody against acetylated tubulin (Fig. 5A). In our experimental conditions, not all the cells in untransfected and transfected monolayers exhibited primary cilia, but the number of ciliated cells appeared markedly increased in the cell lines expressing the POF1B mutant protein (Fig. 5B). Because a direct link between actin dynamics and ciliogenesis has been documented (Kim *et al*., 2010), the altered organization of the actin cytoskeleton observed in Mut cells could account for the increased number of ciliated cells. Moreover, in these cells, we noticed that cilia emerged from the apical surface at a more variable distance from their centre. Statistically, about twice as many cilia emerged closer than 2 µm from the cellular centre in WT and M cells, as compared with cilia in Mut cells (Fig. 5C, histogram). The occasional proximity of cilia, emerging near the cell boundaries, might hence explain the appearance of interlaced cilia tips in Mut-expressing cells (Fig. 5A, arrows).

Primary cilia are microtubule-based structures guided by basal bodies that originate from and have a substructure similar to centrioles. Interestingly, the symmetrical division of epithelial cells to generate two identical daughter cells depends on the correct positioning of centrioles (Jaffe *et al*., 2008; Hao *et al*., 2010; Qin *et al*., 2010; Rodriguez-Fraticelli *et al*., 2010; Zheng *et a*l., 2010), suggesting possible defects in the orientation of cell division in Mut cells. These defects are better visualized in the organotypical 3D extracellular matrix cell culture system (Vieira *et al*., 2006). Mut cells were plated into matrigel and 4-day-old cysts were stained for DAPI to localize mitotic chromosomes (Fig. 6A).

As expected, cell division occurred in a direction parallel to the plane of the cyst apical surface in WT and untransfected MDCK cells (Fig. 6A, arrows), thus generating cells that maintain the polarity of the monolayer. Conversely, mitotic chromosomes were mislocalized in Mut cysts, with a large fraction of Mut cells (approximately 50%) that were not dividing in a direction parallel to the cyst surface. As a consequence, the monolayer will not be maintained and daughter cells will be forced to stratify or to form a new lumen (Fig. 6A). Misorientation of mitotic spindles is known to lead to cysts with multiple lumens (Zegers *et al*., 2003; Mostov *et al*., 2005; Jaffe *et al*., 2008; Zheng *et al*., 2010) and, indeed, we observed a higher percentage of cysts with multiple lumens or no lumens in a period up to 5 days in Mut-expressing cells (Fig. 6C). By contrast, over-expression of POF1B did not interfere with the development of spherical cysts with a single central lumen and a monolayer of cells with correctly polarized apical (facing the lumen) and lateral proteins, as shown by β-catenin and gp135 staining (Fig. 6B), respectively, in 4-day-old cysts. Cell polarity and cyst morphogenesis were therefore the same in cells over-expressing the WT and in untransfected cells examined over the same time period (Fig. 6B). Interestingly, Mut cyst defects were less noticeable after 6 days or more in culture, although the lumens still appeared to be collapsed, as shown by analysis of the circularity index (Akao *et al*., 2003) and gp135 staining (Fig. 6B-D). Misoriented cell division is therefore associated with an alternative mechanism of cyst lumen formation: instead of a single lumen enlarging as the cells divide and cysts grow, cells can first form multiple lumens that eventually generate a single collapsed lumen.

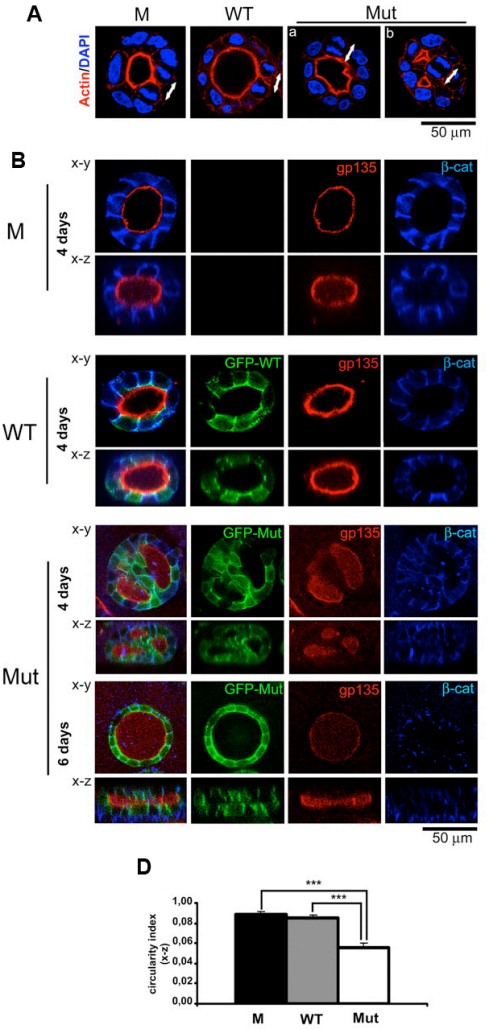

	Parallel	Non-parallel
MDCK	71,9 %	28,1 %
WT	72,6 %	27,3 %
Mut	51,1 %	48,9 %

Figure 6 see next page for legend

Figure 6. Altered mechanism of cystogenesis in cells expressing POF1B R329Q. *Single cells were seeded in an extracellular matrix (Matrigel) and grown for the indicated time. The cysts were fixed in 4% paraformaldehyde, permeabilized, stained for the indicated marker, and analyzed by laser confocal microscopy. The confocal sections were taken at the middle region of the cysts.* ***(A)*** *Representative images (red, F-actin; blue, DAPI) of 4-day-old cysts; the arrows represent the direction of mitotic division. Two examples of Mut cysts showing misoriented division in a single lumen (a) and in a multilumen (b) cyst. Quantification of the direction of mitotic division is shown in the right (n > 80 for each cell line). Experiments were performed in triplicate with at least two stable clones for each transfectant.* ***(B)*** *Cyst polarization was assessed by the extent of lumen formation and by staining for the gp135 apical marker (red) and the β-catenin lateral marker (blue) in horizontal (x-y) and vertical (x-z) confocal sections.* ***(C)*** *Quantitative analysis of cyst morphology in control (M), GFP-POF1B (WT) or GFP-POF1B R329Q (Mut) cell lines cultured for 3-6 days. The values are the percentage of cysts with the indicated lumen morphology (n=100 cysts for each cell line).* ***(D)*** *Quantitative analysis showing the circularity index of lumens of cysts in cells cultured for more than 6 days stained with Texas Red phalloidin (n=28 for each cell line). (C,D) Data are the means +/- S.E.M. of three independent experiments using two stable clones. * p < 0,05; ** p < 0,01; *** p < 0,001 (Padovano et al., 2011).*

The altered mechanism of formation of the cyst lumens, however, did not associate with defects in cell polarity, because the polarity markers β-catenin and gp135 were localized normally to cell-cell contacts and the surface facing the abnormal lumens, respectively, in Mut cysts (Fig. 6B, see apical staining in x-y and x-z sections). Mut expression therefore affects processes, such as cystogenesis and ciliogenesis, that are strictly related to tissue polarity, rather than cell polarity.

4.6 Conclusions and discussion of the results obtained in MDCK cell lines and their implications in the epithelial polarity and POF

In line with the capability of POF1B to bind actin filaments (Lacombe *et al.*, 2006), these experiments demonstrate a key role for POF1B in the organization of epithelial monolayer through regulation of the actin cytoskeleton at the junctional domain.

We here have first investigated the localization of POF1B in human jejunum, where the protein exhibited an enrichment at the tight junction level. In MDCK cells, a model of polarized epithelial cells, we also found localization of the wild type protein at the TJ level, whereas the mutant did not show a precise enrichment at TJs but was more distributed along the entire lateral surface of the cells.

The effects of the over-expression of mutant POF1B on TJs assembly and defects during the acquisition of surface polarity evaluated in cells grown to confluence on Transwell filter supports (two-dimensional cultures, 2D) and in organotypical three-dimensional (3D) cultures using laser confocal and electron microscopy demonstrated clear defects: mutant monolayers were often pseudo-stratified and characterized by the presence of dysmorphic cells, suggesting evident abnormalities in the planar cell polarity of the epithelial sheet. Because cell shape and specialized cellular functions depend on an underlying network of dynamic actin polymers and POF1B is able to bind non-muscle actin (Lacombe *et al.*, 2006), the organization of the actin cytoskeleton was analyzed qualitatively (morphological and biochemical assays) and quantitatively (FACS analysis) in the MDCK stable clones. By these analyses we confirmed that the

R329Q mutant showed decreased levels and altered organization of F-actin, compared to the wild type protein. All the observed defects highlighted the importance of POF1B in regulating epithelial planar cell polarity rather than in the definition of apico-basal polarity, as the mutant did not induce evident alterations in TJs, maintaining proper localization of TJ and polarity markers and their normal ultrastructure. Only the mechanism of TJ formation appeared altered in Mut cells (absence of a TER peak), and this defect might be explained by a difficulty in synchronizing the formation of TJs owing to the irregular polygonal shape and sides of different length of the mutant cells.

In support of a role for POF1B in regulating epithelial PCP, we have also provided data showing altered emergence of cilia docking sites in 2D cultures and misorientation of mitotic divisions in 3D cultures of Mut cells. Several studies have highlighted a primary role for the actin cytoskeleton in centriole positioning (Vaughan and Dawe, 2011) and the described defects in ciliogenesis and cystogenesis might be due to random positioning of centrioles or centriole analogous structures (i.e. basal bodies), controlling the symmetrical cell division in proliferating cells or the cilium emergence in fully polarized cells, respectively. Polarized epithelial tissues regulate ovarian function in a number of ways, and a key organizer of actin dynamics, the formin-related gene DIAPH2 (Diaphanous-related formin-2) (Bione *et al.*, 1998), which also maps to the X chromosome critical region for ovarian function, is another candidate gene for POF. The decision of developing follicles to continue growing and eventually to ovulate or to undergo atresia mainly depends on the intimate relationship between oocytes and the surrounding highly specialized epithelial granulosa cells. During this development, granulosa cells

proliferate, thus contributing to follicle enlargement (Jablonka-Shariff *et al*., 1996; Hirshfield, 1997; Albertini *et al*., 2001) and, by converting testosterone to estrogen, these cells are responsible for the increased level of hormone in the bloodstream. Thus, the low levels of estrogens in POF might be explained by a defect in granulosa cell division. Moreover, ovarian epithelia and the secretory epithelium of the ovarian oviduct have primary cilia, and ovulation was impaired in transgenic mice in which ovarian primary cilia were deleted (Johnson *et al.*, 2008), indicating a crucial role for this organelle in the ovarian functions.

In conclusion, our data provide evidence of a major role for POF1B in controlling cell shape and monolayer organization, which is a key feature that drives morphogenesis during development and is critical for organ function.

5 chapter

Desmosomal localization of POF1B in human intestinal Caco-2 cells

The organs where POF1B is mainly expressed are those in which epithelial tissues are the most important components, such as the skin, the gastro-intestinal tract and the oropharynx. With the purpose to deepen the function of POF1B in the human tissues where it is endogenously expressed, we decided to analyze the localization of the protein in epithelial intestinal Caco-2 cells, a human cell line obtained from colorectal adenocarcinoma cells.

5.1 Colocalization of POF1B with desmosomal proteins in Caco-2 cells

First of all, we analyzed the localization of POF1B at cell-cell adhesions in Caco-2 cells. As well as in MDCK cells, the protein showed a distribution along the entire cell adhesion with an apical enrichment considered *bona fide* TJs by virtue of negative staining with the Na,K-ATPase marker of the AJs (Fig. 7A). However, POF1B exhibited a punctuate staining along the entire cell-cell border, different from the typical indented pattern of TJ marker Claudin2 (Fig. 7B, upper) and the uniform label of the AJ marker β-catenin (Fig. 7B, bottom). Conversely, as shown in Fig. 7C, POF1B nicely colocalized in these spots with the desmosomal markers DSP, PKP2 and DSG (compare the punctuate red staining for POF1B with the green stainings and the corresponding peaks in the in plot profiles, Fig. 7B-C). The dotted distribution of POF1B and desmosomal proteins was confirmed by the analysis of the percentage of staining-free pixels at plasma membrane (Fig. 7D). This quantification reflects the different accumulation patterns of the adhesion markers and

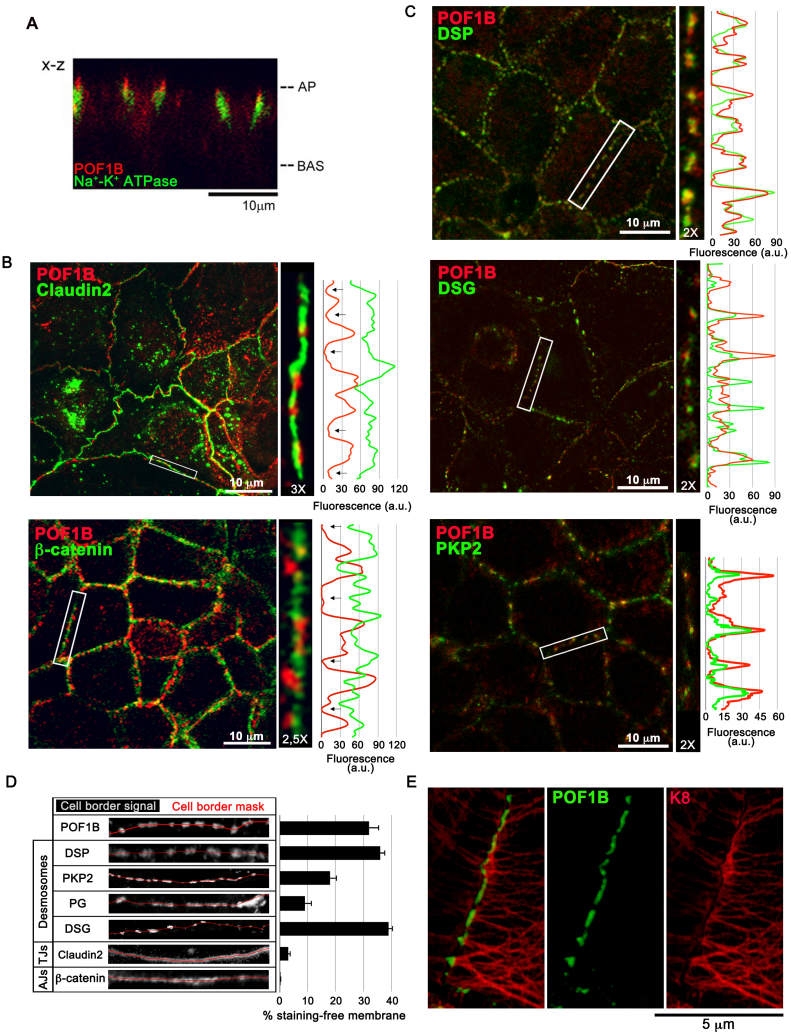

Figure 7

see next page for legend

Figure 7. POF1B colocalization with desmosomal proteins in human intestinal Caco-2 cells. (A) *Vertical confocal section (x-z) of fully polarized Caco-2 cells grown on Transwell filters for > 7 days and stained for POF1B (red) and Na^+/K^+-ATPase (green). AP, apical surface; BAS, basal surface.* ***(B, C)*** *Immunofluorescence confocal analysis of Caco-2 cells probed for POF1B (red) and the indicated markers of TJs and AJs (green) (A) or of desmosomes (B)****;*** *the intensity of fluorescence (in arbitrary units, a.u.) was analyzed by plot profiles.* ***(D)*** *The distribution of the signals in ~ 100 µm of cell-cell adhesion membrane was analyzed for each staining (images of which are presented on the left; the red mask identified the cell-cell contact membrane); the values were expressed as % of staining-free membrane****. (E)*** *Caco-2 cells were co-stained for POF1B (green) and K8 (red). Individual and merged images are presented.*

showed a pattern of POF1B distribution identical only to proteins exclusively found in desmosomes. PG, that can be also found in AJs, only partially co-distributed with POF1B, and a completely different distribution was revealed for β-catenin e Claudin2, markers of AJs and TJs, respectively. The specific recruitment of POF1B to desmosomes was further suggested by its localization in adhesion sites precisely connected to IFs: as illustrated in Fig. 7E, filaments of K8 were attached to plasma membrane exactly where POF1B enriched.

5.2 Detergent insolubility and calcium independence of POF1B and desmosome components in Caco-2 cells

Among cell-cell junctions, only desmosomes are characterized by the capability to form insoluble complexes with IFs and to reach a

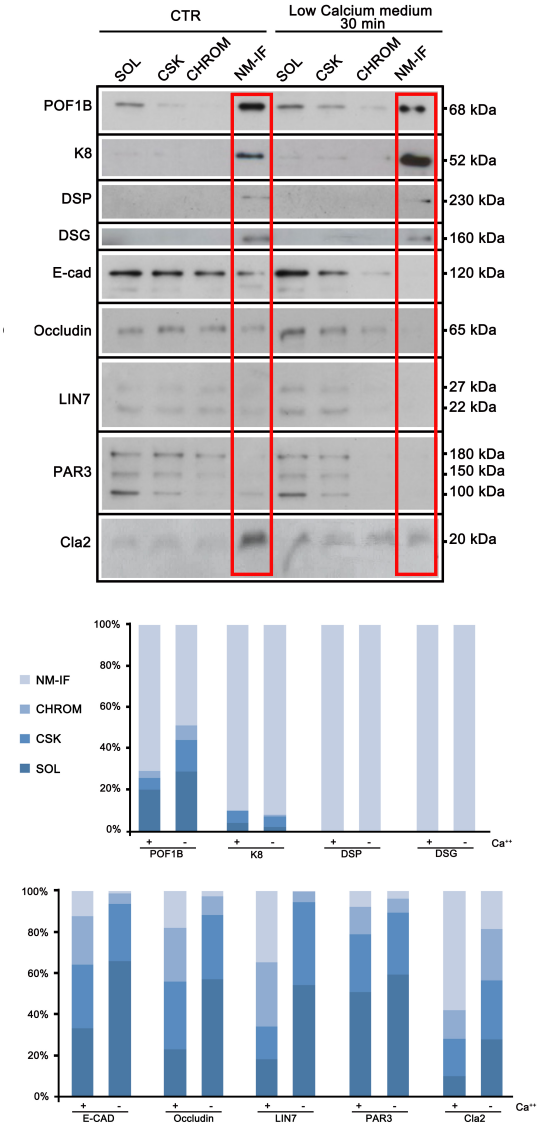

Figure 8

see next page for legend

Figure 8. Insolubility and calcium-independence of POF1B and desmosomes. *Western blot analysis of Caco-2 subfractions obtained according to Fey et al., 1984, in CTR and cells switched to low-calcium medium for 30 min. Equivalent aliquots from the soluble (SOL), cytoskeleton (CSK), chromatin (CHROM) and NM-IF fractions were loaded onto 10% SDS-PAGE and the transferred proteins were immunoprobed for the indicated markers. The molecular weights (kDa) are indicated on the right; the red frames highlight the NM-IF fractions. A quantification (in %) of each fraction for each immunostaining is presented on the bottom.*

calcium-independent mature state, called hyper-adhesion (Garrod and Kimura, 2008). To assess the solubility of POF1B, we performed a Triton X-100 extraction in Caco-2 cells grown confluent for 6 days in regular medium or switched to calcium-deprived medium for the last 30 min (Fig. 8). Three consecutive extractions were used to obtain soluble and cytosolic components (SOL), actin and tubulin cytoskeleton (CSK), chromatin-associated proteins (CHROM) and the insoluble nuclear matrix-intermediate filaments fraction (NM-IF) (Fey *et al.*, 1984). As shown by the Western blot analysis and the corresponding quantification (see graph on bottom), POF1B co-fractionated with desmosomal components (DSP, DSG) and the intermediate filament K8, and not with markers of AJs (E-cadherin and LIN7) and TJs (occludin, LIN7, PAR3). Similar to desmosome components, POF1B distribution in the insoluble NM-IF fraction was mostly independent on calcium, while the Claudin2 TJ marker did not accumulate in the NM-IF fraction in calcium-deprived conditions.

The mature hyper-adhesive desmosomes are highly resistant to disruption, while TJs and AJs break down upon calcium-deprivation (Wallis *et al.*, 2000). To test this condition, Caco-2 cells were grown for 18 days in conventional-calcium culture conditions and then were switched to a calcium-free medium for 60 min before fixation and immunofluorescence staining (Fig. 9). As a result of calcium deprivation, cells largely lost their contacts; nonetheless POF1B and desmosome proteins (PG, PKP2 and DSP) co-accumulated in the remaining adhesion contacts (see arrows), which were devoid of Claudin2 or E-cadherin (not shown). Thus POF1B is a desmosome-associated protein that is a good candidate for the formation of hyper-adhesive contacts in epithelial cells.

5.3 Colocalization of POF1B in intracellular particles closely associated with intermediate filaments in Caco-2 cells

It is known that DSP and PKP2 form particles that slowly traffic to desmosomes in close association with IFs (Kowalczyk and Green, 2013), whereas intracellular trafficking of PG and DSG is vesicle-mediated and microtubule-dependent (Green *et al.*, 2010; Nekrasova *et al.*, 2011). We first observed that also POF1B forms intracellular particles (red) precisely aligned along cytokeratin filaments (green) in sub-confluent Caco-2 cells (Fig. 10A). This POF1B particles accordingly colocalized with DSP and PKP2, but not with DSG or PG particles (Fig. 10B-C). The yellow panels, in Fig. 10B, exclusively display the colocalizing signal between red (POF1B) and green stainings (other markers). Moreover, when

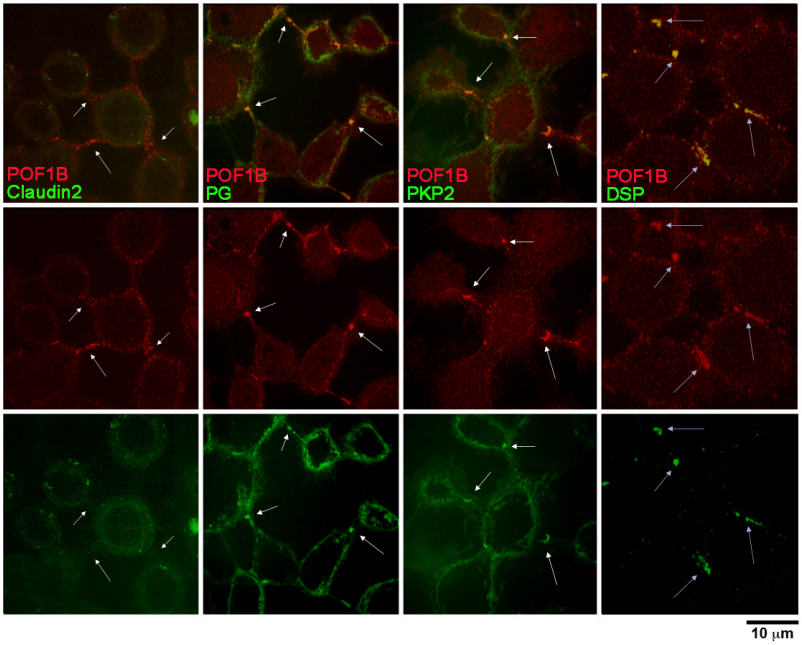

Figure 9

Figure 9. POF1B colocalizes with desmosomal proteins in hyper-adhesive contacts. *Confocal immunofluorescence analysis of calcium switch experiment performed in Caco-2 cells cultured for 18 days in regular medium and then switched for 1 h in calcium-free medium. Merged and single channel images are presented; arrows indicate the hyper-adhesive desmosomes.*

representative strings of particles for each confocal section were magnified and the intensity of fluorescence was analyzed by "plot profiles", a clear colocalization of POF1B particles with DSP and PKP2 was revealed, while only a portion of particles showed an apparent colocalization with PG. Almost no colocalization was

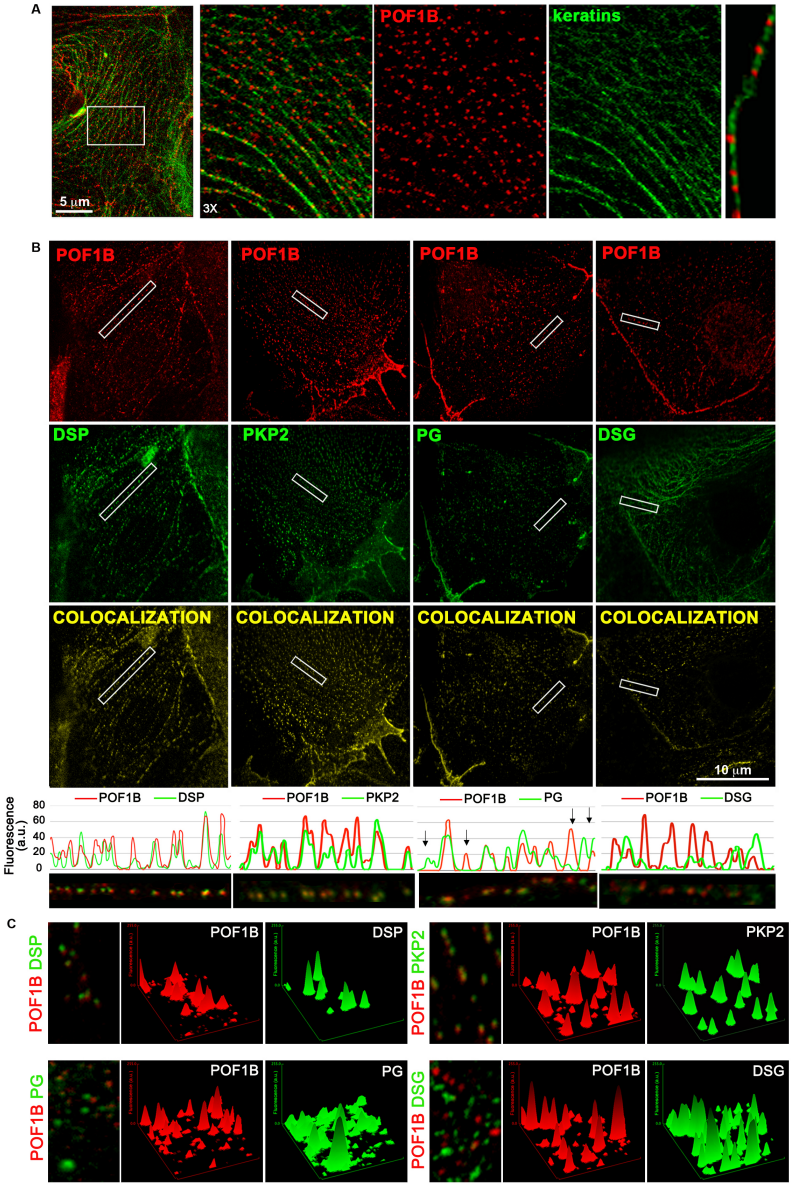

Figure 10

see next page for legend

Figure 10. POF1B colocalization with desmosome-associated proteins in cytoplasmic particles aligned along intermediate filaments. (A-C) *Double immunofluorescence confocal analysis of sub-confluent Caco-2 cells labelled for POF1B (red) and the indicated markers (green). Merged and single channel images are shown. (A) A representative intermediate filament double stained for POF1B is shown, (B) images representing only the colocalizing signal and plot profiles of magnified string of particles are presented. (C) Surface plot analysis of the area shown in the left. Individual fluorescence peaks are presented.*

observed between particles of POF1B and DSG (see the low number of colocalizing pixels in the corresponding yellow panel). These results indicate that POF1B is recruited to cell-cell adhesion in cytoplasmic particles that co-distribute with DSP and PKP2, but not with PG and DSG containing particles. The different distribution of particles stained for POF1B, DSP and PKP2, and particles/vesicles stained for PG and DSG is also demonstrate by the "surface plot" analysis (Fig. 10C). This analysis shows the distribution of all the particles (visualized as a peak of fluorescence) contained in the selected cytoplasmic area (left panels), and indicates a similar peak distribution between POF1B and DSP or PKP2, but not with DSG and PG, thus suggesting that POF1B may traffic to the cell-cell contacts in multiprotein complexes that are in close association with IFs.

5.4 Endogenous POF1B co-immunoprecipitates with K8 in Caco-2 cells

Since POF1B appeared strictly correlated with IFs in Caco-2 cells, we decided to investigate their interaction from a biochemical point of view, taking advantage of the co-immunoprecipitation technique. The analysis was performed both in sub-confluent and in fully confluent Caco-2 cells. As illustrated in Fig. 11 in both the situations POF1B co-immunoprecipitated with K8 suggesting that POF1B actually belonged to a K8-containing complex. It is worth of interest that the interaction occurs before adhesion recruitment and is maintained thereafter.

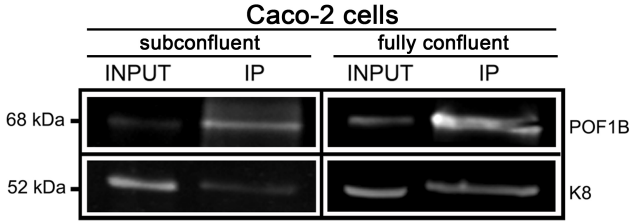

Figure 11

Figure 11. Co-immunoprecipitation of POF1B with K8. *Western blot characterization of the expression of POF1B and K8 in sub-confluent and fully confluent Caco-2 cells by immunoprecipitation with anti-POF1B antibodies. The presence of K8 in the immunocomplexes was determined by immunoprobing the nitrocellulose membranes with anti-K8 antibodies, and immunoprecipitation of POF1B was verified by using anti-POF1B antibodies. Two per cent of cell lysate was probed with the same antibodies (INPUT). Molecular weight (kDa) are indicated on the left.*

5.5 Role of POF1B N- and C-terminal domains in desmosome localization

We next investigated the role of POF1B domains in its localization. cDNAs encoding for human POF1B full-length, N-terminal (N-TER), and C-terminal (C-TER) domains, fused to green fluorescent protein, GFP (Fig. 12A) were transiently transfected in Caco-2 cells and in IOSE523 cells, an epithelial cell line of ovarian origin expressing neither DSP (Auersperg *et al.*, 1994) nor PKP2 and PG (data not shown).

In Caco-2 cells, the over-expressed full-length protein localized at cell-cell contact sites connected with IFs (see K8 staining) like the endogenous protein, thus indicating that the GFP tag did not impair the adhesion recruitment of the protein. In the IOSE523 cells lacking desmosomes, the protein did not show the cytosolic localization expected for a soluble protein, but instead exhibited a filamentous staining regularly aligned along K8 (Fig. 12B), indicating that the interaction between POF1B and IFs did not require DSP or PKP2. POF1B N-TER was largely cytosolic with a higher solubility than full-length, as observed through biochemical fractionation (data not shown). However, POF1B N-TER was also detected at cell-cell adhesion in Caco-2 cells (white arrows, Fig. 12C), but never in IOSE523 cells. Conversely, the C-TER construct is not recruited to cell-cell contacts, but does colocalize with K8 filaments in both Caco-2 and IOSE523 cells (Fig. 12D). The N-terminal domain of POF1B is therefore necessary and sufficient for interaction with desmosomal components, while the C-terminal domain mediate the connection with IFs.

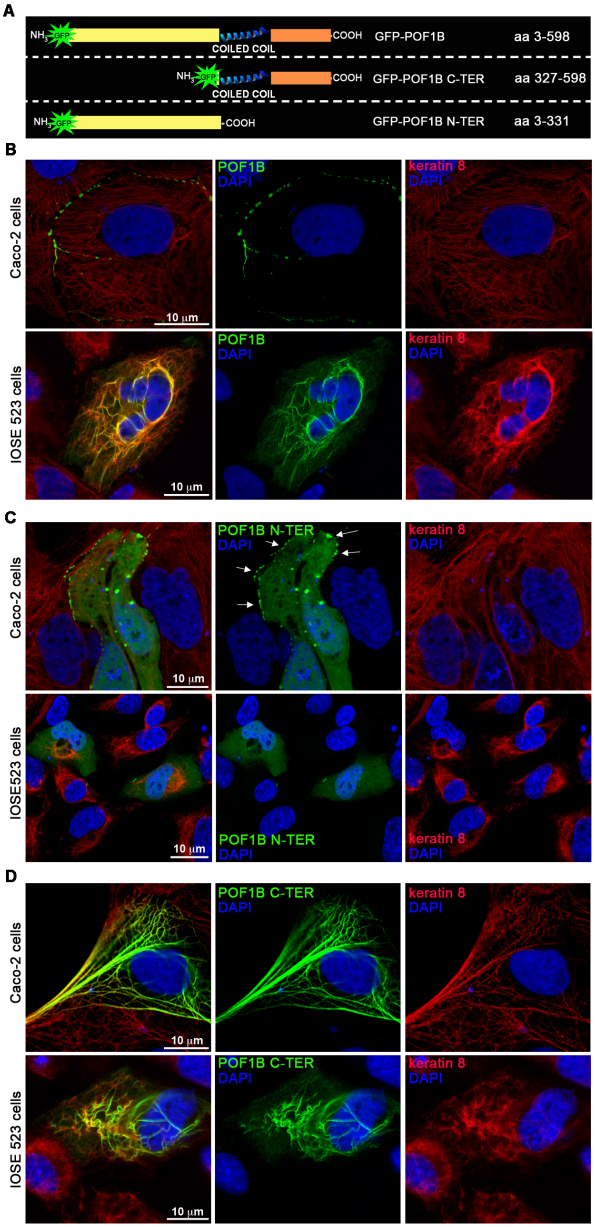

Figure 12 see next page for legend

***Figure 12. Role of POF1B domains for association with desmosomes and intermediate filaments**. **(A)** Schematic representation of GFP-POF1B constructs. Caco-2 and IOSE523 cells were transiently transfected with GFP-POF1B **(B)** GFP-POF1B N-TER **(C)** and GFP-POF1B C-TER **(D)**, and 48 h later they were fixed and stained for K8 (red) and DAPI (blu).*

To demonstrate that the observed POF1B filaments are due to association with IFs non requiring DSP or PKP2, K8-specific siRNA was co-transfected with GFP-POF1B into IOSE523 (Fig. 13). The K8-targeted siRNA was effective in down-regulating the protein (see the red staining of the intermediate filament in the confocal section and the quantification of the Western blot analysis revealing approximately a 50% of downregulation). GFP-POF1B and K8 lost their typical filamentous distribution in K8-downregulated cells, and POF1B showed a cytoplasmic spot-like pattern often colocalizing with residual K8, further suggesting their direct association. Since POF1B and DSP are both coiled-coil domain-containing proteins able to interact and form filaments with IFs through their C-terminal domain, and targeted to desmosomes via their amino-terminal domain (Stappenbeck and Green, 1992; Kouklis *et al.*, 1994), our data reveal structural and functional analogies between DSP and POF1B.

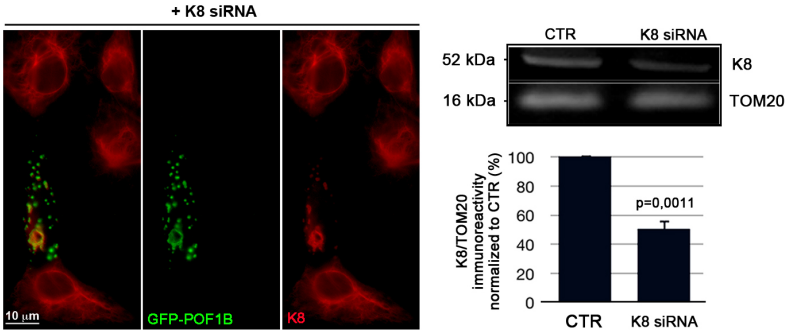

Figure 13

Figure 13. POF1B interacts with intermediate filament keratin 8 in IOSE523 cells. *IOSE523 cells transiently co-trasfected with K8 siRNA and GFP-POF1B were fixed 48 h later and stained for K8 or processed for Western blot analysis where blots were immunoprobed for K8 and TOM20 as a loading control; molecular weights (kDa) are indicated on the right of the blot. The graph on bottom represents the K8/TOM20 immunoreactivity in CTR and K8 siRNA-trasfected cells (%). Data are the mean +/- S.E.M: of three independent experiments; p value is*

5.6 Severe morphological defects in Caco-2 cells expressing POF1B shRNA

To verify the physiological role of POF1B we silenced the endogenous protein in human intestinal Caco-2 cells by transient transfection of shRNA1 and shRNA2 (small hairpin RNA) against POF1B (see Materials and Methods). Approximately 30-35% of the endogenous POF1B in Caco-2 cell lysates was silenced using both shRNAs (Fig. 14A), and this value agreed with the percentage of transfected cells (assessed by measuring the

percentage of GFP-expressing cells). The most relevant phenotype we observed in POF1B-silenced cells is that they lost their epithelial morphology and, when cultured for longer than 3

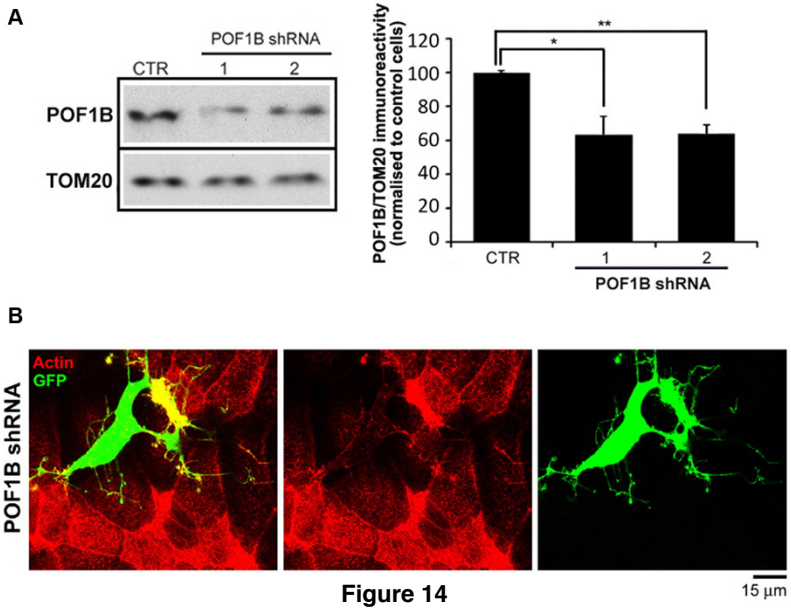

Figure 14

Figure 14. POF1B-silenced Caco-2 cells completely lost their epithelial morphology. (A) *A representative Western blot analysis is shown. Ten µg of total protein extracts from Caco-2 cells transiently transfected with the empty pSUPER vector (CTR) or with the vector containing shRNAs (1 and 2) were probed for POF1B expression, and the mitochondrial marker TOM20 as a loading control. The graph shows the POF1B expression level in silenced cells normalized to control cells; data are the mean +/- S.E.M. of four independent experiments. * p < 0,05; ** p < 0,01.* ***(B)*** *Caco-2 cells transiently expressing POF1B shRNA (green) cultured for > 3 days after transfection were stained with phalloidin (red).*

days, they detached from the monolayer (Fig. 14B). For this reason, we were never able to generate POF1B-downregulated stable clones. Because the apico-basal polarity was completely lost in cells expressing POF1B shRNA, these results indicate a key role for POF1B in the regulation of epithelial morphology.

5.7 Considerations about the results obtained in intestinal Caco-2 cells

In human intestinal Caco-2 cells POF1B is endogenously expressed at high levels, and exhibited the main features of desmosomes. First of all, POF1B clearly colocalized with desmosomal markers at cell-cell adhesion sites; in particular, it showed more similarities with DSP and PKP2 than with PG and DSG. This behavior suggested that POF1B is a desmosome-associated protein that traffics to plasma membrane in multi-protein complexes in tight association with DSP and PKP2. Moreover, these data demonstrated that POF1B is able to interact with intermediate filaments and that forms a complex with keratin 8.

The two most important assays that demonstrated the belonging of POF1B to desmosomal plaque were: 1) its enrichment in the NM-IF fraction (an ensemble of desmosomal proteins and intermediate filaments that showed Triton-X insolubility and calcium independence) and 2) its localization in hyper-adhesive desmosomes. In contrast to the other cell-cell junctions (TJs and AJs), indeed, desmosomes can reach a mature state, in which exhibit a complete calcium independence. When mature epithelial sheets are subjected to calcium

deprivation cells lose almost all their contacts and desmosomes remain the only spot welds persisting between adjacent cells. POF1B, as well as the other desmosomal markers, localized in these remaining contact sites, further supporting its involvement in desmosome functions.

Taking advantages of POF1B constructs, lacking the carboxy- or the amino- terminal of the protein, we suggested that, similarly to DSP, POF1B may interact with desmosomal partners with its N-terminal domain, whereas directly may interact with IFs through its C-terminal half. Further studies are required to clarify the specific partner/partners of POF1B among the desmosomal proteins. Moreover, the function of POF1B in the regulation of epithelial morphology was verified by silencing the endogenous protein using shRNAs. In this condition, POF1B-knockdown epithelial cells completely lost their polarized morphology and detached from the monolayer, indicating a key role for POF1B in the maintenance of cell-cell adhesion and cell survival.

6 chapter

Defects induced by the silencing of POF1B in human HaCaT keratinocytes

Since we demonstrated that POF1B is a desmosomal protein in Caco-2 cells, we investigated its functional role in keratinocytes where desmosomes are essential. The skin is a squamous stratified epithelium that, as well as the cardiac muscle, is routinely subjected to mechanical forces and, for this reason, requires more protection in comparison with other tissues and desmosomes are the cell-cell adhesions most dedicated to ensure the proper strength.

We were never able to generate POF1B-knockdown clones in Caco-2 cells, whereas we were able to establish stable silenced clones in human HaCaT keratinocytes.

6.1 Defects in adhesion strength in POF1B-silenced HaCaT keratinocytes

With the purpose to evaluate the role of POF1B in keratinocytes we first confirm its desmosomal localization also in this kind of cells, taking advantage of the HaCaT cells, a widely used human keratinocyte cell line.

POF1B is expressed in HaCaT cells (see Western blot analysis in Fig. 16) and here it localized at cell-cell adhesions exactly in sites contacting IFs (Fig. 15A). At the plasma membrane POF1B, as well as in Caco-2 cells, colocalized with DSP (Fig. 15C) and a clear colocalization between these two proteins was seen also in cytoplasmatic particles (Fig. 15D), that were aligned along intermediate filaments (Fig. 15B, see K8 staining).

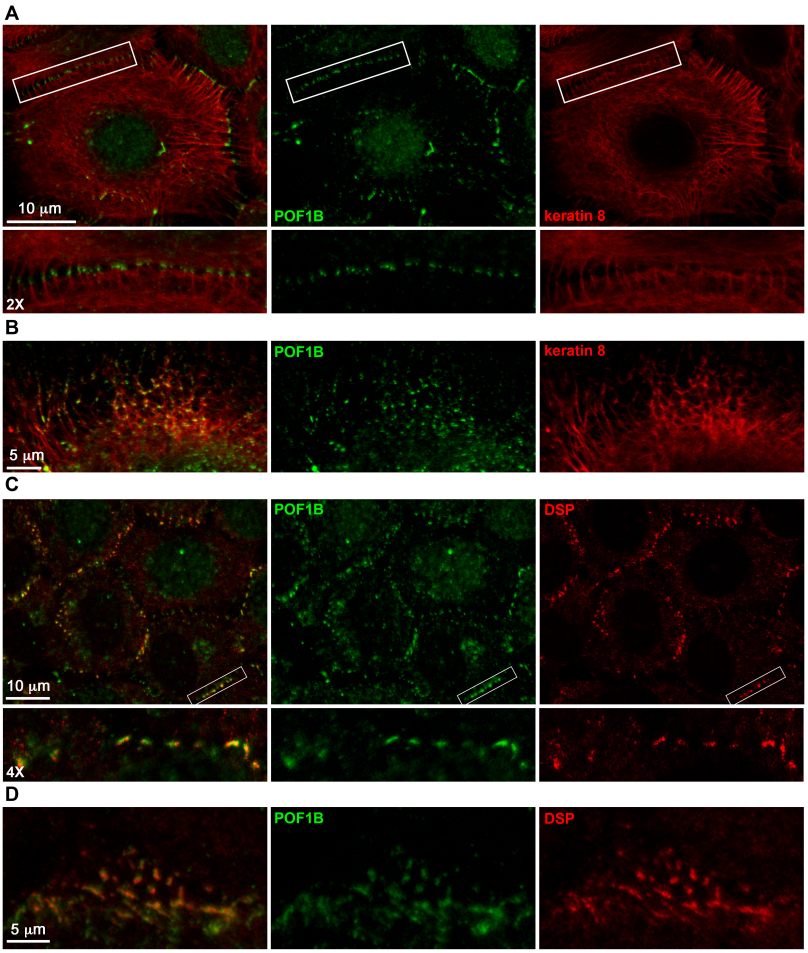

Figure 15

Figure 15. POF1B colocalizes with desmosomal proteins in human HaCaT keratinocytes. (A-D) *Double immunofluorescence staining performed in HaCaT cells fixed in methanol. POF1B is labelled in green while K8 and DSP are stained in red. Single and merged images with magnifications are presented.*

To evaluate the functional role of desmosomal POF1B in HaCaT cells, we generated stable clones expressing POF1B shRNA, already used for transient trasfections in Caco-2 cells (Fig. 14). As shown in Fig. 16, POF1B expression was greatly downregulated in all the characterized clones obtained with shRNA2 (~70-80%) and undetectable levels of the protein were found in shRNA1-expressing cl.1. POF1B-silenced clones maintained the expression of all the analyzed junctional markers and no changes were found in mock transfected pSuper clone.

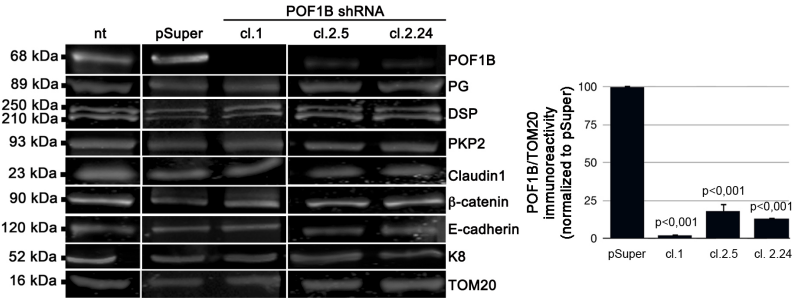

Figure 16

Figure 16. Generation of POF1B-downregulated clones in HaCaT keratinocytes*. A representative Western blot analysis in non transfected (nt), pSuper or POF1B-downregulated clones (cl.1, cl.2.5 and cl.2.24). Equal amounts of cell extracts were immunoprobed for the indicated markers, and TOM20 as a loading control. Molecular weights are presented on the left (kDa). A graph indicating POF1B/TOM20 immunoreactivity in each clone is presented on the right. Data are the mean +/- S.E.M. of three independent experiments; p values are indicated.*

This result differed from the results of POF1B downregulation experiments in Caco-2 cells, where stable clones could not be generated. This suggested that POF1B expression was dispensable for adhesions in HaCaT, but not Caco-2 cells.

To assess whether POF1B plays a role in adhesion strength and in resistance to mechanical stress we measured the ability of POF1B-silenced clones to recover from a scratch in wound healing experiments (Fig. 17), and the mechanical fragmentation of sheets of cells in dispase dissociation assays (Fig. 18). All the downregulated clones recovered more quickly from the scratch, consistently with the observation that defects in desmosome adhesion strength make cells more able to recover from the "wound" (South, 2004; Kundu *et al.*, 2008). However, when proliferation was inhibited by mitomycin C pre-treatment, silenced cells did not recover faster from the scratch than control cells, thus indicating a role for POF1B in the inhibition of proliferation but not in motility. In the absence of mitomycin C, the effect on cell proliferation was proportional to the level of POF1B knockdown, with greater levels of knockdown resulting in faster recovery. Evidence supporting the possibility of both anti- and pro-proliferative roles for desmosomal proteins has been described in the literature, and an inhibitory role on cell proliferation has been documented for PKP3 and PG (Chidgey and Dawson, 2007; Kundu *et al.*, 2008). The increased proliferation in the silenced HaCaT cells is likely to be secondary to a defect in cell-cell adhesion, but the mechanism underlying this effect remains to be clarified.

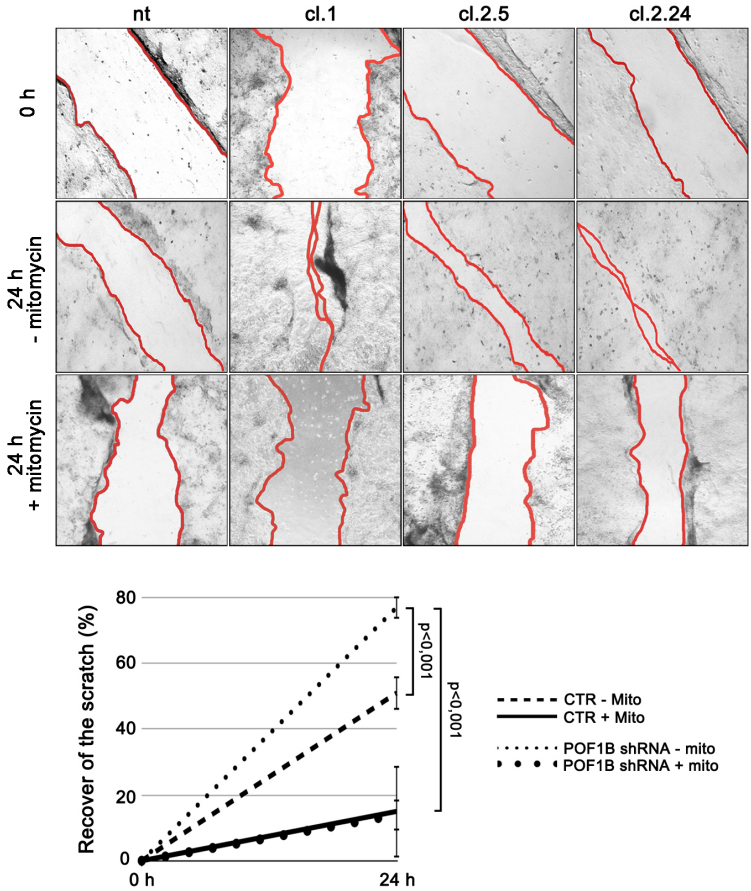

Figure 17

Figure 17. Downregulation of POF1B is associated with increased proliferation in HaCaT keratinocytes. *Wound healing assay in HaCaT cells treated or not with mitomycin C (mito) to block proliferation.The edge of the scratch is highlighted in red. Data in the graph represent the 24 hr recover from the scratch (0 h) and are the mean +/- S.E.M. of three independent experiments performed in triplicate. CTR are data from nt and pSuper transfected cells; p values are indicated.*

Treatment with the enzyme dispase allows cells to detach from the substrate without affecting the adhesion between neighboring cells and the number of fragments obtained after mechanical stress provides a measure of the integrity of the epithelium (Huen *et al*., 2002). Several fragments were measured in POF1B-silenced keratinocytes (Fig. 18), and the number of fragments was inversely related to the level of expression of POF1B, indicating that desmosomes require sufficient POF1B expression to counteract mechanical stress. This fragmentation defect was non observed in pSuper transfected cells.

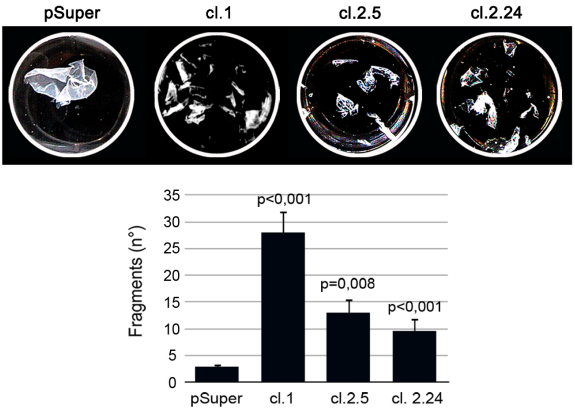

Figure 18

Figure 18. Functional defects in cell-cell adhesion strength in POF1B-downregulated HaCaT clones. *Dispase assay. Representative images (top) of cell sheets after mechanical stress and quantification of fragments (bottom) are shown. Data are the mean +/- S.E.M. of three independent experiments; p values are indicated.*

6.2 Defects in desmosome ultrastructure and cell stratification in POF1B-silenced HaCaT keratinocytes

Ultrastructural defects in desmosomes may account for the altered functions described in POF1B-silenced cells. As shown in Fig. 19, conventional electron microscopy revealed a lower density of desmosomes (see the sections on the left in which desmosomes are indicated by red arrowheads and the corresponding quantification). Magnifications (middle images) of portions of cell-cell contacts showed closely packed desmosomes to form a sort of zip that keep together membranes of adjacent cells in nt/pSuper cells (CTR), while clear defects (see the wide space between neighboring cells) were visible in POF1B-knockdown cells. Quantification of desmosome plaque length from higher magnifications of desmosomes revealed a clear reduction in this parameter in all the analyzed clones. CTR cells showed organized and well defined junctions, while desmosomes of silenced cells (cl.1 and cl.2.5) were interrupted with disorganized electron dense plaque. Moreover, multilayer thickness (reflecting the stratification of keratinocytes) and the length of membranes available for adhesions appeared reduced in POF1B-silenced clones compared to CTR cells, as a result of defective differentiation of the cells.

6.3 Conclusions of the results obtained in POF1B-knockdown HaCaT cells

With the purpose to understand the real function of POF1B in epithelial polarity we stably downregulated the protein in human

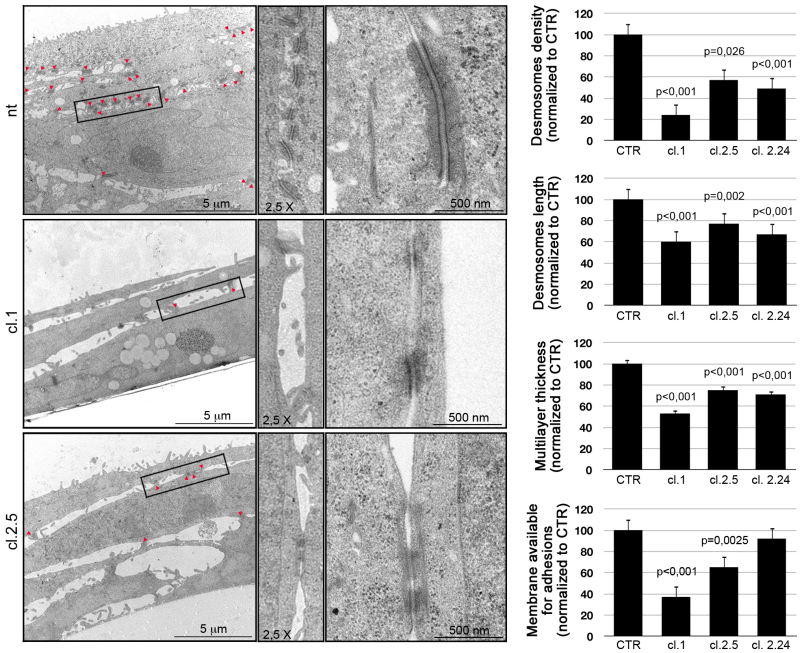

Figure 19

Figure 19. Ultrastructural defects of desmosomes in POF1B-knockdown HaCaT cells. *Conventional TEM. Left, low magnification images showing desmosomes (arrowheads); middle, magnified area; right, higher magnification. Graphs represent the quantification of desmosomes density and length, multilayer thickness and membrane available for adhesions. Data are the mean +/- S.E.M. of at least 15 sections for each clone; p values are indicated. CTR data represents the average between nt and pSuper transfected cells.*

keratinocytes (HaCaT cells) using shRNA. The silencing let us to appreciate the importance of POF1B in the maintenance of proper adhesion in epithelial cells. The downregulation, indeed, led to severe defects in the desmosomal plaque morphology:

POF1B-knockdown cells often exhibited only partial and not well organized desmosomes. As a consequence of these damages, confluent POF1B-downregulated cells were not able to resist to mechanical stress since the shacking of the dispase-treated sheets divided them into numerous fragments, an effect that has been never observed in nt or mock cells. Moreover, the silencing of POF1B caused an increase in cell proliferation without affecting cell migration. All these data confirmed that POF1B is required for the maintenance of proper adhesion strength in human keratinocytes and suggest that proliferation is a consequence of POF1B deficiency in desmosomes.

7
chapter

Localization of POF1B in epithelial tissues

The results obtained in Caco-2 cells and in HaCaT keratinocytes demonstrated that POF1B is a novel desmosomal protein. However, previous paper advanced the hypothesis of POF1B being a tight junction protein (Rizzolio *et al*., 2007), and the apical enrichment of POF1B described in MDCK cells confirmed a possible role of the protein at TJ level. With the purpose to clarify these discrepancies we decided to analyze the distribution of POF1B in different types of epithelia. Histologically, epithelia can be divided in four groups: simple, stratified, pseudo-stratified and transitional (Gartner and Hiatt, 2006).

7.1 POF1B colocalizes with DSP in human duodenum

Rizzolio and colleagues observed that POF1B co-distributed with the desmosomal cadherin DSG in human duodenum (Rizzolio *et al*., 2007). In this simple columnar epithelium we showed that POF1B perfectly colocalized also with DSP (Fig. 20). In particular, the vertical confocal sections (see the panel and magnifications on the right) revealed that POF1B, as well as the desmosomal protein DSP, enriched in the most apical portion of the lateral cell side. This apical accumulation is absolutely similar to that observed in human jejunum (Fig 1A), suggesting that in this type of epithelium desmosomes may accumulate at the upper level of adhesion.

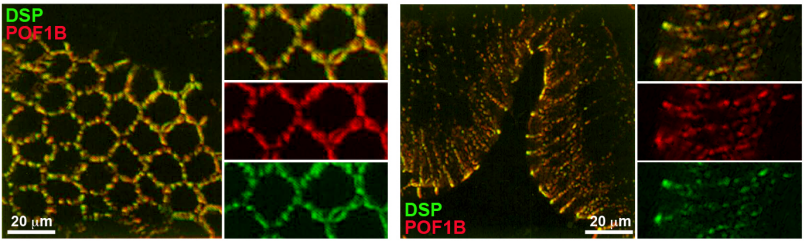

Figure 20

Figure 20. POF1B colocalizes with DSP in human duodenum. *Confocal analysis of immunofluorescence double staining in human duodenum. Staining for POF1B (red) and DSP (green): horizontal (left) and vertical (right) sections with magnifications are presented.*

7.2 Relocation of POF1B in pathological skin

An apparent discordance emerged from our data obtained in HaCaT keratinocytes (Fig. 15-19) and the previous work of Rizzolio and colleagues (Rizzolio *et al*., 2007). In this paper the authors clearly demonstrated that POF1B in human skin did not correlate with desmosome staining, since these cell-cell junctions are mainly localized in the spinous layer of the epidermis, where POF1B expression was undetectable. In healthy epidermis POF1B mainly localizes in the upper granular layers of the skin, where it also showed an atypical cytosolic distribution. DSP, on the contrary, localized in the more basal layers and did not accumulate in the more superficial layer of the skin (Fig. 21A).

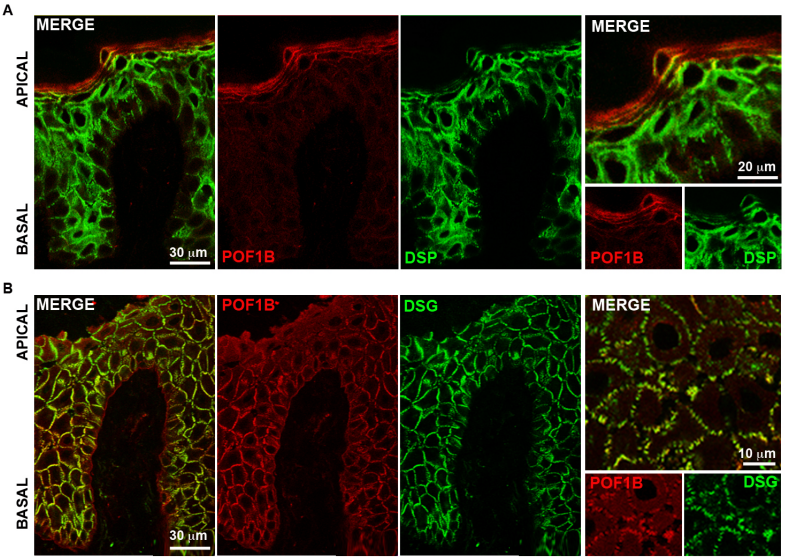

Figure 21

Figure 21. Different distribution of POF1B in human healthy and pathological skin. (A-B) *Confocal section of double staining immunofluorescence of human epidermis in healthy conditions (A) and affected by basal cell carcinoma (B). The tissues was stained for POF1B (red) and DSG or DSP (green). Merged and single channel images are presented for the entire organ length (left) and for a magnified part (right).*

A completely different distribution of POF1B emerged analyzing pathological human skin (Fig 21B). In this section of basal cells carcinoma, as well as in other squamous cells carcinomas (not shown), POF1B localized at cell-cell borders in all the layers and not just in the upper ones. In particular, as illustrated in the magnified panels, POF1B perfectly colocalized

with DSG; this spotted distribution of desmosomes in keratinocytes was visible probably because these tumoral cells were losing their contacts. It is especially worth of interest that these spotted accumulation of POF1B and DSG resembled the hyper-adhesive desmosomes already described in calcium-deprived Caco-2 cells (Fig. 9).

These observations led to the hypothesis that in human skin POF1B physiologically acts in the granular layer and it is not required in the basal layers. Conversely, when differentiation is impaired as it occurs in tumors, POF1B is recruited to desmosomes in all the layers, where it might contribute to maintain cell-cell adhesion.

7.3 Distribution of POF1B and DSG in monkey esophagus

The esophagus is one of the squamous stratified epithelium of the digestive system. As shown in Fig. 22, POF1B here localized again at cell-cell adhesion sites and it was present throughout the organ, from the basal layers to the more apical ones. Analyzing the magnified images we could not observed any difference with the localization of DSG that, anyway, showed a differential accumulation in the layers than POF1B. DSG, indeed, seemed more present in the basal layers and almost no staining was appreciable in the upper part of the tissue, where instead POF1B was expressed.

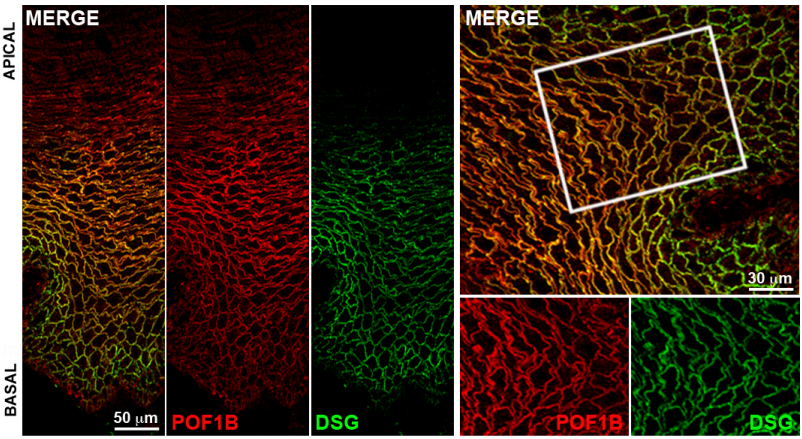

Figure 22

Figure 22. Analysis of the localization of POF1B and DSG in monkey esophagus. *Confocal section of double staining immunofluorescence of monkey esophagus. The tissue was stained for POF1B (red) and DSG 1,2 (green). Merged and single channel images are presented for the entire organ length (left) and for a magnified part (right).*

7.4 POF1B is expressed in all the layers in transitional epithelia

Transitional epithelia are characterized by the capability to considerably modify their appearance with stretching. During the relaxed state cells are small and polyhedral, whereas with the stretching cells become flatten and apparently slide past one another. One typical example of transitional epithelium is the

bladder. We analyzed the localization of POF1B in the murine bladder (Fig. 23). Here we could observe a distribution of POF1B in all the layers of the organ and a clear co-distribution with DSG. Interestingly, although present in all the cell adhesions throughout the organ, POF1B exhibited an enrichment in the most apical layer, where DSG, on the contrary, did not showed any particular accumulation.

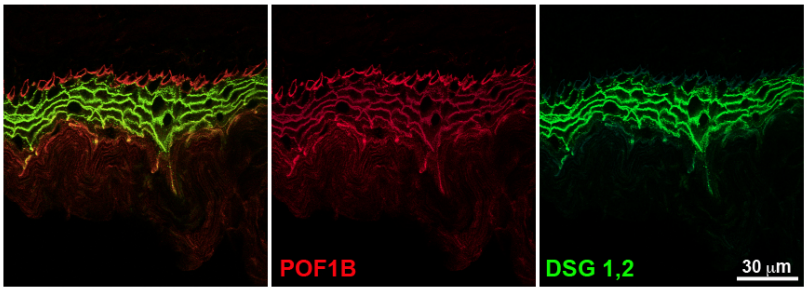

Figure 23

Figure 23. Distribution of POF1B in murine bladder. *Confocal double staining of murine bladder section. The tissue was stained for POF1B (red) and DSG 1,2 (green).*

Thus in all the epithelia, POF1B exhibits a polarized expression in the apical side, respectively corresponding to apical junctions in simple epithelia and upper layers in stratified epithelia. Moreover, the apical enrichment of POF1B, observed both in bladder and esophagus, suggested additional roles for POF1B than other desmosomal proteins in these tissues.

7.5 Final considerations regarding the localization of POF1B in epithelial tissues

POF1B is a protein mainly expressed in epithelial tissues. In simple epithelia, such as duodenum and jejunum, POF1B enriched at the most apical end of the cell sides and colocalized both with marker of TJs (JAM1, Fig 1A) and marker of desmosomes (DSP, Fig. 20). This observation led to two possible hypotheses: the first was that POF1B exhibited a double localization; the second was that in these kind of tissues desmosomes showed an apical localization, in correspondence to TJs.

Relying on the few analyses we have performed in stratified epithelia, we could observe two different behaviors of POF1B, depending on the capability of the tissue to differentiate. The skin is an organ in which cells gradually mature and differentiate from the basal to the cornified layers. In this tissue POF1B did not co-distribute with desmosomal proteins (generally found in the spinous layer), but showed a cytosolic enrichment in the granular layer, suggesting a possible additional role. When the epidermis lost its differentiated phenotype, for example with the onset of a tumoral process, POF1B displayed a distribution in all the epidermis layers (where nicely colocalized with DSG) and not just in the granular one. This localization throughout the tissue was observed also in other stratified tissues not incurring in differentiation processes, such as the bladder and the esophagus. Also in these organs POF1B may accomplish other role than desmosomes, since it exhibited an apical localization in layers devoid of desmosomes.

These observations let us to conclude that the desmosomal protein POF1B exhibits a wide spectrum of expression in both simple and stratified epithelia, where it could participate in processes not only associated with desmosomes.

8 chapter

Discussion and future perspectives

POF1B is a true desmosome-associated protein in epithelial cell lines and in simple and stratified epithelia

POF1B is a cytosolic protein showing selective expression in epithelial tissues and specific polarized localization at their cell-cell junction domain. These data led to the hypothesis of a role for POF1B in junction assembly and acquisition of surface polarization of epithelial cells. To unravel which junctions were dependent on POF1B, we first analyzed the localization of GFP-tagged POF1B stably expressed in MDCK cells. In this widely used polarized cell line, POF1B exhibited a peculiar junctional enrichment in two rings: one apical at the level of the TJs and one more basal. The upper enrichment was more continuous, whereas the basal accumulation of POF1B showed a more spotted pattern of distribution (Fig. 3C). The colocalization of the apical ring with TJ markers and the defects in TER acquisition of the mutant POF1B lacking this peculiar localization prompted the conclusion that POF1B is a TJ associated protein. However, a nice colocalization between POF1B and DSG has been previously documented in human duodenum (Rizzolio *et al.*, 2007), and endogenous POF1B in the Caco-2 human intestinal cell line showed a clear-cut colocalization with desmosomal proteins (Figs 7-10). These observations together with functional assays performed both in Caco-2 and in HaCaT cells confirmed that POF1B is essentially a desmosome-associated protein. Further analyses in MDCK clones performed by a triple immunostaining with the PAR3 marker of TJs and DSP marker of desmosomes and a calcium switch experiment confirmed that POF1B is a desmosome-associated protein also in these cells

(data not shown). The analyses also indicate that desmosomes are adhesions highly enriched at the apical level, between TJs and AJs and thus probably causing the misinterpretation of POF1B at TJs.

All the defects that we have found with the expression of the mutant POF1B (R329Q) in MDCK cells, might be explained by defects in desmosomes. For example our analyses indicate defects in the orientation of the mitotic spindle causing planar cell polarity alterations. Interestingly, DSP has been implicated in the regulation of microtubule organization by recruiting centrosomal proteins (Sumigray and Lechler, 2011).

The colocalization of POF1B with desmosomal markers has been here also demonstrated in the stratified epithelia (Fig. 22, 23), thus POF1B is a desmosomal protein both in simple (Fig. 7-10, Rizzolio et al., 2007, and Fig. 20) and in stratified epithelia. Contradictory results have been reported in epidermis, where POF1B enriches in the granular and not in the spinous layer of epidermis (Rizzolio et al., 2007 and in Fig. 21) as it would be expected for a desmosome-associated protein. Moreover, in the upper granular layers the protein displayed a cytosolic localization not correlating with the distribution of desmosomal markers (Rizzolio *et al.*, 2007).

Since our data demonstrate that POF1B is a desmosomal protein in keratinocytes: it colocalized with desmosomes in HaCaT cells (Fig. 14) and the downregulation of POF1B caused severe defects in the desmosomal plaque of these cells (Fig. 16), it is possible that POF1B expression in the upper layers of epidermis plays an additional role. POF1B could be implicated in the terminal phases of keratinocyte differentiation and, in this context, it may act in the cornification process. It is worth of

interest that, similarly to POF1B, the desmosomal DSG4 isoform does not enrich in the spinous layer and is confined in the granular layer of epidermis (Bazzi *et al*., 2006), and the authors suggested an additional role for this isoform in cornification.

Another not mutually exclusive possibility is that the higher expression of POF1B in the most external layers may confer resistance against the outside environment by strengthening desmosome adhesions in these cells. In line with this possibility, a switch in the localization of the protein was observed in pathological condition. In skin carcinomas, the localization of POF1B in desmosome along the entire length of the tissue was clearly evident. This behavior supports the idea that desmosomes require POF1B especially in cells forming the barrier against the external environments, such as those of the simple epithelia (e.g gastrointestinal tract) or in cells of the upper granular layer of multi-stratified cornified (epidermis) or not cornified epithelia (bladder and esophagus).

Involvement of POF1B in ARVC

Another tissue in which desmosomes are essential is the cardiac muscle. Desmosomes in these cells ensure proper mechanical coupling between cardiomyocytes, permitting the normal propagation of the electric impulse throughout the myocardium. Desmosomes in these cells are enriched at the intercalated discs (IDs) and, together with AJ and gap junction components, are responsible for the integration of structural informations and for cell-cell communications. The heart disease most strictly

correlated with desmosomes is the arrhythmogenic right ventricular cardiomyopathy (ARVC).

ARVC is a cardiac muscle disorder associated with heart failure, ventricular arrhythmias, and it is a prevalent cause of sudden cardiac death among young athletes (Thiene *et al*., 1988). In this disorder, the right ventricular myocardium is progressively replaced by adipose and fibrous tissue (Basso *et al.,* 1996). The disease is mainly caused by mutations of desmosomal proteins, founding the hypothesis that genetically determined disruption of desmosomal integrity and function might be the key factor leading to a cascade of events, including myocyte death and their replacement by fibro-fatty tissue. The myocardial replacement could be a process due to the release of proteins from the destabilized desmosomes and their translocation to the nucleus where they can promote the switch from myogenic to adipogenic gene expression. Progress in identifying mutations in desmosomal genes that lead to ARVC has been made, but in approximately half of the cases the defective proteins have not been identified.

Since we found that POF1B is a desmosomal protein particularly important in the maintenance of cell-cell adhesion strength, a role of the protein in the heart was predicted and preliminary data confirm that the protein is expressed in porcine cardiac muscle and colocalized with DSG at the IDs. The expression of POF1B has been also verified in human hearts by RT-PCR. Further analyses are required to clarify the localization of the protein in human cardiomyocytes and its possible role in this context.

9
chapter

Appendices

9.1 Material and methods

9.1.1 Molecular biology

Molecular biology techniques were used in the preparation of constructs.

PCR, restriction enzyme digestions of DNA, agarose gel electrophoresis, purification of DNA fragments from agarose gel, ligations of DNA fragments in proper vectors, preparation of competent bacteria, transformation of plasmid DNA into *E. Coli* and DNA extractions using alkaline lysis method were performed according to Maniatis protocols. MIDI preparations were performed according to the manufacture's protocol.

PCR

The polymerase chain reaction (PCR) is a biochemical technology widely used to amplify DNA across several orders of magnitude, generating thousands to millions of copies of a particular sequence.

To perform a PCR is fundamental the use of a heat-stable DNA polymerase, such as Taq polymerase, an enzyme originally isolated from the bacterium *Thermus aquaticus*. This DNA polymerase enzimatically assembles a new DNA strand from nucleotides, by using single-stranded DNA as a template and

DNA oligonucleotides (primers), which are required for the initiation of DNA synthesis.

A PCR reaction requires:

- two oligonucleotides primers (17-30 nt of length) that flank the target region (20 pmol each)
- target DNA (0,01-0,1 µg)
- Tris HCl 20 mM [pH 8,0]
- $MgCl_2$ 2 mM
- KCl 25 mM
- dNTPs (50 µM each)
- Taq Polymerase (2 U).

The method relies on thermal cycling, consisting of cycles of repeated heating and cooling of the reaction for DNA melting and enzymatic replication of the DNA. Typically, PCR consists of a series of 20-40 repeated cycles, in which each cycle commonly is composed of three temperature steps. The cycling is often preceded by a single temperature step at a high temperature (initialization step), and is followed by one hold at the end for final product extension (final elongation) or brief storage (final hold). The temperatures used and the time they are applied in each cycle depend on the enzyme used for DNA synthesis, the concentration of divalent ions and dNTPs in the reaction, and the melting temperature of the primers.

Initialization step: 94-96°C for 5 minutes.

Denaturation step: 94-98°C for 30 seconds. It causes the melting of the DNA template, yielding single-stranded DNA molecules.

Annealing step: 50-65°C for 30 seconds allowing annealing of the primers to the single-stranded DNA template. Typically, the

annealing temperature is about 3-5 degrees Celsius below the melting temperature of the primers.

Extension step: 72°C for 1 minute (if DNA template is < 500 bp), or for 3 minutes (if DNA template is > 500 bp). In this step the DNA polymerase synthesizes a new DNA strand complementary to the DNA template strand by adding dNTPs that are complementary to the template in 5' to 3' direction.

Final elongation: 70-74°C for 5-15 minutes after the last PCR cycle to ensure that any remaining single-stranded DNA is fully extended.

Final hold: 4°C for an indefinite time. This step can be employed for short-term storage of the reaction.

The resulting PCR product can be analyzed on an agarose gel.

The primers used for the generation of the constructs are described in the "Constructs" section.

Restriction enzyme digestion

Restriction endonucleases are bacterially derived enzymes that recognize specific sequences within double-stranded DNA. They can be divided into three groups: type I and III enzymes carry modification (methylation) and an ATP-requiring restriction (cleavage) activity in the same protein; type II restriction enzymes consist of a separate restriction endonuclease and modification methylase and are used in molecular cloning These enzymes generally recognize an inverted repeat palindrome and cut DNA leading to a symmetrical cleavage of both strands resulting in either blunt- or sticky-ends. Blunt ends are universally compatible

with other blunt-ended DNA and possess a 5' phosphate group to promote ligation. Sticky ends, on the other hand, are stretches of single-stranded DNA that is capable of self-ligation or ligation with a complementary region of DNA.

Each restriction enzyme requires optimal reaction conditions; the most important parameters are the temperature of incubation and the composition of the buffer. Generally, restriction enzymes can be divided in three groups according to the buffer characteristics: those that work best at high ionic strength (NaCl 100 mM, Tris HCl 50 mM [pH 7,5], $MgCl_2$ 10 mM, and Dithiothreitol (DTT) 1 mM), those that prefer medium ionic strength (NaCl 50 mM, Tris HCl 10 mM [pH 7,5], $MgCl_2$ 10 mM, and DTT 1 mM) and those that have a preference for buffers of low ionic strength (Tris HCl 10 mM [pH 7,5], $MgCl_2$ 10 mM, and DTT 1 mM).

The digestions of DNA with restriction enzymes were carried out in a total volume of 20 µl as follows:

- 0,2-1 µg of DNA was mixed with water to give rise a volume of 18 µl in a sterile Eppendorf tube.
- 2 µl of the appropriate 10X digestion buffer was added, and the tube was mixed by tapping.
- 1 U of restriction enzyme was added and, after mixing, the tube was incubated at the appropriate temperature for the required time.

After the incubation, the cleavage of the DNA could be checked directly on an agarose gel.

Agarose gel electrophoresis

Electrophoresis performed on agarose gel is the standard method used to separate, identify and purify DNA fragments.

Bands of DNA in the gel were stained with low concentrations of the fluorescent, intercalating dye ethidium bromide. The electrophoretic migration rate of DNA through agarose gels depends on the molecular size of DNA, the agarose concentration, the conformation of the DNA and the applied current. The buffer in which the electrophoresis was performed is the Tris-acetate buffer (TAE: Tris-acetate 40 mM and ethylenediaminetetraacetic acid [EDTA] 2 mM).

The preparation of the agarose gel consisted of:

- The correct amount of powered agarose was added to a measured quantity of TAE.
- The slurry was boiled in a microwave until the agarose dissolving.
- Ethidium bromide was added to a final concentration of 0,5 µg/ml.
- A mold for the agarose gel was created sealing the edges of a glass plate with a tape.
- The warm agarose solution was poured into the mold and, near one end of the gel, the comb was put to create the sample wells with the teeth of the comb.
- When the gel was completely set, the comb and the tape were removed and the gel was put into the electrophoresis tank.
- The electrophoresis buffer was added just enough too cover the gel.

- Samples were mixed with the loading buffer (30% glycerol and 0,025% bromophenol blue in water) and were loaded into the wells of the submerged gel.
- After a proper time of run, the DNA bands could be detected and analyzed at the ultraviolet light.

Purification of DNA fragments from agarose gel

This protocol was performed using the QIAEX II Gel Extraction Kit (QIAGEN). With this protocol DNA fragments were extracted and purified from agarose as follows:

- The DNA band was excised from the agarose gel with a clean and sharp scalpel.
- The slice of gel containing the band of interest was solubilized in a specific volume of buffer QX 1, according to the weight of the slice. This reaction occurred at 50°C for 10 minutes.
- The DNA was absorbed to the QIAEX II silica-gel particles in the presence of high salt.
- The solubilized mix was centrifuged for 30 sec and the supernatant was removed.
- The pellet was washed with the buffer QX 1.
- After one centrifugation and the removal of the supernatant the pellet was washed twice with the buffer PE.
- The pellet was then air-dried for 15 minutes.
- The DNA was finally eluted with a low-salt solution, such as Tris buffer or water.

Ligation of DNA fragments in proper vectors

Ligation consists of joining two strands of DNA between the 5´-phosphate and the 3´-hydroxyl groups of adjacent nucleotides. It allows the insertion of a DNA fragment into a plasmid. The ligase we have used is the T4 Ligase that can ligate cohesive ends of DNA and blunt ended DNA.

The ligation mix was assembled in 10 µl of total volume and consisted of:

- 15 ng of linearized plasmid DNA.
- Threefold molar excess (compared to the plasmid) of the fragment to be subcloned.
- A proper amount of ligation buffer (Tris HCl 50 mM [pH 7,4], $MgCl_2$ 10 mM, DTT 10 mM, spermidine 0,5 mM, ATP 2 mM, hexamine cobalt chloride 2,5 mM, and bovine serum albumin [BSA] 20 µg/ml).
- A proper amount of T4 Ligase.

The reaction occurred at 19°C overnight and, after that, the enzyme was inactivated heating the mix up to 60°C for 20 minutes. Then, 1-5 µl of the reaction were transformed into 100 µl competent cells.

Preparation of competent bacteria

The competence of bacteria is a prerequisite by which cells can accept extra-chromosomal DNA such as plasmids. The protocol used was the following:

- One colony from LB (Luria Bertani) plate (BactoAgar 1,5%, Bacto-tryptone 1%, Bacto-yeast extract 0,5%, and NaCl 1%) was inoculated into 2 ml of LB medium (Bacto-tryptone 1%, Bacto-yeast extract 0,5%, and NaCl 1%) and was shaken at 37°C overnight.
- 1 ml of overnight cell culture was inoculated into 100 ml LB medium and was shaken vigorously at 37°C to $OD_{600} \sim 0,4$.
- The culture was chilled on ice for 10 minutes.
- Cells were centrifuged for 20 minutes at 4°C at 2500 rpm and then the supernatant was removed completely.
- Bacteria were resuspended in 20 ml of $CaCl_2$ 0,1 M.
- Cells were kept on ice for 30 minutes.
- Cells were centrifuged as above and, after the removal of the supernatant, they were resuspended in 4 ml of $CaCl_2$ 0,1 M and incubated on ice for 1 hour.
- 15% glycerol was added to the solution and 0,5 ml aliquots of the competent bacteria were frozen on liquid nitrogen and then transferred to -80°C freezer.

Transformation of plasmid DNA into *E. coli*

The transformation allows the insertion of plasmid DNA into competent bacteria. The procedure was the following:

- 1-10 ng of DNA plasmid were added to 100 µl competent bacteria in a tube.
- The mix was kept on ice for 30 minutes.
- The tube was transferred to a water bath, preheated to 42°C for 45 sec, and then incubated on ice for 1 minute.

- 900 µl of LB medium were added to the mix and the tube was incubated at 37°C, where it was shaken for 1 hour.This period allowed the bacteria to recover and to begin to express antibiotic resistance.
- 300 µl of transformed bacteria were spread onto selective plate of top agar, and the inverted plate was incubated overnight at 37°C.
- After this period colonies appeared.

DNA extraction (MINI and MIDI preparations)

Different procedures are available for isolating DNA plasmids grown from bacterial colonies. These techniques yield enough DNA for analysis by restriction enzymes, gel electrophoresis, Southern blot and DNA sequencing.

Small-scale isolation of plasmid DNA (MINI preparations)

The protocol was the following:

- 2 ml of LB, containing the appropriate antibiotic, was inoculated with a single bacterial colony and incubated overnight at 37°C with vigorous shaking.
- The following morning 1,5 ml of the overnight culture were centrifuged in a 2 ml sterile Eppendorf tube for 5 minutes.
- The supernatant was removed and the pellet was resuspended in 100 µl of Solution 1 (glucose 50 mM, Tris HCl 25 mM [pH 8,0], and EDTA 10 mM [pH 8,0]).

- 200 µl of Solution 2 (sodium dodecyl sulfate [SDS] 1% and NaOH 0,2 N) were added to the tube.
- The tube was mixed gently by inverting.
- 150 µl of Solution 3 (potassium acetate 5 M and 11,5% glacial acetic acid) were then added and the tube was vigorously mixed on vortex for 10 sec.
- Tube was kept on ice for 5 minutes.
- The tube was centrifuged for 5 minutes in an Eppendorf centrifuge.
- The obtained supernatant contained the plasmid DNA; to achieve its precipitation an equal volume of isopropanol was added and the tube was kept at room temperature for 2 minutes.
- The tube was centrifuged at room temperature for 15 minutes.
- 150 µl of 70% cold ethanol were then added.
- The tube was centrifuged and, after the removal of the supernatant, the pellet was air-dried for 15 minutes.
- The DNA was resuspended in 50 µl of TE (Tris HCl 10 mM [pH 7,6] and EDTA 1 mM [pH 8,0]), containing RNase 100 µg/ml.

Large-scale isolation of plasmid DNA (MIDI preparations)

The MIDI preparations were performed according to QIAGEN Plasmid *Plus* Midi kit. The protocol was the following:

- 2 ml of LB, containing the appropriate antibiotic were inoculated with a single bacterial colony and incubated overnight at 37°C with vigorous shaking.

- The following day, 400 ml of LB medium were inoculated with 400 µl of the overnight culture, always in the presence of the antibiotic, and were shaken overnight at 37°C. At this point, there were enough bacteria to permit proper extraction of large amount of plasmid DNA.
- Bacteria were centrifuged at 4°C, for 15 minutes at 6000 g.
- The pelleted cells were resuspended in 4 ml of Buffer P1, allowing the lysis of bacteria.
- 4 ml of Buffer P2 were added to the tube and, after gentle inverting, the tube was incubated at room temperature for 3 minutes.
- 4 ml of Buffer S3 were added and immediately the lysate was mixed by inverting the tube 4-6 times. With this buffer in the tube appeared a precipitate containing the genomic DNA, proteins, and cell debris.
- The lysate was then transferred to a QIAfilter cartridge and incubated at room temperature for 10 minutes; in this period the precipitate started to float.
- With a plunger the cell lysate was filter through the QIAfilter cartridge in a new tube.
- 2 ml of Buffer BB were added to the cleared lysate and mixed by inverting 4-6 times.
- The lysate was transferred to a spin column with a tube extender attached on the vacuum manifold.
- Switching on the vacuum, rapidly the solution seeped through the filter in the spin column.
- 700 µl of Buffer ETR were added to the spin column to wash the DNA.
- The column was attached to a new tube and then was centrifuged for 1 minute.

- DNA was washed again in the same way using the Buffer PE.
- The column was placed in a new clean Eppendorf tube and the DNA was eluted in 60 µl of TE with a 1 minute-centrifugation.
- The obtained purified plasmid DNA was stored at -20°C and, then used for cell trasfections.

Constructs

Full-length human POF1B (see *Cartoon 17*), corresponding to amino acids 3-589 of POF1B (NCBI database accession #Q8WVV4), was fused to the C-terminus of GFP by subcloning the PCR product into the XhoI-BamHI restriction fragment of the mammalian expression vector pAcGFP1-C1 (Clonetech).

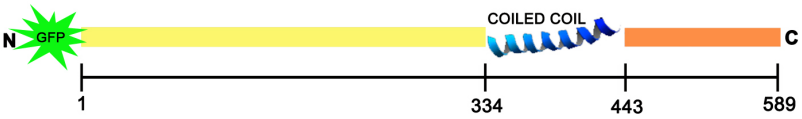

Cartoon 17. *Structure of GFP-POF1B*

POF1B R329Q (*Cartoon 18*) was generated by means of QuikChange Site-directed Mutagenesis (Stratagene) PCR using GFP-POF1B as template and complementary oligo-nucleotides containing AG instead of GA at position 986-987 of the coding sequence (oligo upper 5'-GTCTGATAAGTCACTCC**AG**CTAGT GCTGTCCAC-3' and the complementary oligo lower). A BpmI site

was created by the substitution and used to identify the mutagenized product.

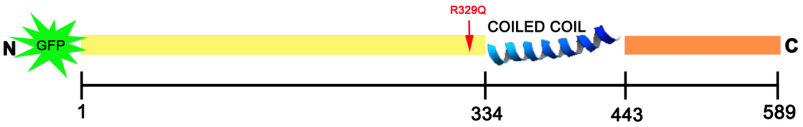

Cartoon 18. *Structure of GFP-POF1B R329Q*

POF1B N-TER (aa 3-331 of POF1B, see *Cartoon 19*) was generated by introducing an in-frame stop codon at amino acid position 331. A PCR was performed using GFP-POF1B as template and the following oligonucleotides: upper 5'-TCCG GACTGAATTCTCGATCGA-3' and lower 5'-TAAGGA TCCACTACACTAGTCGGA-3'; the product was inserted into EcoRI-BamHI restriction fragment of the mammalian expression vector pAcGFP1-C1.

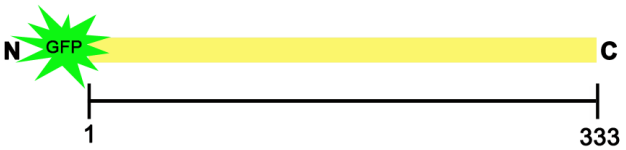

Cartoon 19. *Structure of GFP-POF1B N-TER*

POF1B C-TER (aa 327-589 of POF1B, see *Cartoon 20*) was obtained carrying out a PCR with the following oligonucleotides: upper 5'-GTCTGAGAATTCACTCCGACTA-3' and lower 5'-TCAGTTATCGAATTCCGGTG-3'; the PCR product was inserted into the mammalian expression vector pEGFP-C1 (EcoRI-BamHI restriction fragment).

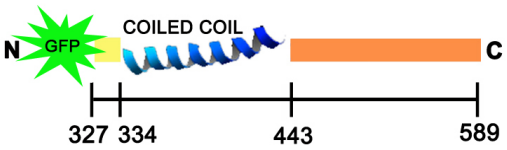

Cartoon 20. *Structure of GFP-POF1B C-TER*

To create the GFP-POF1B shRNA constructs, two 19-base pair sites within human POF1B were chosen using on-line biocomputer tools, and pairs of complementary oligonucleotides containing the following target sequences were synthesized by Sigma Aldrich: 5'-GCAAGGACTTCAAGACTCA-3' (shRNA1), corresponding to the amino acids 375-381 in the coiled-coil domain region, and 5'-AATGCCATCATCACATTAT-3' (shRNA2), corresponding to the amino acids 181-187. These sequences did not have any significant homology to other genes in the human genome database. The forward and reverse oligos were annealed and cloned into BglII-XhoI restriction sites of the pSUPER.gfp/neo RNAi system (OligoEngine), and the resulting plasmid was amplified. All the plasmid sequences were verified by means of automated sequencing to exclude unwanted substitutions.

mCherry-Keratin 8 was a kind gift of Dr R.E. Leube (Leube *et al.*, 2011) and double-stranded siRNA oligonucleotides against K8 were purchased from Sigma Aldrich, the sequence used is 5'-CAUGUUGCUUCGAGCCGUCtt-3' (Long *et al*., 2006).

9.1.2 Cell cultures

MDCK cells

MDCK (Madin-Darby canine kidney) cells were derived by S.H. Madin and N.B. Darby from the kidney tissue of an adult female cocker spaniel in 1958 (Madin and Darby, 1958). This cell line is widely used as epithelial model to study cell polarity. MDCK cells form polarized monolayers that maintain the morphological and functional properties of the tissue of origin (Misfeldt *et al.*, 1976; Cereijido *et al*., .1978). Moreover, when cultured in 3D systems such as type I collagen or matrigel, they form cysts, spherical monolayers of polarized cells that enclose a central lumen. This culture system, simulating the real environment of these cells, allow to study polarity in a more physiological condition.

This cell line was cultured in MEM (Minimum Essential Medium, Euroclone), supplemented with 1% L-glutamine (Euroclone), 100 U/ml Penicillin/Streptomycin (P/S, Euroclone) and 10% Fetal Bovine Serum (FBS, Euroclone). Cells were grown at 37°C and 5% CO_2. For morphological and functional (transepithelial electrical resistance, TER and Ca^{++} switch) studies, the MDCK cell lines were seeded at a density of $2{,}5x10^5$ cells/cm^2 onto Transwell filter inserts (0,4 µm pore size; Corning Costar) and analyzed more than 3 days later unless otherwise indicated. For the biochemical assays, the cells were plated at the same density on Iwaki or Falcon tissue culture dishes and used 3 days or more after plating unless otherwise indicated. For the calcium-switch protocol, the original method (Cereijido *et al.*, 1978) was modified as follows: MDCK cell lines grown to confluency ($2{,}5x10^5$ cells/cm^2) on Transwell filter inserts for 4

days were incubated in calcium-free DMEM (Gibco) supplemented with 1% L-glutamine and calcium to a final concentration of 5 µM for 2 hours. The cells were then grown in complete medium (1,8 mM Ca^{++}) for 24 hours, and cell-cell contact formation was assessed at the indicated time by measuring TER.

Caco-2 cells

Caco-2 cell line is an epithelial continuous line of human cells derived from colorectal adenocarcinoma. They were isolated by Dr J. Fogh in 1975 (Fogh and Trempe, 1975), as a heterogeneous cell line having both enterocytic and colonocytic characteristics. These cells in culture are able to differentiate and polarize, morphologically and functionally recapitulating enterocytes main features. Caco-2 cells express cell-cell junctional proteins and, generally, they are used not as individual cells, but as a confluent polarized monolayer. The electrical properties and ionic conductivity characteristics of Caco-2 cells resemble those of colonic crypt cells (Volpe, 2008). Often, Caco-2 cells are widely used in the pharmaceutical industry as an *in vitro* model of the human small intestinal mucosa to predict the absorption of orally administered drugs (Hidalgo *et al*., 1989). Caco-2 cells growing medium is composed by DMEM (Dulbecco's Modified Eagle Medium, Euroclone) supplemented with 1% L-glutamine, 100 U/ml P/S and 10% FBS. Cells were grown at 37°C and 5% CO_2. For x-z confocal sections Caco-2 cells were grown for 7 days on Transwell filters, whereas for x-y confocal images cells were plated sub-confluent or fully confluent on glass

coverslips. For the biochemical assay, the cells were plated confluent on Corning tissue culture dishes and were processed for fractionation assay 3 days later. For transfection experiments Caco-2 cells were plated sub-confluent on glass coverslips. In some experiments Caco-2 cells were maintained in a low-calcium medium, composed of calcium-free DMEM, 1% L-glutamine, 100 U/ml P/S and 10% dialyzed FBS, supplemented with 5 µm $CaCl_2$.

IOSE 523 cells

IOSE523 cell line is a human cell clone immortalized from the ovarian surface epithelium (OSE cells), that is a modified mesothelium leading to most human ovarian carcinomas (Auersperg *et al.*, 1994). The immortalized cell lines were attained by transfecting low-passage cultures of OSE cells with SV40 large-T antigen by Researchers at the University of British Columbia and the affiliated BC Children's & Women's Hospital. IOSE cells uniformly express laminin and collagen IV but do not express E-cadherin and desmoplakin. These cells grow in a medium composed of DMEM supplemented with 1% L-glutamine, 100 U/ml P/S and 10% FBS. IOSE523 cells were grown at 37°C and 5% CO_2. For transfection experiments cells were plated on glass coverslips and analyzed by biochemical and morphological assays 3 days later.

HaCaT cells

HaCaT cells are human spontaneously immortalized keratinocytes that have been demonstrated to exhibit a high differentiation potential under *in vivo* and *in vitro* conditions and, for these reasons, are widely used as a substitute for normal human keratinocytes (Boukamp *et al.*, 1988; Breitkreutz *et al.*, 1998). HaCaT cells growing medium consists of DMEM supplemented with 1% L-glutamine, 100 U/ml P/S, 1% non-essential amino acids (NEAA, Sigma Aldrich), 1% vitamin (Sigma Aldrich) and 10% FBS. Cells were grown at 37°C and 5% CO_2. The method for the generation of stable clones is described below. For immunofluorescence experiments performed on non trasfected cells (nt), HaCaT cells were plated on glass coverslips.

9.1.3 Transfections

Transient trasfections

Caco-2 cells were transiently transfected with polyethylenimine (PEI, PolyScience Inc.) according to the manufacturer's protocol. Briefly, 20.000 cells were seeded in a 12-wells plate on glass coverslips. After 24 hours the cells were transfected using 40 µl of PEI and 0,5 µg of DNA. The cells were then incubated in the mix containing PEI-DNA in complete medium. After 4 hours incubation, the mix was replaced with fresh growing medium. The cells were fixed 20 minutes in 4% paraformaldehyde + 4% sucrose or 10 minutes in ice-cold methanol 48 hours after transfection.

IOSE523 cells were transiently transfected with Lipofectamine 2000 (Invitrogen) following the manufacturer's protocol with modifications. In particular, the cells were seeded at a density of $0,15x10^5$ cells/cm^2 in a 12-wells plate, on glass coverslips. After 24 hours the cells were transfected using 2 µl of Lipofectamine 2000 and 0,5 µg of DNA or 50 nM siRNA. The cells were then incubated in the mix containing Lipofectamine and DNA in the absence of serum and antibiotics. After 4 hours incubation, the mix was replaced with complete growing medium. Forty-eight hours later cells were fixed 20 minutes in 4% paraformaldehyde + 4% sucrose or 10 minutes in ice-cold methanol for immunofluorescence or were harvested for Western blot analysis.

Stable trasfections

MDCK were stably transfected using the Ca-PO_4 method as previously described (Perego *et al.*, 1999). The stable cell lines were selected on the basis of growth in the antibiotic G418 (0,6 mg/ml) (Sigma Aldrich), and the expression of the constructs was assessed by fluorescence microscopy and Western blotting. Four cell lines expressing the full-length protein (WT 5, 7, 10 and 13) and three cell lines expressing the R329Q variant (Mut 5, 6 and 12) were chosen on the basis of their homogeneity and levels of expression.

HaCaT cells were stably transfected using PEI. This method was used to generate HaCaT cells stably expressing GFP-pSuper (mock), GFP-POF1B shRNA 1 (cl. 1), GFP-POF1B shRNA 2 (cl. 2.5 and cl. 2.24). HaCaT cells were seeded at the

density of 0,25x10^5 cells/cm^2 in a 6-wells plate. Twenty-four hours later cells were trasfected using 1 µg of plasmid DNA and 80 µL of PEI following the manufacturer's protocol. Clones were selected on the basis of growth in the antibiotic G418 (0,6 mg/ml) (Euroclone), and the expression of the constructs was assessed by fluorescence microscopy and Western blotting. Clones were chosen on the basis of their homogeneity and levels of exogenous construct expression.

9.1.4 Transepithelial electrical resistance (TER)

TER measurement is considered the most convenient, reliable and non-destructive method to evaluate the growth of epithelial tissue cultures *in vitro and the functionality of TJs.* It is, in fact, a measure of the barrier to small ions in an experimentally applied electrical field in the bathing media (Fanning *et al*., 1999).

The TER values were obtained by subtracting the contributions of the filter (no cells) and bathing solution and were expressed as ohms x cm^2 (Balda *et al*., 1996), following the manufacturer's instructions. Three experiments, each one with three parallel filters from control and transfected MDCK cell lines were measured for each time point.

9.1.5 Organotypical 3D cultures

Organotypical 3D MDCK cell cultures were used for cyst formation as previously described (Vieira *et al*., 2006). Briefly, 25 µl of cell suspension containing 5x10^4 cells were mixed with 50 µl

of matrigel (Becton Dickinson); 12 µl drops were placed on glass coverslips into a 6-wells plate and allowed to solidify for 1 h at 37°C before culture medium was added. The cultures were grown for the indicated time and then were fixed for 1 hour in 4% paraformaldehyde + 4% sucrose and processed by immuno-fluorescence.

9.1.6 Detergent extraction experiments

Detergent extraction experiments were carried out as described (Blikstad and Carlsson, 1982). MDCK cells were treated for 30 minutes using extraction buffer (1% Triton X-100, NaF 100 mM, KCl 50 mM, $MgCl_2$ 2 mM, EGTA 1 mM, KPO_4, 10 mM [pH 7,5], sucrose 0,5 M) supplemented with phenylmethylsulfonylfluoride (PMSF) and protease cocktail inhibitor (Sigma Aldrich) to block the partial depolymerization of actin seen in other buffers. After extraction, the cell extracts (G-actin fraction) were centrifuged at 13.000 g for 20 minutes, cell matrices (F-actin fraction) were collected by scraping the dish in 0,1 ml extraction buffer with a rubber policeman, and both fractions were solubilized in 0,1 ml SDS denaturation buffer and equal volumes of each fraction were analyzed by immunoblotting for actin content.

9.1.7 F-actin FACS assay

CTR MDCK cells (M) and cells expressing POF1B WT and POF1B R329Q (Mut) were trypsinized and fixed in 4% paraformaldehyde in phosphate-buffered saline (PBS) for 5

minutes before and after permeabilization. Cells were stained with FITC-phalloidin (Jackson ImmunoResearch) to detect F-actin. For all samples, 10.000 gated cells were analyzed, and the mean F-actin content, as determined by the phalloidin staining, was quantified using the Cell Quest software system in FACSCalibur flow cytometer (Becton Dickinson). The values were expressed as percentage relative to untransfected MDCK cells.

9.1.8 Fractionation assay

Human intestinal Caco-2 cells were used to performed fractionation assay according to Fey *et al.*, 1984. Cells were plated and grown for 4-5 days in a 12-wells plate, then cells were rinsed twice with PBS and extracted in cytoskeleton buffer (CSK: NaCl 100 mM, sucrose 300 mM, PIPES 10 mM [pH 6,8], $MgCl_2$, 3 mM, Triton X-100 0,5% and PMSF 1,2 mM) for 10 min at 0°C. The resulting "soluble" fraction was removed. An extraction buffer (EB: ammonium sulfate 250 mM, sucrose 300 mM, PIPES 10 mM [pH 6,8], $MgCl_2$, 3 mM PMSF 1,2 mM, and Triton X-100 0,5%) was added to the Triton X-100-insoluble structures for 10 min at 0°C and, in this way, the "cytoskeleton" fraction was removed. The "chromatin" fraction was removed from the remaining structural elements by digestion in a buffer identical to the CSK buffer except that NaCl 50 mM was present. To this buffer 100 µg/ml bovine pancreatic DNase and 100 µg/ml pancreatic RNase A were added and the digestion proceeded for 20 min at room temperature (RT). Ammonium sulfate was added to a final concentration of 0,25 M and incubation continued for 5 min at RT. The "chromatin" fraction was removed as a supernatant leaving

the NM-IF (nuclear matrix-intermediate filaments) fraction. Each fraction was diluted in SDS solubilization buffer (Tris HCl 0,3 M [pH 8,9], SDS 5%, β-mercaptoethanol 10%, glycerol 20% and bromophenol blue 0,02%) and boiled 2 minutes before being used for SDS-PAGE experiments.

9.1.9 Co-immunoprecipitation

The co-immunoprecipitation is a technique used to pull down intact protein complexes and to identify protein-protein interactions and novel members of protein complexes. The assay was performed as described previously (Crespi *et al.*, 2012) with some modifications. Briefly, sub-confluent and fully confluent Caco-2 cells were grown in 100 mm dishes and then harvested in 1,5 ml of ice-cold lysis buffer (Tris-HCl 25 mM [pH 7,5], NaCl 100 mM, EDTA 5 mM, Triton X-100 0,5%, DTT 1 mM, PMSF and a cocktail of protease inhibitors) for 30 min at 4˚C. The lysates were then spun at 14.000 g for 20 min at 4˚C. For input samples, 50 µl of the cell lysate were mixed with 2X SDS samples loading buffer and heated at 100˚C for 5 min. For affinity precipitation, 700 µl of lysate were incubated with 25 µl bead volume of protein-A-Sepharose (Sigma Aldrich) cross linked to anti-POF1B antibodies at 4˚C for 3 h. The immunocomplexes washed and released from the beads by boiling the samples in SDS solubilization buffer, and the input samples (2% of the total) were loaded onto a 10% SDS-PAGE.

9.1.10 SDS-PAGE and Western blot

SDS-PAGE, sodium dodecyl sulfate polyacrylamide gel electrophoresis, is a technique widely used in biochemistry to separate proteins according to their electrophoretic mobility (a function of length of polypeptide chain or molecular weight, as well as higher order protein folding, post-translational modifications and other factors). Besides the addition of SDS, proteins may optionally be briefly heated to near boiling in the presence of a reducing agent, such as mercaptoethanol (β-mercaptoethanol), which further denatures the proteins by reducing disulfide linkages, thus overcoming some forms of tertiary protein folding, and breaking up quaternary protein structure (oligomeric subunits). This is known as reducing SDS-PAGE, and is the most commonly used.

In this study, samples were diluted in SDS solubilization buffer and boiled 2 minutes. Proteins were separated on 10% or 11% polyacrylamide gels and transferred onto nitrocellulose membranes (Schleicher and Shull). The blots were probed with the indicated primary antibodies, followed by peroxidase- or infrared-conjugated anti-mouse or anti-rabbit secondary antibodies. In the first case the bands were visualized with ECL Western blotting detection system (Perkin-Elmer Life Science) and the signal intensity was quantified densitometrically using NIH ImageJ software. In the second case, blots were scanned with the Odyssey CLx Infrared Imaging System (LI-COR, Bioscence) and the bands were quantified with Image Studio software (LI-COR, Bioscence).

9.1.11 Dispase assay

To test the strength of cell-cell adhesion, a dispase fragmentation assay was performed as described elsewhere (Huen *et al.*, 2002). HaCaT cells (nt, mock and POF1B-knockdown clones 1, 2.5 and 2.24) were plated in triplicate and grown at confluence for 7 days in a 12-wells plate and washed twice in PBS before being incubated in 1 mg/ml dispase (STEMCELL technologies) at 37°C until the cells detached from the substrate. Cell sheets were transferred to a 15 ml tube containing 2 ml PBS and subjected to mechanical stress (20-40 rapid shaking of the tube). The number of the fragments in each well was then manually counted.

9.1.12 Wound healing assay

To compare the proliferation and migration capability of mock and POF1B-silenced cells, a wound healing assay was performed in confluent HaCaT cells. Briefly, cells were cultured in a 12-wells plate for 7 days and then scratched with a 2 µl pipette tip; the medium was changed and images were taken at different time point using an AxioCam MRm camera with a 10X phase 1 objective. The percentage of recover was quantified using ImageJ software. When indicated, mitomycin C was added to the medium 3 h before the scratch to avoid proliferation.

9.1.13 Immunofluorescence

The cells grown on glass coverslips were fixed for 20 min in 4% paraformaldehyde + 4% sucrose or 10 min in ice-cold methanol, and permeabilized with 0,5% Triton X-100. Immunostaining with primary antibodies (2 hours) was followed by incubation with fluorophore-conjugated anti-rabbit or anti-mouse secondary antibodies for 1 hour. Cysts were immunoprobed with primary antibodies overnight and an incubation of 3 hours was required for secondary antibody stainings. Samples were mounted using Vectashield (VectorLabs) containing DAPI for visualize nuclei. The confocal images were obtained using a LSM Zeiss META confocal microscope.

Sections of the frozen unfixed human jejunum, human duodenum, murine bladder, monkey esophagus, human skin, human basal cell carcinoma and porcine heart (6 µm thick) were flattened over a gelatin-coated glass slide, fixed with acetone for 3 seconds and allowed to dry out overnight at RT. Sections were permeabilized with 0,5% Triton X-100, incubated overnight at 4°C with primary antibodies, washed and incubated for 1 hour at RT with secondary antibodies.

9.1.14 Transmission electron microscopy (TEM)

MDCK cells grown on Transwell filters or HaCaT cells grown for 7 days in a 6-wells plate were fixed in 2% (v/v) glutaraldehyde in cacodylate buffer 0,1 M [pH 7,4], and post-fixed with 1% (w/v) OsO_4 in cacodylate buffer 0,1 M. The samples were then stained en bloc, dehydrated in ethanol and embedded in

EPON 812 (Fluka) following standard procedures. Ultrathin sections were obtained using an Ultracut E ultramicrotome (Reichert-Jung) equipped with a diamond knife (Diatome), counterstained with uranyl acetate and lead citrate. Finally they were examined using a Philips CM10 transmission electron microscope (TEM).

9.1.15 Antibodies

In this studies, antibodies were used in both biochemical and immunofluorescence assays. The protocols used require an incubation with a primary antibody followed by an incubation with a secondary antibody. For immunofluorescence experiments, the secondary antibodies are conjugated with a fluorophore, while for Western blot experiments, the secondary antibodies are conjugated with peroxidase or with infrared fluorophores.

Primary antibodies

Primary antibodies are immunoglobulins raised against an antigenic target of interest (a protein, peptide, carbohydrate, or other small molecule) and are typically unconjugated (unlabelled). Primary antibodies that recognize and bind with high affinity and specificity to unique epitopes across a broad spectrum of molecules are available as high specificity monoclonal antibodies and/or as polyclonal antibodies. These antibodies are useful also to detect modifications mediated by processes such as

phosphorylation, methylation, or glycosylation. The primary antibodies used in this study are listed below.

- rabbit polyclonal antibody against human POF1B was raised against the corresponding fusion proteins (Rizzolio *et al*., 2007)
- monoclonal mouse anti-claudin1, anti-claudin2 and anti-ZO-2 (Zymed Laboratories)
- polyclonal rabbit anti-β-catenin was produced and characterized in our laboratory (Massari *et al*., 2005)
- monoclonal mouse anti-β-catenin (BD Transduction Laboratories)
- monoclonal mouse anti-JAM1 BV16 (Cell Science)
- monoclonal mouse anti-E-cadherin, anti-keratin 8, anti-acetylated tubulin, anti-PG and anti-actin (Sigma Aldrich)
- monoclonal mouse anti-GFP (MBL, Eppendorf)
- polyclonal rabbit anti-occludin (Zymed Laboratories)
- polyclonal rabbit anti-PAR3 (Upstate)
- polyclonal rabbit anti-LIN7 antiserum was raised against the histidine-LIN7A fusion protein (Perego *et al*., 2002)
- rabbit polyclonal antibodies against α1 Na^+/K^+-ATPase were raised against specific peptides (Pietrini *et al*., 1992)
- monoclonal mouse anti-desmoplakin (SIC)
- monoclonal mouse anti-DSG1, 2 (PROGEN)
- polyclonal rabbit anti-β-tubulin and anti-TOM20 and monoclonal mouse anti-PKP2 (Santa Cruz Biotechnology)
- monoclonal mouse anti-cytokeratins (DAKO)
- the hybridoma cell line 3F2-secreting antibodies against gp135 were kindly provided by G. K. Ojakian (Ojakian and Schwimmer, 1988).

Secondary antibodies

A secondary antibody is an antibody that binds to primary antibodies or antibody fragments. They are typically labelled with probes that make them useful for detection, such as peroxidase or fluorophore. The secondary antibodies used in this study are listed below.

- rhodamine-conjugated anti-rabbit and fluorescein isothiocyanate (FITC)-conjugated anti-mouse IgG (Jackson ImmunoResearch Laboratories, Inc.)
- CY3-labelled anti-mouse and AlexaFluor 488-labelled anti-rabbit IgG (Jackson ImmunoResearch Laboratories, Inc.)
- rhodamine-labelled phalloidin (Cytoskeleton) and FITC-labelled phalloidin (Jackson ImmunoResearch Laboratories, Inc.) were used to detect filamentous actin
- peroxidase-conjugated anti-rabbit and anti-mouse IgG (Jackson ImmunoResearch Laboratories, Inc.)
- infrared-conjugated anti-rabbit IgG IRDye 800CW or anti-mouse 680RD (LI-COR Bioscience).

9.1.16 Image analysis

In MDCK clones the approximate values of angles at multiple cell-to-cell contacts, as well as the distance between the cell centre and the point of emergence of the primary cilium, were calculated by means of semi-automatic, custom procedures using ImageJ software. To obtain values of angles from a planar image of MDCK cells, binary maps of cell locations was manually constructed, drawing the cell contours on an image. This image

was then used as input for an ImageJ macro, which used it to identify cells, cell corners and internal angles. Centroids were calculated using ImageJ measurement functions and represented the average of the x and y coordinates of all of the pixels assigned to a cell. To obtain distances from cell centre and points of cilium emergence, we used stacks obtained by z-series of polarized cultures of MDCK cells. A binary map of cell locations was constructed by manually drawing cell contours, as observed in the most apical portion of the stack. This image, and the stack, were then used as inputs for a second ImageJ macro, which used the map to identify cells and cell centroids and used the stack to recognize the point of emergence of every cilium. The aforementioned procedures were validated manually.

The length of MDCK cells sides and orientation of their mitotic division were calculated manually by considering the distance between two corners along the connecting cell wall and the position of mitotic chromosomes relative to the apical luminal surface, respectively.

The 3D image reconstructions were conducted using z-series of MDCK cell lines taken with the same confocal parameters and processed with the "make isotropic" plug-in and "volume reconstruction rendering" (ImageJ 3D viewer).

Colocalization of POF1B with F-actin in MDCK cells was quantified by Manders' colocalization coefficients (ImageJ "JACoP" plug-in analysis) (Bolte and Cordelieres, 2006), while the colocalizing signals between POF1B and the desmosomal markers in Caco-2 cells were obtained with ImageJ software performing the "MIN" operation between the red and green channels.

The circularity of the MDCK cyst lumens was determined using the formula $4\pi(\text{area})/(\text{perimeter})^2$; the values obtained with this formula closer to 1,0 indicate a circularity profile (Akao *et al.*, 2003).

In immunofluorescence confocal sections (MDCK and Caco-2 cells), the quantification of the signals was evaluated by using ImageJ "surface plot" and "plot profile".

The analysis of the percentage of staining-free membrane in Caco-2 cells was performed using "plot profile" values obtained from approximately 100 µm of membrane for each single staining.

The analysis on desmosome morphology was performed in HaCaT cells (nt, mock, cl. 1, cl. 2.5 and cl. 2.24). TEM images (at least 15 for each clone) were analyzed using ImageJ. Data represent the desmosome density (normalized for 100 µm of membrane), the desmosome plaque length, the membrane available for adhesion and the multilayer thickness.

The recover of HaCaT scratched cells was evaluated measuring the width of the scratch with ImageJ software at different time points.

9.1.17 Statistical analysis

All quantitative data are presented as mean +/- S.E.M. Multiple comparisons among groups were carried out by Student's t-test using Prism software (GraphPad PrismTM software). Where not specified: * = $p < 0,05$, ** = $p < 0,01$ and *** = $p < 0,001$.

9.2 List of abbreviations

2D	Two-dimensional
3D	Three-dimensional
a.u.	Arbitrary units
ADP	Adenosine diphosphate
AP	Apical
ATP	Adenosine triphosphate
Arm	Armadillo
ARVC	Arrhythmogenic right ventricular cardiomyopathy
AJ	Adherens junction
aPKC	atypical protein kinase C
BAS	basal
BSA	bovine serum albumin
C-TER	carboxy-terminal
CASK	Calcium/calmodulin-dependent serine protein kinase
CE	cell envelope
CHROM	chromatine
Crb	Crumbs
CSK	cytoskeleton
Dlg	Discs large
DMEM	Dulbecco's modified Eagle medium

dNTPs	deoxynucleotide triphosphates
DSC	Desmocollin
DSG	Desmoglein
DSP	Desmoplakin
DTD	Desmoglein terminal domain
DTT	dithiothreitol
EC	extracellular domain
ECM	extracellular matrix
EDTA	Ethylenediaminetetraacetic acid
EGTA	Ethylene glycol tetra acetic acid
EM	electron microscopy
FACS	fluorescence-activated cell sorting
Fat/Ds/Fj	Fat/Dachsous/Four-jointed
FBS	fetal bovine serum
FITC	fluorescein isothiocyanate
Fmi	Flamingo
Fz	Frizzled
GDP	guanoside diphosphate
GFAP	Glial fibrillary acidic protein
GFP	green fluorescent protein
GSK3b	Glycogen synthase kinase 3b
GSR	glycine-serine-arginine rich domain
GTP	guanoside triphosphate

GUK	guanylate kinase
hPOF1B	human POF1B
IA	intracellular anchor
ICD	intercalated disc
ICS	cadherin-like sequence
IDP	inner dense plaque
IF	intermediate filaments
IOSE	immortalized ovarian surface epithelium
IPL	prolin-rich linker
JAM	Junctional adhesion molecule
JUP	Junction plakoglobin
K8	Keratin 8
LB	Luria Bertani
Lef	lymphoid enhancer factor
Lgl	Lethal giant larvae
MAGI-1	Membrane-associated guanylate kinase with inverted domain structure 1
MAGUK	Membrane-associated guanylate kinase
MAP	microtubule-associated proteins
MDCK	Madin-Darby canine kidney
MEM	Minimum Essential Medium
MTOC	microtubule organizing center
MUPP1	Multi-PDZ domain protein 1

N-TER	amino-terminal
NEAA	non essential amminoacids
NF	Neurofilament
NM-IF	nuclear matrix-Intermediate filaments
ODP	outer dense plaque
OSE	ovarian surface epithelium
P/S	penicillin/Streptomycin
p120ctn	P120 catenin
PALS1	Protein associated with Lin-7 1
Par3	Partitioning defective-3
Par6	Partitioning defective-6
PATJ	PALS1-associated tight junction protein
PBS	phosphate-buffered saline
PCP	planar cell polarity
PCR	polymerase chain reaction
PDZ	Postsynaptic density 95/disc-large/zona occludens
PEI	poly ethilen immine
PF	pemphigus foliaceus
PG	Plakoglobin
PKC	Protein kinase C
PKP	Plakophilin
PM	plasma membrane
PMSF	phenylmethylsulfonylfluoride

PNP	paraneoplastic pemphigus
POF	premature ovarian failure
POF1B	premature ovarian failure 1B
PPK	palmoplantar keratodermas
PV	pemphigus vulgaris
RT	room temperature
RT-PCR	reverse trascriptase PCR
RUD	repeat unit domain
SCRIB	Scribble
SDS	sodium dodecyl sulfate
SDS-PAGE	sodium dodecyl sulfate-polyacrylamide gel electrophoresis
SH3	Src homology 3
shRNA	small hairpin RNA
siRNA	small interference RNA
SOL	soluble
SSSS	Staphylococcal scalded skin syndrome
TAE	tris-acetate
Tcf	T-cell factor
TE	tris-EDTA
TEM	transmission electron microscopy
TER	transepithelial electrical resistance
TJ	tight junction

Wnt/Fz	Wnt/Frizzled
YMO1	Yurt/ mosaic eyes like 1
ZO	Zonula occludens
ZONAB	ZO-1-associated nucleic acid-binding protein

10 chapter

References

Akao, M., O'Rourke, B., Kusuoka, H., Teshima, Y., Jones, S.P., and Marban, E. **(2003)**. Differential actions of cardioprotective agents on the mitochondrial death pathway. *Circ Res.* 92:195-202.

Al-Amoudi, A., Castaño-Diez, D., Devos, D.P., Russell, R.B., Johnson, G.T., and Frangakis, A.S. **(2011)**. The three-dimensional molecular structure of the desmosomal plaque. *PNAS USA*. 108(16):6480-6485.

Albertini, D.F., Combelles, C.M., Benecchi, E., and Carabatsos, M.J. **(2001)**. Cellular basis for paracrine regulation of ovarian follicle development. *Reproduction.* 121:647-653.

Amagai, M. **(1999)**. Autoimmunity against desmosomal cadherins in pemphigus. *J Dermatol Sci*. 20(2):92-102.

Arin, M.J. **(2009).** The molecular basis of human keratin disorders. *Hum Genet*. 125:355-73.

Asimaki, A., Syrris, P., Wichter, T., Matthias, P., Saffitz, J.E., and McKenna, W.J. **(2007).** A novel dominant mutation in plakoglobin causes arrhythmogenic right ventricular cardiomyopathy. *Am J Hum Genet.* 81:964-973.

Assémat, E., Bazellières, E., Pallesi-Pocachard, E., Le Bivic, A., and Massey-Harroche, D. **(2008)**. Polarity complex proteins. *Biochimica et biophysica acta.* 1778:614-30.

Auersperg, N., Maines-Bandiera, S.L., Dyck, H.G., and Kruk, P.A. **(1994).** Characterization of cultured human ovarian surface epithelial cells: phenotypic plasticity and premalignant changes. *Lab Invest.* 71:510-518.

Aurrand-Lions, M., Johnson-Leger, C., Wong, C., Du Pasquier, L., and Imhof, B.A. **(2001)**. Heterogeneity of endothelial junctions is reflected by differential expression and specific subcellular

localization of the three JAM family members. *Blood.* 98: 3699-3707.

Balda, M.S., Garrett, M.D., and Matter, K. **(2003)**. The ZO-1-associated Y-box factor ZONAB regulates epithelial cell proliferation and cell density. *J Cell Biol.* 160:423-432.

Balda, M.S., and Matter, K. **(2000)**. Transmembrane proteins of tight junctions. *Semin Cell Dev Biol.* 11:281-289.

Balda, M.S., Whitney, J.A., Flores, C., Gonzalez, S., Cereijido, M., and Matter, K. **(1996)**. Functional dissociation of paracellular permeability and transepithelial electrical resistance and disruption of the apical-basolateral intramembrane diffusion barrier by expression of a mutant tight junction membrane protein. *J Cell Biol*. 134:1031-1049.

Bass-Zubek, A.E., Godsel, L.M., Delmar, M., and Green, K.J. **(2009)**. Plakophilins: multifunctional scaffolds for adhesion and signaling. *Curr Opin Cell Biol.* 21:708-716.

Bass-Zubek, A.E., Hobbs, R.P., Amargo, E.V, Garcia, N.J., Hsieh, S.N., Chen, X., Wahl, J.K., Denning, M.F., and Green, K.J. **(2008)**. Plakophilin 2: a critical scaffold for PKC alpha that regulates intercellular junction assembly. *J Cell Biol.* 181:605-613.

Basso, C., Thiene, G., Corrado, D., Angelini, A., Nava, A., and Valente, M. **(1996)**. Arrhythmogenic right ventricular cardiomyopathy. Dysplasia, dystrophy, or myocarditis? *Circulation.* 94:983-991.

Bauce, B., Rampazzo, A., Basso, C., Mazzotti, E., Rigato, I., Steriotis, A., Beffagna, G., Lorenzon, A., De Bortoli, M., Pilichou, K., *et al*. **(2011)**. Clinical phenotype and diagnosis of arrhythmogenic right ventricular cardiomyopathy in pediatric

patients carrying desmosomal gene mutations. *Heart Rhythm.* 8:1686-1695.

Bazzi, H., Getz, A., Mahoney, M.G., Ishida-Yamamoto, A., Langbein, L., Wahl, J.K., and Christiano, A.M. **(2006)**. Desmoglein 4 is expressed in highly differentiated keratinocytes and trichocytes in human epidermis and hair follicle. *Differentiation*. 74:129-40.

Bazzoun, D., Lelièvre, S., and Talhouk, R. **(2013)**. Pharmacology and Therapeutics Polarity proteins as regulators of cell junction complexes: Implications for breast cancer. *Pharmacology & Therapeutics*. 138:418-427.

Berbari, N.F., Connor, A.K.O., Haycraft, C.J., and Yoder, B.K. **(2010)**. The Primary Cilium as a Complex Signaling Center. *Curr Biol.* 19(13):1-21.

Bione, S., Rizzolio, F., Sala, C., Ricotti, R., Goegan, M., Manzini, M.C., Battaglia, R., Marozzi, A., Vegetti, W., Dalprà, L., *et al*. **(2004)**. Mutation analysis of two candidate genes for premature ovarian failure, DACH2 and POF1B. *Human reproduction.* 19:2759-2766.

Bione, S., Sala, C., Manzini, C., Arrigo, G., Zuffardi, O., Banfi, S., Borsani, G., Jonveaux, P., Philippe, C., Zuccotti, M. *et al*. **(1998)**. A human homologue of the Drosophila melanogaster diaphanous gene is disrupted in a patient with premature ovarian failure: evidence for conserved function in oogenesis and implications for human sterility. *Am J Hum Genet*. 62:533-541.

Blikstad, I., and Carlsson, L. **(1982)**. On the dynamics of the microfilament system in HeLa cells. *J Cell Biol.* 93:122-128.

Bolling, M.C., Veenstra, M.J., Jonkman, M.F., Diercks, G.F.H., Curry, C.J., Fisher, J., Pas, H.H., and Bruckner, L. **(2010)**. Lethal

acantholytic epidermolysis bullosa due to a novel homozygous deletion in DSP: expanding the phenotype and implications for desmoplakin function in skin and heart. *Br J Dermatol*. 162:1388-1394.

Bolling, M.C., and Jonkman, M.F. **(2009)**. Skin and heart: une liaison dangereuse. *Exp Dermatol.* 18:658-668.

Bolte, S., and Cordelieres, F.P. **(2006)**. A guided tour into subcellular colocalization analysis in light microscopy. *J Microsc.* 224:213-232.

Boukamp, P., Petrussevka, R.T., Breitkreutz, D., Hornung, J., Markham, A., Fusenig, N. **(1988)**. Normal Keratinization in a Spontaneously Immortalized Aneuploid Human Keratinocyte Cell Line. *J Cell Biol* 106:761-771.

Bragulla, H.H. and Homberger, D.G. **(2009)**. Structure and functions of keratin proteins in simple, stratified, keratinized and cornified epithelia. *J Anat.* 214:516-59.

Breitkreutz, D., Schoop, V.M., Mirancea, N., Baur, M., Stark, H., Fusenig, N. **(1998)**. Epidermal differentiation and basement membrane formation by HaCaT cells in surface transplants. *European journal of cell biology.* 75:273-286.

Brooke, M., Nitoiu, D., and Kelsell, D.P. **(2012)**. Cell-cell connectivity: desmosomes and disease. *J Pathol.* 226:158-171.

Bryant, D.M., and Mostov, K.E. **(2008)**. From cells to organs: building polarized tissue. *Nature reviews. Molecular cell biology.* 9:887-901.

Bulgakova, N., and Knust, E. **(2009)**. The Crumbs complex: from epithelial-cell polarity to retinal degeneration. *J Cell Sci.* 122:2587-2596.

Burdett, I.D., and Sullivan, K.H. **(2002).** Desmosome assembly in MDCK cells: transport of precursors to the cell surface occurs by two phases of vesicular traffic and involves major changes in centrosome and Golgi location during a Ca(2+) shift. *Exp Cell Res*. 276(2):296-309.

Calkins, C.C., and Setzer, S.V. **(2007)**. Spotting desmosomes: The first 100 years. *J Invest Dermatol.* 127:E2-E3.

Campuzano, O., Alcalde, M., Iglesias, A., Barahona-Dussault, C., Sarquella-Brugada, G., Benito, B., Arzamendi, D., Flores, J., Leung, T.K., Talajic, M., *et al*. **(2012)**. Arrhythmogenic right ventricular cardiomyopathy: severe structural alterations are associated with inflammation. *J Clin Pathol*. 65:1077-1083.

Carthew, R.W. **(2005)**. Adhesion proteins and the control of cell shape. *Curr Opin Genet Dev*. 15:358-363.

Cereijido, M., Robbins, E.S., Dolan, W.J., Rotunno, C.A., and Sabatini, D.D. **(1978)**. Polarized monolayers formed by epithelial cells on a permeable and translucent support. *J Cell Biol.* 77:853-880.

Chen, J., and Zhang, M. **(2013)**. The Par3/Par6/aPKC complex and epithelial cell polarity. *Experimental cell research*. 319:1357-1364.

Chiba, H., Osanai, M., Murata, M., Kojima, T., and Sawada, N. **(2008)**. Transmembrane proteins of tight junctions. *Biochim Biophys Acta Biomembr.* 1778:588-600.

Chidgey, M., and Dawson, C. **(2007)**. Desmosomes: a role in cancer? *Br J Cancer.* 96:1783-1787.

Chidgey, M. **(2002)**. Desmosomes and disease: an update. *Histol. Histopathol.* 17:1179-1192.

Choi, H.J., Park-Snyder, S., Pascoe, L.T., Green, K.J., and Weis, W.I. **(2002)**. Structures of two intermediate filament-binding

fragments of desmoplakin reveal a unique repeat motif structure. *Nature Structural Biology*. 9:612-620.

Clark, E.A., and Brugge, J.S. **(1995)**. Integrins and signal transduction pathways: the road taken. *Science.* 268:233-239.

Clevers, H., and Nusse, R. **(2012)**. Wnt/β-catenin signaling and disease. *Cell.* 149:1192-1205.

Coulam, C.B., Adamson, S.C., and Annegers, J.F. **(1986)**. Incidence of premature ovarian failure. *Obstet Gynecol*. 67:604-606.

Crespi, A., Ferrari, I., Lonati, P., Disanza, A., Fornasari, D., Scita, G., Padovano, V., and Pietrini, G. **(2012)**. LIN7 regulates the filopodium- and neurite-promoting activity of IRSp53. *J Cell Sci* 125:4543-4554.

Davis, C.J., Davison, R.M., Payne, N.N., Rodeck, C.H., and Conway, G.S. **(2000)**. Female sex preponderance for idiopathic familial premature ovarian failure suggests an X chromosome defect: opinion. *Hum Reprod*. 15:2418-2422.

De Forges, H., Bouissou, A., and Perez, F. **(2012)**. Interplay between microtubule dynamics and intracellular organization. *Int J Biochem Cell Biol*. 44:266-74.

Delorme-Axford, E., and Coyne, C.B. **(2011)**. The actin cytoskeleton as a barrier to virus infection of polarized epithelial cells. *Viruses.* 3:2462-2477.

Delva, E., Tucker, D.K., and Kowalczyk, A.P. **(2009)**. The desmosome. *Cold Spring Harbor perspectives in biology.* 1 (2):a002543. doi: 10.1101/cshperspect.a002543.

de Moraes-Ruehsen, M., and Jones, G.S. **(1967)**. Premature ovarian failure. *Fertil Steril.* 18:440-461.

Drubin, D.G., and Nelson, W.J. **(1996)**. Origins of Cell Polarity. *Cell* 84:335-344.

Dusek, R.L., and Attardi, L.D. **(2011).** Desmosomes: new perpetrators in tumour suppression. *Nat Rev Cancer.* 11:317-323.

Ebnet, K., Suzuki, A., Horikoshi, Y., Hirose, T., Meyer Zu Brickwedde, M.K., Ohno, S., and Vestweber, D. **(2001).** The cell polarity protein ASIP/PAR-3 directly associates with junctional adhesion molecule (JAM). *Embo J.* 20:3738-3748.

Etienne-Manneville, S. **(2011)**. Control of polarized cell morphology and motility by adherens junctions. *Semin Cell Dev Biol*. 22:850-857.

Fanning, A.S., Mitic, L.L. and Anderson, J.M. **(1999)**. Transmembrane proteins in the tight junction barrier. *J Am Soc Nephrol.* 10:1337-1345.

Feldman, G.J., Mullin, J.M., and Ryan, M.P. **(2005)**. Occludin: structure, function and regulation. *Adv Drug Deliv Rev.* 57:883-917.

Fey, E.G., Wan, K.I., and Penman, S. **(1984)**. Epithelial Cytoskeletal Framework and Nuclear Matrix-Intermediate Filament Scaffold: Three-dimensional Organization and Protein Composition. *J Cell Biol.* 98:1973-1984.

Fogh, J., and Trempe, G. **(1975)**. Human Tumor Cells In Vitro. *Plenum*. 115-141.

Fontao, L., Favre, B., Riou, S., Geerts, D., Jaunin, F., Saurat, J., Green, K.J., Sonnenberg, A., and Borradori, L. **(2003)**. Interaction of the bullous pemphigoid antigen 1 (BP230) and desmoplakin with intermediate filaments is mediated by distinct sequences within their COOH terminus. *Mol Biol Cell.* 14:1978-1992 .

Garcia-Gras, E., Lombardi, R., Giocondo, M.J., Willerson, J.T., Schneider, M.D., Khoury, D.S., and Marian, A.J. **(2006)**.

Suppression of canonical Wnt/beta-catenin signaling by nuclear plakoglobin recapitulates phenotype of arrhythmogenic right ventricular cardiomyopathy. *J Clin Invest.* 116:2012-2021.

Garrod, D. **(2010)**. Desmosomes in vivo. *Dermatology research and practice.* 212439. doi:10.1155/2010/212439.

Garrod, D., and Kimura, T.E. **(2008)**. Hyper-adhesion: a new concept in cell-cell adhesion. *Biochemical Society Transactions*. 36(2): 195-201.

Garrod, D., and Chidgey, M. **(2008)**. Desmosome structure, composition and function. *Bioch biophys Acta.* 1778:572-587.

Garrod, D.R., Berika, M.Y., Bardsley, W.F., Holmes, D., and Tabernero, L. **(2005)**. Hyper-adhesion in desmosomes: its regulation in wound healing and possible relationship to cadherin crystal structure. *J Cell Sci*. 118(24):5743-5754.

Gartner, L.P., and Hiatt, J.L. **(2006)**. Gartner & Hiatt: Color Textbook of Histology, 3rd ed. ISBN-13: 978-0-8089-2356-5 ISBN-10: 0-8089-2356-0.

Getsios, S., Amargo, E.V, Dusek, R.L., Ishii, K., Sheu, L., Godsel, L.M., and Green, K.J. **(2004a)**. Coordinated expression of desmoglein 1 and desmocollin 1 regulates intercellular adhesion. *Differentiation*. 72:419-433.

Getsios, S., Huen, A.C., and Green, K.J. **(2004b).** Working out the strength and flexibility of desmosomes. *Nature Reviews Molecular Cell Biology.* 5:271-281.

Godsel, L.M., Hsieh, S.N., Amargo, E.V., Bass, A.E., Pascoe-McGillicuddy, L.T., Huen, A.C., Thorne, M.E., Gaudry, C.A., Park, J.K., Myung, K., *et al.* **(2005)**. Desmoplakin assembly dynamics in four dimensions: multiple phases differentially regulated by intermediate filaments and actin. *J Cell Biol.* 171:1045-1059.

Gonzalez-Mariscal, L., Betanzos, A., and Avila-Flores, A. **(2000).** MAGUK proteins: structure and role in the tight junction. *Semin Cell Dev Biol.* 11:315-324.

Green, K.J., Getsios, S., Troyanovsky, S., and Godsel, L.M. **(2010)**. Intercellular junction assembly, dynamics, and homeostasis. *Cold Spring Harbor perspectives in biology.* 2, a000125. doi: 10.1101/cshperspect.a000125.

Gumbiner, B.M. **(2005)**. Regulation of cadherin-mediated adhesion in morphogenesis. *Nat Rev Mol Cell Biol*. 6(8):622-634.

Haines, R.L., and Lane, E.B. **(2012)**. Keratins and disease at a glance. *J Cell Sci*. 125:3923-3928.

Halbleib, J.M., and Nelson, W.J. **(2006).** Cadherins in development: cell adhesion, sorting, and tissue morphogenesis. *Genes Dev.* 20:3199-3214.

Hao, Y., Du, Q., Chen, X., Zheng, Z., Balsbaugh, J.L., Maitra, S., Shabanowitz, J., Hunt, D.F., and Macara, I.G. **(2010)**. Par3 controls epithelial spindle orientation by aPKC-mediated phosphorylation of apical pins. *Curr Biol*. 20:1809-1818.

Hartsock, A., and Nelson, W.J. **(2007)**. Adherens and tight junctions: structure, function and connections to the actin cytoskeleton. *Biochim Biophys Acta.* 1778:660-669.

Hatzfeld, M. **(2007)**. Plakophilins: Multifunctional proteins or just regulators of desmosomal adhesion? *Bioch Biophys Acta.* 1773:69-77.

Hidalgo, I.J., Raub, T.J., Borchardt, R.T. **(1989)**. Characterization of the human colon carcinoma cell line (Caco-2) as a model system for intestinal epithelial permeability. *Gastroenterology.* 96:736-749.

Hirshfield, A.N. **(1997)**. Overview of ovarian follicular development: considerations for the toxicologist. *Environ Mol Mutagen.* 29,10-15.

Hofer, D., Jons, T., Kraemer, J., Drenckhahn, D. **(1998).** From cytoskeleton to polarity and chemoreception in the gut epithelium. *Ann N Y Acad Sci*. 859:75-84.

Holthofer, B., Windoffer, R., Troyanovsky, S., Leube, R.E. **(2007)**. Structure and function of desmosomes. *Int Rev Cytol.* 264:65-163.

Huber, A.H., Nelson, W.J., Weis, W.I. **(1997)**. Three-dimensional structure of the armadillo repeat region of beta-catenin. *Cell.* 90:871-882.

Huen, A.C., Park, J.K., Godsel, L.M., Chen, X., Bannon, L.J., Amargo, E.V, Hudson, T.Y., Mongiu, A.K., Leigh, I.M., Kelsell, D.P., *et al*. **(2002)**. Intermediate filament-membrane attachments function synergistically with actin-dependent contacts to regulate intercellular adhesive strength. *J Cell Biol*. 159:1005-1017.

Hynes, R. O. **(1992)**. Integrins: versatility, modulation, and signaling in cell adhesion. *Cell.* 69:11-25.

Itoh, M., Sasaki, H., Furuse, M., Ozaki, H., Kita, T., and Tsukita, S. **(2001).** Junctional adhesion molecule (JAM) binds to PAR-3: a possible mechanism for the recruitment of PAR-3 to tight junctions. *J Cell Biol.* 154:491-497.

Itoh, M., Nagafuchi, A., Yonemura, S., Kitani-Yasuda, T., Tsukita, Sa., and Tsukita, S. **(1993)**. The 220-kD protein colocalizing with cadherins in non-epithelial cells is identical to ZO-1, a tight junction-associated protein in epithelial cells: cDNA cloning and immunoelectron microscopy. *J Cell Biol*. 121:491-502.

Jablonka-Shariff, A., Reynolds, L.P., and Redmer, D.A. **(1996)**. Effects of gonadotropin treatment and withdrawal on follicular growth, cell proliferation, and atresia in ewes. *Biol Reprod.* 55:693-702.

Jaffe, A.B., Kaji, N., Durgan, J., and Hall, A. **(2008)**. Cdc42 controls spindle orientation to position the apical surface during epithelial morphogenesis. *J Cell Biol.* 183:625-633.

Johnson, E.T., Nicola, T., Roarty, K., Yoder, B.K., Haycraft, C.J., and Serra, R. **(2008)**. Role for primary cilia in the regulation of mouse ovarian function. *Dev Dyn.* 237:2053-2060.

Keil, R., Wolf, A., Huttelmaier, S., and Hatzfeld, M. **(2007)**. Beyond regulation of cell adhesion: local control of RhoA at the cleavage furrow by the p0071 catenin. *Cell Cycle.* 6:122-127.

Kim, J., Lee, J.E., Heynen-Genel, S., Suyama, E., Ono, K., Lee, K., Ideker, T., Aza-Blanc, P., and Gleeson, J.G. **(2010)**. Functional genomic screen for modulators of ciliogenesis and cilium length. *Nature.* 464:1048-1051.

Koch, P.J., Mahoney, M.G., Ishikawa, H., Pulkkinen, L., Uitto, J., Shultz, L., Murphy, G.F., Whitaker-Menezes, D., and Stanley, J.R. **(1997)**. Targeted disruption of the pemphigus vulgaris antigen (desmoglein 3) gene in mice causes loss of keratinocyte cell adhesion with a phenotype similar to pemphigus vulgaris. *J Cell Biol*. 137:1091-1102.

Kölsch, A., Windoffer, R., Würflinger, T., Aach, T., and Leube, R.E. **(2010)**. The keratin-filament cycle of assembly and disassembly. *J Cell Sci.* 123:2266-2272.

Kouklis, P.D., Hutton, E., and Fuchs, E. **(1994)**. Making a connection: direct binding between keratin intermediate filaments and desmosomal proteins. *J Cell Biol*. 127:1049-1060.

Kowalczyk, A.P., and Green, K.J. **(2013)**. Structure, function and regulation of desmosomes. *Progress in Molecular Biology and Translational Science*. 116:95-113.

Krauss, C.M., Turksoy, R.N., Atkins, L., McLaughlin, C., Brown, L.G., and Page, D.C. **(1987)**. Familial premature ovarian failure due to an interstitial deletion of the long arm of the X chromosome. *N Engl J Med*. 317:125-131.

Kundu, S.T., Gosavi, P., Khapare, N., Patel, R., Hosing, A.S., Maru, G.B., Ingle, A., Decaprio, J., and Dalal, S.N. **(2008)**. Plakophilin3 downregulation leads to a decrease in cell adhesion and promotes metastasis. *Int J Cancer.* 123:2303-2314.

Lacombe, A., Lee, H., Zahed, L., Choucair, M., Muller, J.M., Nelson, S.F., Salameh, W., and Vilain, E. **(2006)**. Disruption of POF1B binding to nonmuscle actin filaments is associated with premature ovarian failure. *American journal of human genetics* 79:113-9.

Lee, C.H., Kim, M.S., Chung, B.M., Leahy, D.J., and Coulombe, P.A. **(2012)**. Structural basis for heteromeric assembly and perinuclear organization of keratin filaments. *Nat Struct Mol Biol*. 19:707-715.

Leube, R.E., Moch, M., Kölsch, A., and Windoffer, R. **(2011)**. "Panta rhei": Perpetual cycling of the keratin cytoskeleton. *Bioarchitecture.* 1:39-44.

Leung, C.L., Green, K.J., and Liem, R.K. **(2002)**. Plakins: a family of versatile cytolinker proteins. *Trends Cell Biol*. 12:37-45.

Long, H.A., Boczonadi, V., McInroy, L., Goldberg, M., and Määttä, A. **(2006)**. Periplakin-dependent reorganisation of keratin cytoskeleton and loss of collective migration in keratin-8-downregulated epithelial sheets. *J Cell Sci*. 119:5147-59.

Madin, S.H., and Darby, N.B. **(1958)**. Established kidney cell lines of normal adult bovine and ovine origin. *Proc Soc Exp Biol Med*. 98(3):574-576.

Mandell, K.J., and Parkos, C.A. **(2005)**. The JAM family of proteins. *Adv Drug Deliv Rev.* 57:857-867.

Maniatis, T., Fritsch, E.F., and Sambrook, J. **(1982)**. Molecular cloning. A laboratory manual. ISBN 0-87969-136-0.

Mattison, D.R., Evans, M.I., Schwimmer, W.B., White, B.J., Jensen, B., and Schulman, J.D. **(1984)**. Familial premature ovarian failure. *Am J Hum Genet*. 36:1341-1348.

McCrea, P.D., Turck, C.W., and Gumbiner, B. **(1991).** A homolog of the armadillo protein in Drosophila (plakoglobin) associated with E-cadherin. *Science.* 254:1359-1361.

McGrath, J.A., McMillan, J.R., Shemanko, C.S., Runswick, S.K., Leigh, I.M., Lane, E.B., Garrod, D.R., and Eady, R.A.J. **(1997).** Mutations in the plakophilin 1 gene result in ectodermal dysplasia/skin fragility syndrome. *Nat Genet.* 17:240-244.

McKoy, G., Protonotarios, N., Crosby, A., Tsatsopoulou, A., Anastasakis, A., Coonar, A., Norman, M., Baboonian, C., Jeffery, S., and McKenna, W.J. **(2000)** Identification of a deletion in plakoglobin in arrhythmogenic right ventricular cardiomyopathy with palmoplantar keratoderma and woolly hair (Naxos disease). *Lancet.* 355:2119-2124.

McNally, F.J. **(2013)**. Mechanisms of spindle positioning. *J Cell Biol.* 200:131-140.

Mertens, C., Kuhn, C., and Franke, W.W. **(1996)**. Plakophilins 2a and 2b: Constitutive proteins of dual location in the karyoplasm and the desmosomal plaque. *J Cell Biol.* 135:1009-1025.

Misfeldt, D.S., Hamamoto, S.T., and Pitelka, D.R. **(1976)**. Transepithelial transport in cell culture. *Proc Natl Acad Sci USA*. 73:1212-1216.

Miyoshi, J., and Takai, Y. **(2008)**. Structural and functional associations of apical junctions with cytoskeleton. *Biochim Biophys Acta.* 1778:670-691.

Morita, K., Miyachi, Y. and Furuse, M. **(2011).** Tight junctions in epidermis: from barrier to keratinization. *Eur J Dermatol*. 21:12-7.

Mostov, K., Brakeman, P., Datta, A., Gassama, A., Katz, L., Kim, M., Leroy, P., Levin, M., Liu, K., Martin, F. *et al*. **(2005)**. Formation of multicellular epithelial structures. *Novartis Found Symp.* 269:193-200; discussion 200-195:223-130.

Muroyama, A., and Lechler, T. **(2013)**. Polarity and Stratification of the Epidermis. *Semin Cell Dev. Biol.* 23:890-896.

Nekrasova, O. and Green, K. J. **(2013)**. Desmosome assembly and dynamics. *Trends Cell Biol.* 23, 537-546.

Nekrasova, O.E., Amargo, E.V, Smith, W.O., Chen, J., Kreitzer, G.E., and Green, K.J. **(2011)**. Desmosomal cadherins utilize distinct kinesins for assembly into desmosomes. *J Cell Biol.* 195:1185-1203.

Nelson, W.J. **(2003)**. Adaptation of core mechanisms to generate cell polarity. *Nature.* 422:766-774.

Nikolic, B., Mac Nulty, E., Mir, B., and Wiche, G. **(1996)**. Basic amino acid residue cluster within nuclear targeting sequence motif is essential for cytoplasmic plectin-vimentin network junctions. *J Cell Biol.* 134:1455-1467.

Noren, N.K., Liu, B.P., Burridge, K., and Kreft, B. **(2000).** p120 catenin regulates the actin cytoskeleton via Rho family GTPases. *J Cell Biol.* 150:567-580.

Oishi, I., Kawakami, Y., Raya, A., Callol-Massot, C., and Izpisua Belmonte, J.C. **(2006)**. Regulation of primary cilia formation and left-right patterning in zebrafish by a noncanonical Wnt signaling mediator, duboraya. *Nat Genet*. 38:1316-1322.

Ojakian, G. K., and Schwimmer, R. **(1988)**. The polarized distribution of an apical cell surface glycoprotein is maintained by interactions with the cytoskeleton of Madin-Darby canine kidney cells. *J Cell Biol.* 107:2377-2387.

Oriolo, A.S., Wald, F.A., Ramsauer, V.P., and Salas, P.J.I. **(2007)**. Intermediate filaments: a role in epithelial polarity. *Exp Cell Res*. 313:2255-2264.

Otten, E., Asimaki, A., Maass, A., van Langen, I.M., van der Wal, A., de Jonge, N., van den Berg, M.P., Saffitz, J.E., Wilde, A.M., Jongbloed, J.D.H., *et al.* **(2010)**. Desmin mutations as a cause of right ventricular heart failure affect the intercalated disks. *Heart Rhythm.* 7:1058-1064.

Padovano, V., Lucibello, I., Alari, V., Della Mina, P., Crespi, A., Ferrari, I., Recagni, M., Lattuada, D., Righi, M., Toniolo, D., *et al.* **(2011)**. The POF1B candidate gene for premature ovarian failure regulates epithelial polarity. *J Cell Sci.* 124:3356-3368.

Peifer, M., McCrea, P.D., Green, K.J., Wieschaus, E., and Gumbiner, B.M. **(1992)**. The vertebrate adhesive junction proteins beta-catenin and plakoglobin and the Drosophila segment polarity gene armadillo form a multigene family with similar properties. *J Cell Biol.* 118:681-691.

Perego, C., Vanoni, C., Massari, S., Raimondi, A., Pola, S., Cattaneo, M.G., Francolini, M., Vicentini, L.M., and Pietrini, G. **(2002)**. Invasive behaviour of glioblastoma cell lines is associated with altered organisation of the cadherin-catenin adhesion system. J Cell Sci. 115:3331-3340.

Perego, C., Vanoni, C., Villa, A., Longhi, R., Kaech, S.M., Frohli, E., Hajnal, A., Kim, S.K., and Pietrini, G. **(1999)**. PDZ-mediated interactions retain the epithelial GABA transporter on the basolateral surface of polarized epithelial cells. *EMBO J.* 18:2384-2393.

Peters, M.N., Katz, M.J., and Alkadri, M.E. **(2012).** Diagnosis of arrhythmogenic right ventricular cardiomyopathy. *Proc (Bayl Univ Med Cent)*. 25:349-353.

Pieczynski, J., and Margolis, B. **(2011).** Protein complexes that control renal epithelial polarity. *Am J Physiol Renal Physiol.* 300:F589-F601.

Pieperhoff, S., Barth, M., Rickelt, S., and Franke, W.W. **(2010)**. Desmosomal molecules in and out of adhering junctions: normal and diseased States of epidermal, cardiac and mesenchymally derived cells. *Dermatology research and practice*. Article ID 139167. doi:10.1155/2010/139167.

Pietrini, G., Matteoli, M., Banker, G., and Caplan, M.J. **(1992)**. Isoforms of the Na,K-ATPase are present in both axons and dendrites of hippocampal neurons in culture. *Proc Natl Acad Sci USA.* 89:8414-8418.

Pilichou, K., Bezzina, C.R., Thiene, G., and Basso, C. **(2011)**. Arrhythmogenic cardiomyopathy: transgenic animal models provide novel insights into disease pathobiology. *Circ Cardiovasc Genet*. 4:318-326.

Qin, Y., Meisen, W.H., Hao, Y., and Macara, I.G. **(2010)**. Tuba, a Cdc42 GEF, is required for polarized spindle orientation during epithelial cyst formation. *J Cell Biol.* 189:661-669.

Rampazzo, A. **(2006)**. Genetic bases of arrhythmogenic right ventricular Cardiomyopathy. *Heart Int*. 2, 17.

Rasmussen, B., Hansen, J., Nissen, P.H., Palmfeldt, J., Dalager, S., Jensen, U.B., Kim, W.Y., Heickendorff, L., Mølgaard, H., Jensen, H.K., *et al.* **(2013)**. Protein expression studies of desmoplakin mutations in cardiomyopathy patients reveal different molecular disease mechanisms. *Clin Genet.* 84:20-23.

Rickelt, S., and Pieperhoff, S. **(2012)**. Mutations with pathogenic potential in proteins located in or at the composite junctions of the intercalated disk connecting mammalian cardiomyocytes: a reference thesaurus for arrhythmogenic cardiomyopathies and for Naxos and Carvajal diseases. *Cell Tissue Res.* 348:325-33.

Riva, P., Magnani, I., Fuhrmann Conti, A.M., Gelli, D., Sala, C., Toniolo, D., and Larizza, L. **(1996)**. FISH characterization of the Xq21 breakpoint in a translocation carrier with premature ovarian failure. *Clin Genet.* 50:267-269.

Rizzolio, F., Bione, S., Villa, A., Berti, E., Cassetti, A., Bulfone, A., Tribioli, C., and Toniolo, D. **(2007)**. Spatial and temporal expression of POF1B, a gene expressed in epithelia. *Gene expression patterns.* 7:529-34.

Rodriguez-Fraticelli, A.E., Vergarajauregui, S., Eastburn, D.J., Datta, A., Alonso, M.A., Mostov, K., and Martin-Belmonte, F. **(2010)**. The Cdc42 GEF Intersectin 2 controls mitotic spindle orientation to form the lumen during epithelial morphogen- esis. *J Cell Biol.* 189:725-738.

Rudini, N., and Dejana, E. **(2008).** Adherens junctions. *Curr Biol.* 18: R1080-1082.

Runkle, E.A., and Mu, D. **(2013)**. Tight junction proteins: from barrier to tumorigenesis. *Cancer letters.* 337:41-48.

Saito, M., Tucker, D.K., Kohlhorst, D., Niessen, C.M., and Kowalczyk, A.P. **(2012).** Classical and desmosomal cadherins at a glance. *J Cell Sci.* 125(11):2547-2552.

Schmidt, A., Langbein, L., Rode, M., Pratzel, S., Zimbelmann, R., and Franke, W.W. **(1997)**. Plakophilins 1a and 1b: Widespread nuclear proteins recruited in specific epithelial cells as desmosomal plaque components. *Cell Tissue Res.* 290:481-499.

Segalen, M., and Bellaïche, Y. **(2009).** Cell division orientation and planar cell polarity pathways. *Seminars in cell & developmental biology.* 20:972-977.

Sharma, N., Berbari, N.F.,and Yoder, B.K. **(2008)**. Ciliary dysfunction in developmental abnormalities and diseases. *Curr Top Dev Biol*. 85:371-427.

Shin, K., Fogg, V.C., and Margolis, B. **(2006)**. Tight junctions and cell polarity. *Annual review of cell and developmental biology.* 22:207-35.

Shirakata, Y., Amagai, M., Hanakawa, Y., Nishikawa, T., and Hashimoto, K. **(1998)**. Lack of mucosal involvement in pemphigus foliaceus may be due to low expression of desmoglein 1. *J Invest Dermatol*. 110:76-78.

Siegrist, S.E., and Doe, C.Q. **(2007)**. Microtubule-induced cortical cell polarity. *Genes Dev*. 21:483-496.

Simons, M., and Mlodzik, M. **(2008)**. Planar cell polarity signaling: from fly development to human disease. *Annu Rev Genet*. 42:517-540.

Simpson, C.L., Patel, D.M. and Green, K.J. **(2011)**. Deconstructing the skin: cytoarchitectural determinants of epidermal morphogenesis. *Nat Rev Mol Cell Biol.* 12:565-80.

Simpson, M.A., Mansour, S., Ahnood, D., Kalidas, K., Patton, M.A., McKenna, W.J., Behr, E.R., and Crosby, A.H. **(2009).** Homozygous mutation of desmocollin-2 in arrhythmogenic right

ventricular cardiomyopathy with mild palmoplantar keratoderma and woolly hair. *Cardiology.* 113:28-34.

Singla, V., and Reiter, J.F. **(2006).** The primary cilium as the cell's antenna: signaling at a sensory organelle. *Science.* 313:629-633.

Song, H., Hu, J., Chen, W., Elliott, G., Andre, P., Gao, B., and Yang, Y. **(2010)**. Planar cell polarity breaks bilateral symmetry by controlling ciliary positioning. *Nature.* 466:378-382.

Sonnenberg, A., and Liem, R.K.H. **(2007)**. Plakins in development and disease. *Experimental cell research.* 313:2189-2203.

Stappenbeck, T.S., and Green, K.J. **(1992)**. The Desmoplakin Carboxyl Terminus Coaligns with and Specifically Disrupts Intermediate Filament Networks When Expressed in Cultured Cells. *J Cell Biol*. 116:1197-1209.

Stepniak, E., Radice, G.L., and Vasioukhin, V. **(2009).** Adhesive and signaling functions of cadherins and catenins in vertebrate development. *Cold Spring Harb Perspect Biol.* 1(5):a002949. doi: 10.1101/cshperspect.a002949.

Stevenson, B.R., Siliciano, J.D., Mooseker, M.S., and Goodenough, D.A. **(1986)**. Identification of ZO-1: a high molecular weight polypeptide associated with the tight junction (zonula occludens) in a variety of epithelia. *J Cell Biol.* 103:755-766.

Sugioka, K., and Sawa, H. **(2012)**. Formation and functions of asymmetric microtubule organization in polarized cells. *Curr Opin Cell Biol*. 24:517-25.

Sumigray, K.D. and Lechler, T. **(2011)**. Control of cortical microtubule organization and desmosome stability by centrosomal proteins. Bioarchitecture 1, 221-224.

Swope, D., Li, J., and Radice, G.L. **(2013)**. Beyond cell adhesion: The role of armadillo proteins in the heart. *Cell Signal*. 25:93-100.

Therman, E., Laxova, R., and Susman, B. **(1990).** The critical region on the human Xq. *Hum Genet.* 85:455-461.

Thiene, G., Nava, A., Corrado, D., Rossi, L., and Pennelli, N. **(1988)**. Right ventricular cardiomyopathy and sudden death in young people. *N Engl J Med.* 318:129-133.

Thompson, B.J. **(2013)**. Cell polarity: models and mechanisms from yeast, worms and flies. *Development.* 21:13-21.

Toivola, D.M., Strnad, P., Habtezion, A., and Omary, M.B. **(2011)**. Intermediate filaments take the heat as stress proteins. *Cell.* 20:79-91.

Tsukita, S. and Furuse, M. **(2002)**. Claudin-based barrier in simple and stratified cellular sheets. *Curr Opin Cell Biol.* 14:531-536.

Van Itallie, C.M., Fanning, A.S., Bridges, A., and Anderson, J.M. **(2009)**. ZO-1 stabilizes the tight junction solute barrier through coupling to the perijunctional cytoskeleton. *Mol Biol Cell.* 20:3930-3940.

Vaughan, S., and Dawe, H.R. **(2011)**. Common themes in centriole and centrosome movements. *Trends Cell Biol*. 21:57-66.

Vega Salas, D.E., Salas, P.J., Gunderson, D.,and Rodriguez-Boulan, E. **(1987)**. Formation of the apical pole of epithelial (Madin-Darby canine kidney) cells: polarity of an apical protein is independent of tight junctions while segregation of a basolateral marker requires cell-cell interactions. *J Cell Biol*.104:905-916.

Vieira, O.V., Gaus, K., Verkade, P., Fullekrug, J., Vaz, W.L. and Simons, K. **(2006)**. FAPP2, cilium formation, and compartmentalization of the apical membrane in polarized

Madin-Darby canine kidney (MDCK) cells. *Proc. Natl. Acad. Sci USA.* 103:18556-18561.

Volpe, D.A. **(2008)**. Variability in Caco-2 and MDCK Cell-Based Intestinal Permeability Assays. *Journal of Pharmaceutical Sciences.* 97:712-725.

Wallingford, J.B. **(2012)**. Planar cell polarity and the developmental control of cell behavior in vertebrate embryos. *Annual review of cell and developmental biology.* 28:627-53.

Wallis, S., Lloyd, S., Wise, I., Ireland, G., Fleming, T.P., and Garrod, D. **(2000)**. The alpha isoform of protein kinase C is involved in signaling the response of desmosomes to wounding in cultured epithelial cells. *Molecular Biology of the Cell.* 11(3):1077-1092.

Wells, W.A. **(2005)**. Defining junctional complexes. *J Cell Biol.* 168:989.

Windoffer, R., Beil, M., Magin, T.M., and Leube, R.E. **(2011)**. Cytoskeleton in motion: the dynamics of keratin intermediate filaments in epithelia. *J Cell Biol*. 19:669-678.

Yin, T., and Green, K.J. **(2004)**. Regulation of desmosome assembly and adhesion. *Seminars in cell & developmental biology.* 15:665-677.

Zegers, M.M., O'Brien, L.E., Yu, W., Datta, A., and Mostov, K.E. **(2003)**. Epithelial polarity and tubulogenesis in vitro. *Trends Cell Biol*. 13:169-176.

Zheng, Z., Zhu, H., Wan, Q., Liu, J., Xiao, Z., Siderovski, D.P., and Du, Q. **(2010)**. LGN regulates mitotic spindle orientation during epithelial morphogenesis. *J Cell Biol.* 189:275-288.